

2

NAVAL POSTGRADUATE SCHOOL

Monterey, California

DTIC ERL COPY

AD-A202 188



THESIS

PASSIVE VIBRATION CONTROL USING
VISCOELASTIC AND CONSTRAINED LAYER
BEAM WAVEGUIDE ABSORBERS

by

Charles T. Horne III

September 1988

Thesis Advisor

Young S. Shin

Approved for public release; distribution is unlimited

DTIC
ELECTE
DEC 29 1988
S D

H

88 12 29 014

Unclassified

security classification of this page

REPORT DOCUMENTATION PAGE

1a Report Security Classification Unclassified		1b Restrictive Markings	
2a Security Classification Authority		3 Distribution Availability of Report Approved for public release; distribution is unlimited.	
2b Declassification Downgrading Schedule			
4 Performing Organization Report Number(s)		5 Monitoring Organization Report Number(s)	
6a Name of Performing Organization Naval Postgraduate School	6b Office Symbol (if applicable) 34	7a Name of Monitoring Organization Naval Postgraduate School	
6c Address (city, state, and ZIP code) Monterey, CA 93943-5000		7b Address (city, state, and ZIP code) Monterey, CA 93943-5000	
8a Name of Funding Sponsoring Organization	8b Office Symbol (if applicable)	9 Procurement Instrument Identification Number	
8c Address (city, state, and ZIP code)		10 Source of Funding Numbers	
		Program Element No	Project No
		Task No	Work Unit Accession No
11 Title (include security classification) PASSIVE VIBRATION CONTROL USING VISCOELASTIC AND CONSTRAINED LAYER BEAM WAVEGUIDE ABSORBERS			
12 Personal Author(s) Charles T. Horne III			
13a Type of Report Master's Thesis	13b Time Covered From To	14 Date of Report (year, month, day) September 1988	15 Page Count 101
16 Supplementary Notation The views expressed in this thesis are those of the author and do not reflect the official policy or position of the Department of Defense or the U.S. Government.			
17 Cosati Codes		18 Subject Terms (continue on reverse if necessary and identify by block number)	
Field	Group	Subgroup	
		waveguide absorber, viscoelastic, constrained layer, impedance	
19 Abstract (continue on reverse if necessary and identify by block number)			
<p>Reduction of noise and vibrations within structural systems has been a long standing problem. Recent studies have indicated that waveguide absorbers have been effective in the reduction of noise and vibrations over a broad frequency range. A waveguide absorber is a structure along which vibrational waves can travel. If the waveguide absorber is treated with an energy dissipation scheme, the amplitudes of the waves will decrease as they travel along the waveguide absorber.</p> <p>The test structure consisted of a rectangular aluminum plate with clamped boundary conditions. A finite element analysis approach theoretically predicted the test structure's mode shapes and modal strain energies. An experimental modal survey was conducted to compare with the theoretically predicted mode shapes and natural frequencies. The mode shapes and modal strain energies determined the optimum locations of the waveguide absorbers and their orientation on the test structure. The frequency range of interest and mode shapes determined the required number of waveguide absorbers.</p> <p>Experiments were conducted using viscoelastic and constrained layer beam waveguide absorbers over a 2000 Hertz frequency range. Significant reduction of the test structure's frequency response was demonstrated through the effective use of multiple beam waveguide absorbers. <i>Theses, (Aug)</i></p>			
20 Distribution Availability of Abstract <input checked="" type="checkbox"/> unclassified unlimited <input type="checkbox"/> same as report <input type="checkbox"/> DTIC users		21 Abstract Security Classification Unclassified	
22a Name of Responsible Individual Young S. Shin		22b Telephone (include Area code) (408) 646-2568	22c Office Symbol 69Sg

DD FORM 1473,84 MAR

83 APR edition may be used until exhausted
All other editions are obsolete

security classification of this page

Unclassified

Approved for public release; distribution is unlimited.

Passive Vibration Control Using Viscoelastic and Constrained Layer
Beam Waveguide Absorbers

by

Charles T. Horne III
Lieutenant, United States Navy
B.M.E., Auburn University, 1981


" Submitted in partial fulfillment of the
requirements for the degree of

MASTER OF SCIENCE IN MECHANICAL ENGINEERING

from the

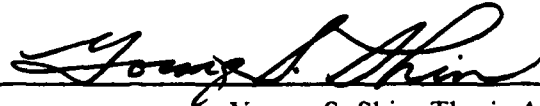
NAVAL POSTGRADUATE SCHOOL
September 1988

Author:

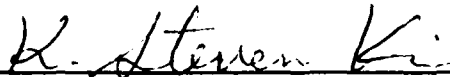


Charles T. Horne III

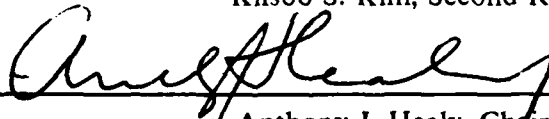
Approved by:



Young S. Shin, Thesis Advisor



Kilsoo S. Kim, Second Reader



Anthony J. Healy, Chairman,
Department of Mechanical Engineering



Gordon E. Schacher,
Dean of Science and Engineering

ABSTRACT

Reduction of noise and vibrations within structural systems has been a long standing problem. Recent studies have indicated that waveguide absorbers have been effective in the reduction of noise and vibrations over a broad frequency range. A waveguide absorber is a structure along which vibrational waves can travel. If the waveguide absorber is treated with an energy dissipation scheme, the amplitudes of the waves will decrease as they travel along the waveguide absorber.

The test structure consisted of a rectangular aluminum plate with clamped boundary conditions. A finite element analysis approach theoretically predicted the test structure's mode shapes and modal strain energies. An experimental modal survey was conducted to compare with the theoretically predicted mode shapes and natural frequencies. The mode shapes and modal strain energies determined the optimum locations of the waveguide absorbers and their orientation on the test structure. The frequency range of interest and mode shapes determined the required number of waveguide absorbers.

Experiments were conducted using viscoelastic and constrained layer beam waveguide absorbers over a 2000 Hertz frequency range. Significant reduction of the test structure's frequency response was demonstrated through the effective use of multiple beam waveguide absorbers.



Accession For	
NTIS GRA&I	<input checked="" type="checkbox"/>
DTIC TAB	<input type="checkbox"/>
Unannounced	<input type="checkbox"/>
Justification	
By	
Distribution/	
Availability Codes	
Dist	Avail and/or Special
A-1	

TABLE OF CONTENTS

I. INTRODUCTION	1
A. BACKGROUND	1
B. PREVIOUS INVESTIGATIONS	1
C. CURRENT RESEARCH	3
II. FINITE ELEMENT ANALYSIS	4
A. MODAL ANALYSIS	4
B. STRAIN ENERGY ANALYSIS	6
III. WAVEGUIDE ABSORBER DESIGN	11
A. LENGTH AND MATERIAL PROPERTIES	11
B. LOCATION AND ORIENTATION	11
IV. EXPERIMENTAL METHOD	13
A. EXPERIMENTAL MODEL	13
B. EQUIPMENT ARRANGEMENT	13
1. MODAL SURVEY IMPACT TESTING	13
2. STRUCTURAL DAMPING OF THE PLATE	18
3. PLATE IMPEDANCE	18
C. GENERAL TEST PLAN	18
V. RESULTS	21
A. COMPARISONS	21
1. THEORETICAL AND EXPERIMENTAL	21
2. VISCOELASTIC AND CONSTRAINED LAYER	21
B. ORIENTATION	23
C. MULTIPLE WAVEGUIDE ABSORBERS	26
VI. CONCLUSIONS	30
VII. RECOMMENDATIONS	32

APPENDIX A. THEORETICAL PERSPECTIVE VIEWS AND Z - PLANE DEFORMATION CONTOURS	33
APPENDIX B. MODAL SURVEY PERSPECTIVE VIEWS	58
APPENDIX C. FREQUENCY RESPONSE FUNCTIONS OF THE TEST PLATE WITH BEAM WAVEGUIDE ABSORBERS ATTACHED	68
LIST OF REFERENCES	88
INITIAL DISTRIBUTION LIST	89

LIST OF FIGURES

Figure 1.	Theoretical undeformed shape and grid structure	7
Figure 2.	Theoretical perspective view - mode #1 (312.31 Hz).	8
Figure 3.	Theoretical z-plane deformation contour - mode #1 (312.31 Hz).	9
Figure 4.	Waveguide absorber in torsion and bending.	12
Figure 5.	The test model.	14
Figure 6.	Viscoelastic and constrained layer beam waveguide absorbers.	15
Figure 7.	Modal survey test equipment arrangement.	16
Figure 8.	Modal survey undeformed shape and grid structure.	17
Figure 9.	Equipment arrangement for the test plate frequency response measurements (with beam waveguide absorbers attached).	19
Figure 10.	Modal survey perspective view - mode #1 (195.76 Hz).	22
Figure 11.	Baseline (DP) frequency response (solid); with a 20" viscoelastic waveguide (dashed) at locations A, B and C.	24
Figure 12.	Baseline (DP) frequency response (solid); with a 20" constrained layer waveguide (dashed) at locations A, B and C.	25
Figure 13.	Baseline (DP) frequency response (solid); with a 20" viscoelastic waveguide parallel to the X axis (dashed)	27
Figure 14.	Baseline (DP) frequency response (solid); with a 20" viscoelastic waveguide parallel to the Y axis (dashed)	28
Figure 15.	Baseline (DP) frequency response (solid); with a 20" viscoelastic waveguide absorber attached at locations A - F (dashed).	29
Figure 16.	Theoretical perspective view - mode #2 (475.25 Hz)	34
Figure 17.	Theoretical perspective view - mode #3 (755.67 Hz).	35
Figure 18.	Theoretical perspective view - mode #4 (762.99 Hz)	36
Figure 19.	Theoretical perspective view - mode #5 (897.72 Hz)	37
Figure 20.	Theoretical perspective view - mode #6 (1136.16 Hz)	38
Figure 21.	Theoretical perspective view - mode #7 (1145.22 Hz)	39
Figure 22.	Theoretical perspective view - mode #8 (1438.39 Hz)	40
Figure 23.	Theoretical perspective view - mode #9 (1484.84 Hz)	41
Figure 24.	Theoretical perspective view - mode #10 (1558.78 Hz)	42
Figure 25.	Theoretical perspective view - mode #11 (1636.15 Hz)	43

Figure 26.	Theoretical perspective view - mode #12 (1766.34 Hz)	44
Figure 27.	Theoretical perspective view - mode #13 (1945.23 Hz)	45
Figure 28.	Theoretical z-plane deformation contour - mode #2.	46
Figure 29.	Theoretical z-plane deformation contour - mode #3.	47
Figure 30.	Theoretical z-plane deformation contour - mode #4.	48
Figure 31.	Theoretical z-plane deformation contour - mode #5.	49
Figure 32.	Theoretical z-plane deformation contour - mode #6.	50
Figure 33.	Theoretical z-plane deformation contour - mode #7.	51
Figure 34.	Theoretical z-plane deformation contour - mode #8.	52
Figure 35.	Theoretical z-plane deformation contour - mode #9.	53
Figure 36.	Theoretical z-plane deformation contour - mode #10.	54
Figure 37.	Theoretical z-plane deformation contour - mode #11.	55
Figure 38.	Theoretical z-plane deformation contour - mode #12.	56
Figure 39.	Theoretical z-plane deformation contour - mode #13.	57
Figure 40.	Modal survey perspective view - mode #2 (276.04 Hz).	59
Figure 41.	Modal survey perspective view - mode #3 (338.71 Hz).	60
Figure 42.	Modal survey perspective view - mode #4 (429.66 Hz).	61
Figure 43.	Modal survey perspective view - mode #5 (499.84 Hz).	62
Figure 44.	Modal survey perspective view - mode #6 (665.73 Hz).	63
Figure 45.	Modal survey perspective view - mode #7 (708.52 Hz).	64
Figure 46.	Modal survey perspective view - mode #8 (815.66 Hz).	65
Figure 47.	Modal survey perspective view - mode #9 (1005.73 Hz).	66
Figure 48.	Modal survey perspective view - mode #10 (1062.31 Hz).	67
Figure 49.	Baseline (DP) frequency response (solid); with a 20" constrained layer waveguide attached at location A (dashed)	69
Figure 50.	Baseline (DP) frequency response (solid); with a 20" constrained layer waveguide attached at locations A and B (dashed)	70
Figure 51.	Baseline (DP) frequency response (solid); with a 16" constrained layer waveguide absorber at location A (dashed)	71
Figure 52.	Baseline (DP) frequency response (solid); with a 16" constrained layer waveguide absorber at locations A and B (dashed)	72
Figure 53.	Baseline (DP) frequency response (solid); with a 16" constrained layer waveguide absorber at locations A, B and C (dashed)	73
Figure 54.	Baseline (DP) frequency response (solid); with a 20" viscoelastic	

	waveguide absorber attached at location A (dashed)	74
Figure 55.	Baseline (DP) frequency response (solid); with a 20" viscoelastic waveguide absorber at locations A and B (dashed)	75
Figure 56.	Baseline (DP) frequency response (solid); with a 20" viscoelastic waveguide absorber at locations A, B, C and D (dashed)	76
Figure 57.	Baseline (DP) frequency response (solid); with a 20" viscoelastic waveguide absorber at locations A, B, C, D and E (dashed)	77
Figure 58.	Baseline (DP) frequency response (solid); with a 16" viscoelastic waveguide absorber at location A (dashed)	78
Figure 59.	Baseline (DP) frequency response (solid); with a 16" viscoelastic waveguide absorber at locations A and B (dashed)	79
Figure 60.	Baseline (DP) frequency response (solid); with a 16" viscoelastic waveguide absorber at locations A, B and C (dashed)	80
Figure 61.	Real part of the test plate's impedance at location A.	81
Figure 62.	Real part of the test plate's impedance at location B.	82
Figure 63.	Real part of the test plate's impedance at location C.	83
Figure 64.	Real part of the 20" constrained layer waveguide absorber's impedance.	84
Figure 65.	Real part of the 16" constrained layer waveguide absorber's impedance.	85
Figure 66.	Real part of the 20" viscoelastic waveguide absorber's impedance.	86
Figure 67.	Real part of the 16" viscoelastic waveguide absorber's impedance.	87

ACKNOWLEDGEMENTS

The author would like to express his appreciation to Professor Young S. Shin and Dr. Kilsoo S. Kim for their guidance, theoretical support and technical expertise in performing this research, and to Tom Christian, Jim Scholfield and Mardo Blanco for providing the material, equipment knowledge and lab support to complete this research. And finally, to my wife [REDACTED] whose love, devotion and patience ensured that I always maintained a "true" perspective of the big picture.

I. INTRODUCTION

A. BACKGROUND

The reduction of noise and vibrations in structural systems has been a long standing problem. Structural damping is an indication of a structure's ability to dissipate energy. This energy, which is a prime source of acoustics and resonant fatigue, may be transferred to connected structures, removed as heat or transferred to other structural motions. Classical methods such as isolation, detuning, viscoelastic damping and dynamic absorbtion have been researched with their limitations and resultant actions fully documented. [Ref. 1]

A new technique for passive vibration control has recently been developed [Ref. 2] that invokes the concept of removing the energy away from the structure through vibrational, (flexural) waveforms. The "waveguide", when attached to a vibrating structure acts as a medium along which these vibration waves can travel. If the waveguide is treated with or designed from a high energy dissipation material the vibrational waves will decrease in amplitude with increasing distance. With this, the waveguide absorber reduces the structure's vibration energy over a broad frequency range.

B. PREVIOUS INVESTIGATIONS

Although Bschorr and Albrecht [Ref. 2] conducted initial investigations into the use of waveguide absorbers with tapered cross-sections, the conceptual understanding of a waveguide absorber's interactions in dissipating a structure's vibration energy was not fully understood until after Ungar and Kurzweil's studies in 1983 [Ref. 3]. In their studies, the theory for understanding the contributions of the waveguide absorber in increasing the damping of a structure was developed. The major concept centered around the matching of impedances between the structure and the waveguide absorber. The energy loss per cycle was shown to be:

$$D = \frac{\pi R_b}{\omega} \frac{|V_s|^2}{\left|1 + \frac{Z_b}{Z_s}\right|^2} \quad (1.1)$$

where, ω , denotes the vibration frequency, V_s , is the structure's velocity amplitude at the attachment point (before attaching a waveguide), Z_b and Z_s , denote the impedance of the

waveguide and structure, respectively and R_b , represents the magnitude of the real part of Z_b . The structure will vibrate with the energy of vibration:

$$W_0 = \frac{1}{2} M V_m^2 \quad (1.2)$$

where, M , is the total mass of the structure and V_m , denotes the magnitude of the average spatial velocity. By combining equations (1.1) and (1.2) the loss factor, η , due to the contribution of an attached waveguide absorber can be expressed as:

$$\eta = \frac{D}{2\pi W_0} = \frac{R_b}{\omega M} \frac{\left| \frac{V_s}{V_m} \right|^2}{\left| 1 + \frac{Z_b}{Z_s} \right|^2} \quad (1.3)$$

The loss factor was found to be a function of both the velocity and impedances at the attachment point. The loss factor contribution could then be maximized by matching the impedances of the waveguide absorber and the structure at the attachment point.

Ungar and Williams [Ref. 4] conducted experiments with several types of waveguide absorbers which were attached to a free-free flat plate and a fixed-free beam. Significant damping resulted from the addition of the waveguide absorber. However, theoretical predictions of the waveguide absorber's driving point impedances (using semi-infinite Bernoulli-Euler beam theory) varied significantly from experimentally measured values. The experiments were conducted with finite beams, but the results were compared with the theoretical predictions of semi-infinite beams.

Lee [Ref. 5], showed that the Timoshenko beam theory and harmonic wave propagation approach improved the predictions of the driving point impedances for viscoelastic beams, while sixth-order beam theory was successful in predicting the impedances of constrained layer beams. Lee, experimenting with various lengths of both the viscoelastic and constrained layer beams, found that the waveguide absorber and the test plate's impedances were similar in magnitude, thus concluding that equation (1.3) could not be used to accurately predict the loss factor contribution. Further he concluded that the impedance and the location of the waveguide absorber had a direct impact on maximizing the waveguide absorber's effectiveness in damping a structure.

C. CURRENT RESEARCH

Previous studies [Refs. 3, 4 ,5] primarily focused on the theoretical predictions of the waveguide absorber's impedance and experimental analysis when attached to a test structure. In order to maximize the effectiveness of a waveguide absorber, an optimization process was required. The location, number, orientation, and design of the waveguide absorber were considered the essential elements of this process. The design of the waveguide absorber was not considered in this research. The viscoelastic and constrained layer beam waveguide absorbers of Lee's research [Ref. 5] were used. However, the thought process in designing a waveguide absorber is discussed.

A finite element analysis approach predicted the mode shapes and modal strain energies for a 2000 Hertz frequency range. An experimental modal survey was conducted to compare with theoretical predictions. Based on the theoretical modal energies, mode shapes and frequency range the location, number and orientation of beam waveguide absorbers were determined. The effective use of multiple beam waveguide absorbers was demonstrated during random vibration experiments.

II. FINITE ELEMENT ANALYSIS

A. MODAL ANALYSIS

The finite element method is a simulation of a physical "Real World" problem. In the finite element method, a mathematical model is formed by subdividing the real-world structure into a finite number of small regions called elements. Each element is connected to the surrounding elements at a finite number of points called grids. This establishes the structure's geometry. Other structural information utilized within the analysis includes; a global reference coordinate system, material properties, loading, etc. A single degree of freedom system, subjected to a time varying input force can be described by a linear second order differential equation in the following form:

$$m\ddot{x}(t) + c\dot{x}(t) + kx(t) = f(t) \quad (2.1)$$

where,

$\ddot{x}(t)$ = acceleration response

$\dot{x}(t)$ = velocity response

$x(t)$ = displacement response

m = mass

c = damping

k = stiffness

$f(t)$ = applied force

A multiple degree of freedom system can be described in a similar manner:

$$[M]\{\ddot{x}\} + [C]\{\dot{x}\} + [K]\{x\} = \{F\} \quad (2.2)$$

where,

$\{x\}$ = acceleration response vector

$\{\dot{x}\}$ = velocity response vector

$\{x\}$ = displacement response vector

$[M]$ = mass matrix, $n \times n$

$[C]$ = damping matrix, $n \times n$

$[K]$ = stiffness matrix, $n \times n$

$\{F\}$ = applied force vector

Modal analysis of the structure assumes an undamped, unforced case, whereas, equation (2.2) becomes:

$$[M]\{\ddot{x}\} + [K]\{x\} = 0 \quad (2.3)$$

and if it is assumed that, x , is of the form:

$$\{x\} = \{\phi\} \exp(j\omega t) \quad (2.4)$$

$\{\phi\}$ = modal vector

ω = excitation frequency

then, substitution of equation (2.4) into equation (2.3) gives:

$$[K - \omega^2 M]\{\phi\} = 0 \quad (2.5)$$

which reduces the dependent equations (in x) of equation (2.3), to a set of independent equations (in ϕ) of equation (2.5). A nontrivial solution exists if the matrix of equation (2.4) is singular. It can be shown that this will occur only at a discrete set of frequencies called eigenfrequencies (modal frequencies). Corresponding to each frequency there is a vector $\{\phi_i\}$, called an eigenvector (modal vector) which solves equation (2.5). Each modal frequency and modal vector defines the structure's natural frequency, geometry and the magnitude of the structural deformation. The vibrational response of the structure can then be expressed as a sum of the responses of its vibration modes. [Refs. 6,7]

Using MSC/NASTRAN [Ref. 6], a T6061 aluminum plate, with clamped boundary conditions is sectioned into 96 elements and 117 grid points as shown in Figure 1. The selection of the number of elements in the finite element model is an obviously important topic because of its relation to accuracy. In many cases the minimum number of elements is set by topological considerations. The number of elements and their spacing used to model the test plate, describes the mode shapes over a 2000 Hz frequency range. A perspective view of each mode's geometry as shown in Figure 2 and a z-plane deformation contour as shown in Figure 3 are plotted. The deformation contours are used to determine the node lines for each mode. Along node lines, structural deformation does not occur. By analyzing the node lines for each mode over the desired frequency range, a composite group of node lines is established. This composite group represents a detailed description of the individual grid point's deformation within the modeled

structure. A modal strain energy analysis is conducted to examine the strain energy of each element within a particular mode [Ref. 7].

B. STRAIN ENERGY ANALYSIS

The strain energy of each element is a function of the displacement of that element and thereby, the excitation. The displacements of any point are expressed as a function of the elemental displacements. The strain within an element is expressed as:

$$\{\epsilon\} = [B]\{u\} \quad (2.5)$$

where, $[B]$ = element strain displacement matrix and $\{u\}$ = element displacement vector. Since the elemental stress is a function of the strain within the element, it is expressed as:

$$\{\sigma\} = [C]\{\epsilon\} \quad (2.6)$$

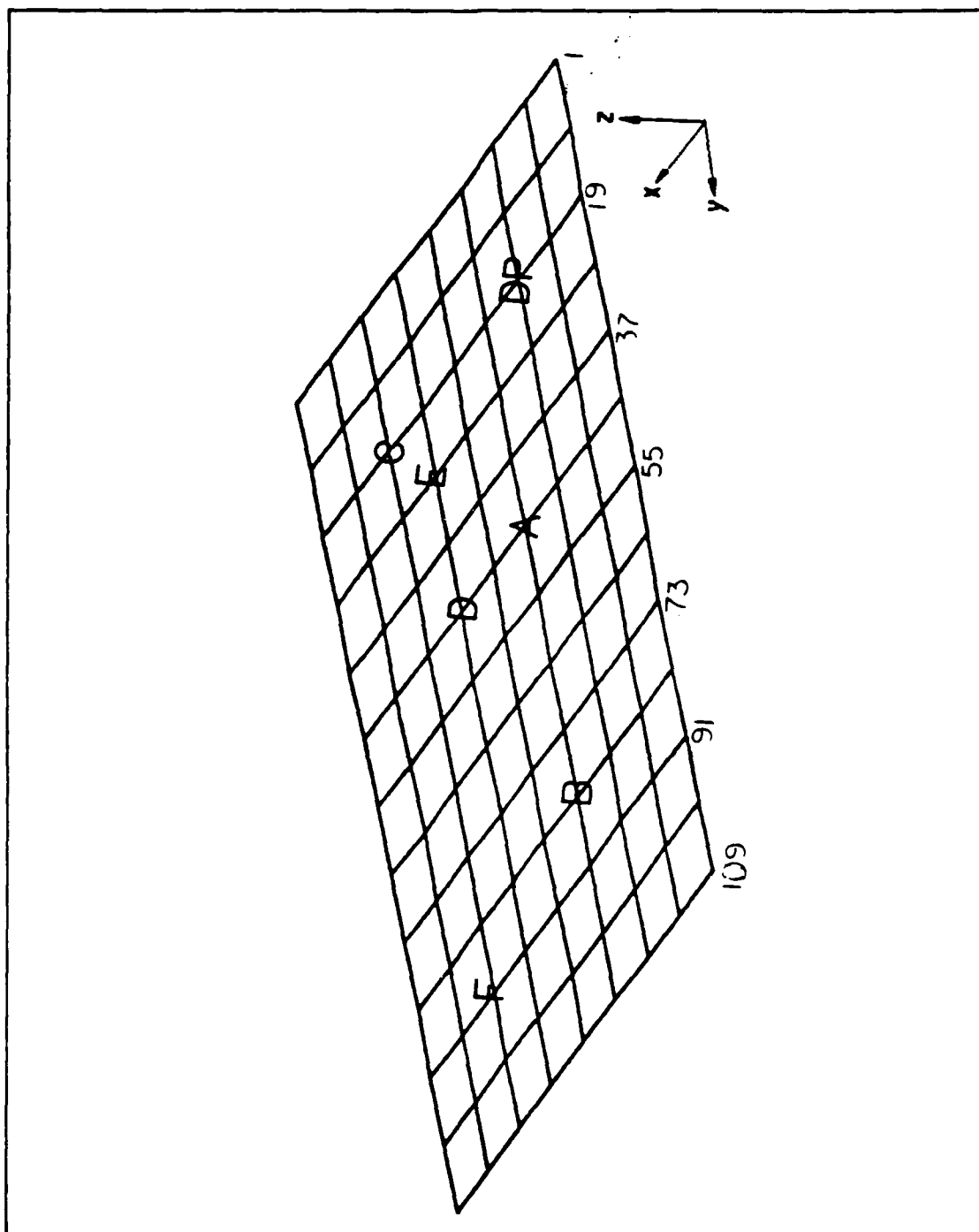
where, $[C]$, is the element stress-strain matrix. Then, the internal strain energy of each element is expressed as:

$$[U] = \frac{1}{2} \{\sigma\}^T \{\epsilon\} \quad (2.7)$$

Substituting equations, (2.5) and (2.6) into (2.7) and using the relationship, $[K] = [B]^T[C][B]$, the internal strain energy is expressed as:

$$U = \frac{1}{2} \{u\}^T [K] \{u\} \quad (2.9)$$

For a given excitation, the internal strain energy, U , is determined for each mode and the elements containing the highest strain energy for each mode are identified. The elements which repeat in having the highest strain energy over all modes within the desired frequency range, theoretically determine the location of the waveguide absorbers. The frequency response is to be affected over a broad frequency span, therefore, the grid points surrounding those elements with the highest strain energy are identified as the attachment points for the waveguide absorbers. As an example, elements 28, 29, 68 and 69 as shown in Figure 1, repeated as having the highest strain energy for all modes (0-2000 Hz). Based on the theoretical mode shapes and modal strain energies, six grid points were selected as waveguide absorber attachment points. These grid points, 49, 85, 25, 51, 33, and 97 are indicated by locations A through F respectively, in Figure 1.



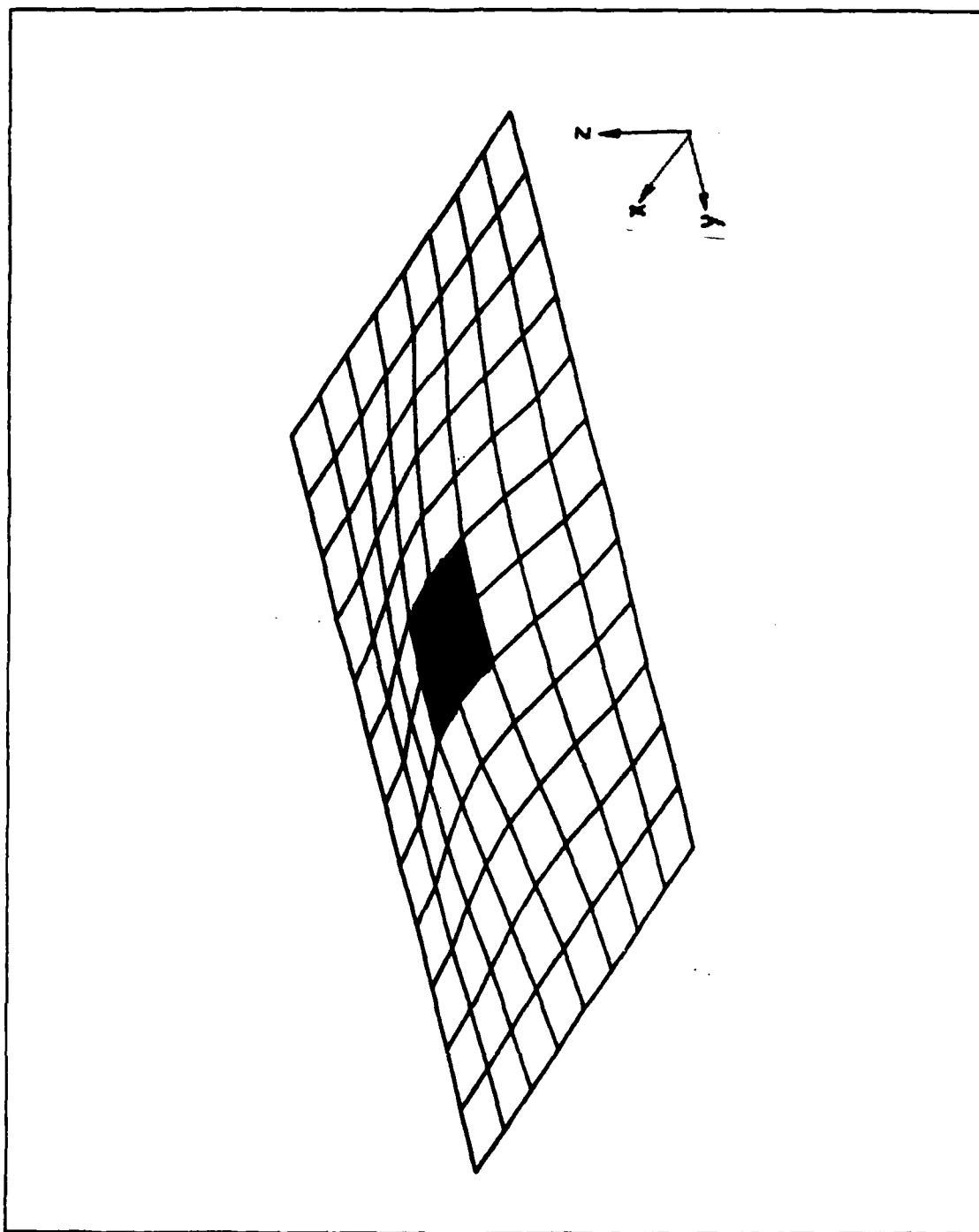


Figure 2. Theoretical perspective view - mode #1 (312.31 Hz).: Shaded elements
- area of highest strain energy.

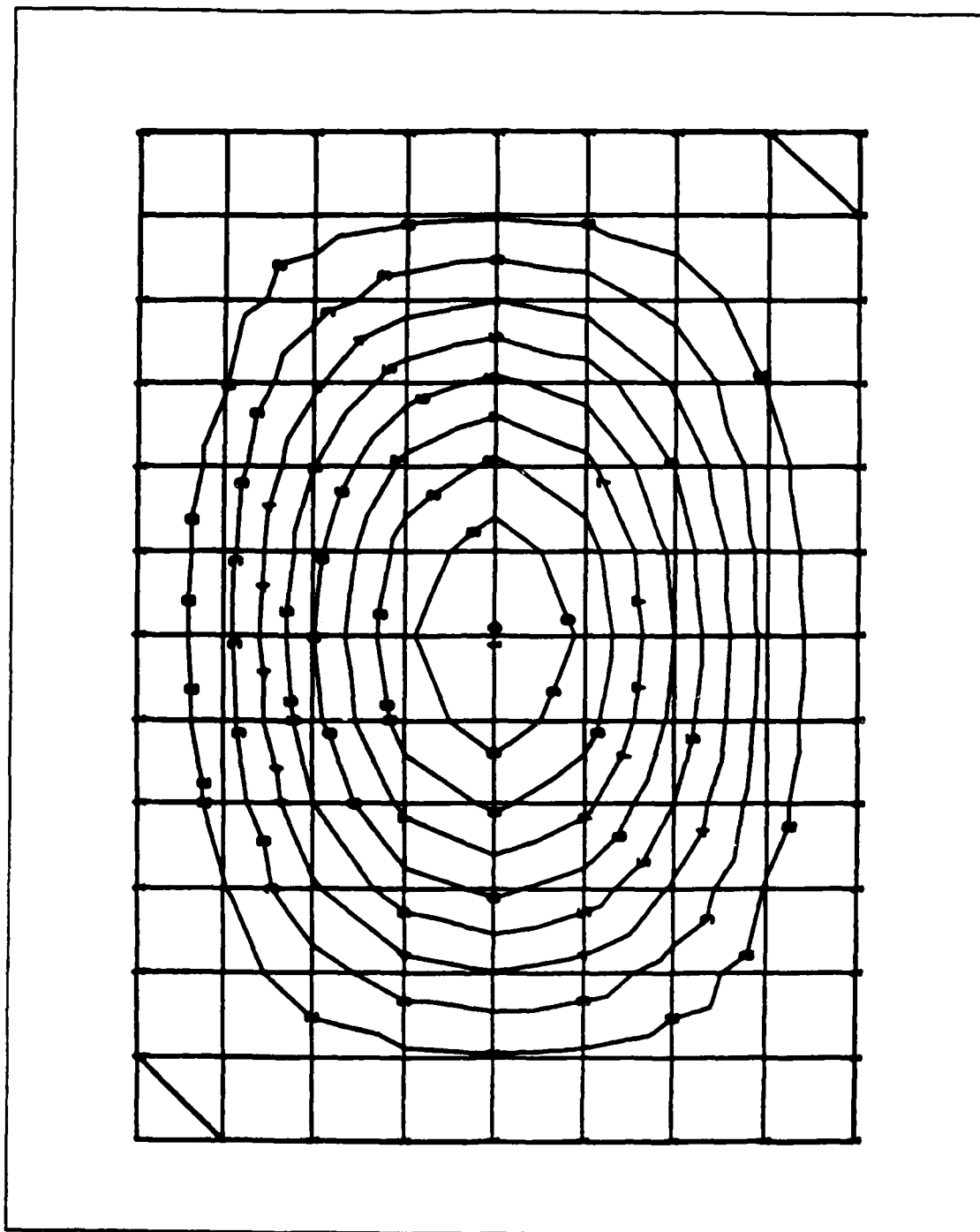


Figure 3. Theoretical z-plane deformation contour - mode #1 (312.31 Hz).

After predicting the mode shapes, modal strain energies and knowing the structure's impedance, the waveguide absorber would then be designed to maximize the loss factor of equation (1.3).

III. WAVEGUIDE ABSORBER DESIGN

A. LENGTH AND MATERIAL PROPERTIES

In almost all Naval applications, the vibrating structure would require the retrofit of a waveguide absorber. To achieve the optimal performance of the waveguide absorber, many variables must be considered. Almost all of the variables in question are a function of the waveguide absorber's physical and material properties. For example, if the area of concern is in a lower frequency range, a longer waveguide absorber would generally be more effective, since the wavelength, λ is inversely proportional to the frequency.

In equation (1.3), the loss factor is a function of the waveguide absorber's impedance, Z_b , the structure's impedance, Z_s , the velocity, V , and V_m , and the term $\frac{R_b}{\omega M}$. Matching the impedance of the waveguide absorber to the structure's impedance at the attachment point, maximizes the damping loss factor. If the impedance of the waveguide absorber, Z_b , is much greater than that of the structure at the attachment point, the loss factor is reduced. The velocity, V , and V_m , which describe the velocity of the attachment point and the average spatial velocity of the structure are both functions of the two impedances. However, the change in the structure's average spatial velocity, V_m is not considered in equation (1.3). This change is difficult to predict in equation form. It can be predicted using a finite element approach. The addition of the waveguide absorber to the structure alters the structure's mass, damping and stiffness matrices. These matrices can be altered within the finite element program to predict the frequency response and resultant damping. Knowing the location and orientation with respect to the structure, the design of the waveguide absorber can then be evaluated.

B. LOCATION AND ORIENTATION

The location and orientation of the waveguide on the structure is almost totally, mode shape dependent. In past studies [Refs. 3, 4, 5], the effects of torsional waves are not considered in the development of theoretical predictions of the waveguide absorber's impedance. Torsional waves are in fact shear waves which are induced from the lateral rotation of the waveguide absorber as shown in Figure 4, in contrast to flexural waves, which are induced due to a force or bending moment along the waveguide absorber's length [Ref. 8]. As previously stated by Ungar [Ref. 4], the power transfer to a semi-infinite beam is higher due to torsional waves than flexural, which is considered

similar in nature to that of a finite beam. Therefore, the location must take into consideration the effects of both waves. For example, in the first classical mode as shown in Figure 2, the center of the plate experiences vertical motion only. This attachment point would induce flexural waves, with the waveform independent of orientation. However, if the waveguide absorber's attachment point is off-center and the waveguide absorber is rotated off axis, both waveforms are induced with the flexural part being dominant. Therefore, the induced waveform is dependent on the mode shape and location of the attachment point. In most cases it is dependent on the orientation of the waveguide absorber with respect to the structure's coordinate system. Understanding the total concept of location, number and orientation, experiments utilizing multiple waveguide absorbers were conducted to evaluate their contribution in reducing the driving point frequency response amplitude.

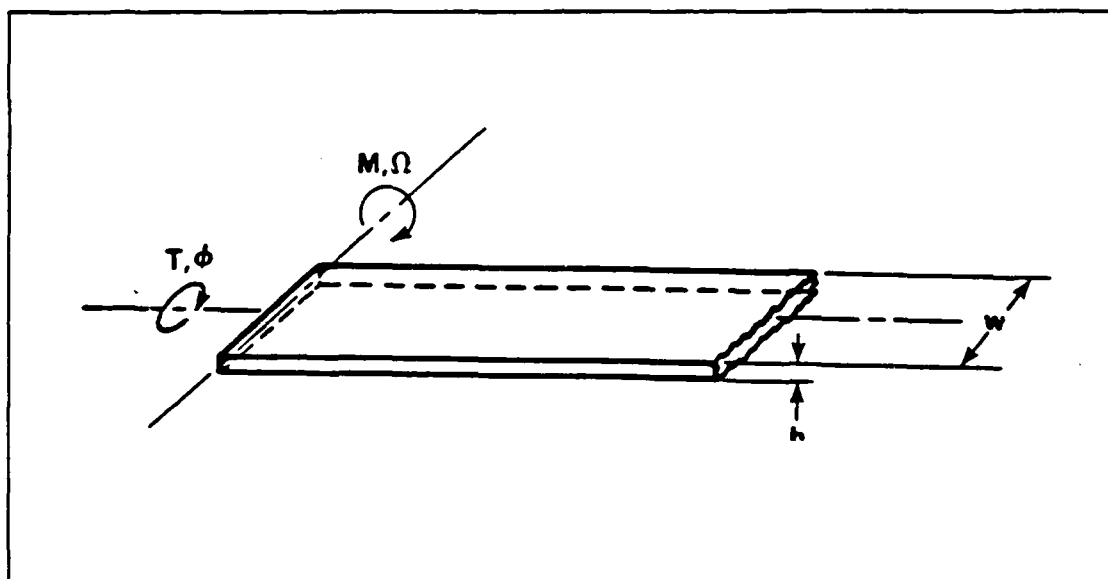


Figure 4. Waveguide absorber in torsion and bending.

IV. EXPERIMENTAL METHOD

A. EXPERIMENTAL MODEL

The experimental model was the same model used by Lee [Ref. 5] in his investigation of beam waveguide absorbers to increase structural damping. A rectangular aluminum plate with clamped boundary conditions was selected as the test structure, because there are a sufficient number of modes for analysis within the 2000 Hz frequency range. A T6061 aluminum test model (30" x 22" x 2"), as shown in Figure 5, was milled to include a test plate (24" x 16" x 0.3125") and a three inch border which simulated the clamped boundary condition. The model was supported with styrofoam to limit the transmission of random noise from the environment to the test structure.

During the experimentation phase, two viscoelastic and two constrained layer beams, which were previously developed by Lee [Ref. 5] and as shown in Figure 6, were used as waveguide absorbers.

B. EQUIPMENT ARRANGEMENT

1. Modal Survey Impact Testing

The testing equipment arrangement used during the investigation is shown in Figure 7. An impact analysis, using a PCB modally tuned impact hammer (model 086B03) was performed on the test model which included the test plate and surrounding border. Each of the 48 grid points as shown in Figure 8, was excited ten times and averaged to obtain the input and output signals. The input signal was obtained from a force transducer located in the tip of the impact hammer. The signal was amplified by a PCB signal conditioner (model 480B06). The response of the test model was measured at grid point 15 using an Endevco accelerometer (model 2250A10). The response signal was amplified by a PCB signal conditioner (model 480D06), which was set with a gain factor of ten. The input and response signals were analyzed by a Hewlett Packard (HP) 3562A Dynamic Signal Analyzer. The frequency response function was then transferred to a HP 216 system computer, where utilizing a Structural Measurement Systems (Modal 3.0) modal analysis package, the modal properties were determined. The modal analysis package also animated the vibrational motion of each mode.

2. Structural Damping of the Plate

The structural damping of the test plate with waveguide absorbers attached was determined from frequency response transfer functions. The testing equipment used

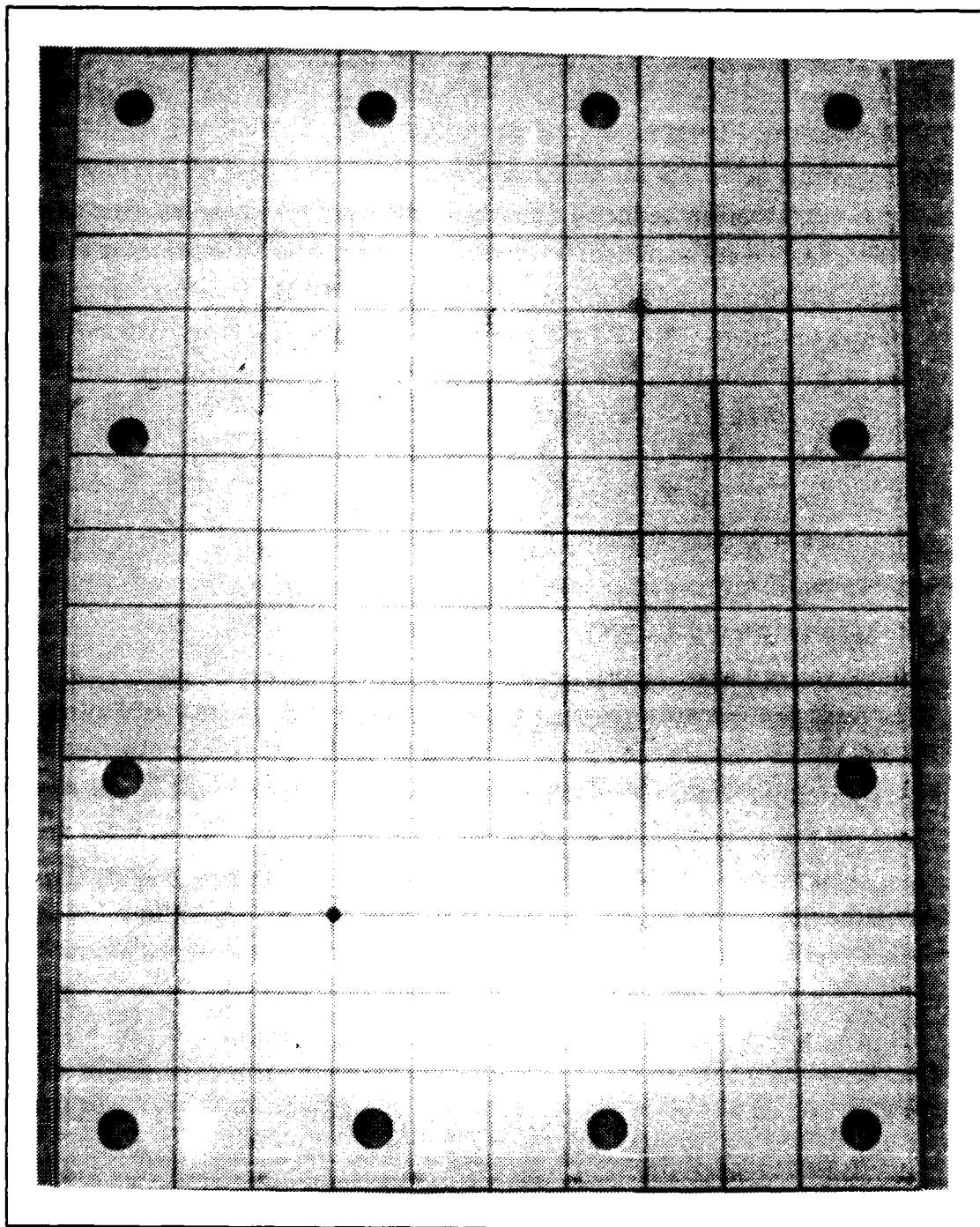


Figure 5. The test model.

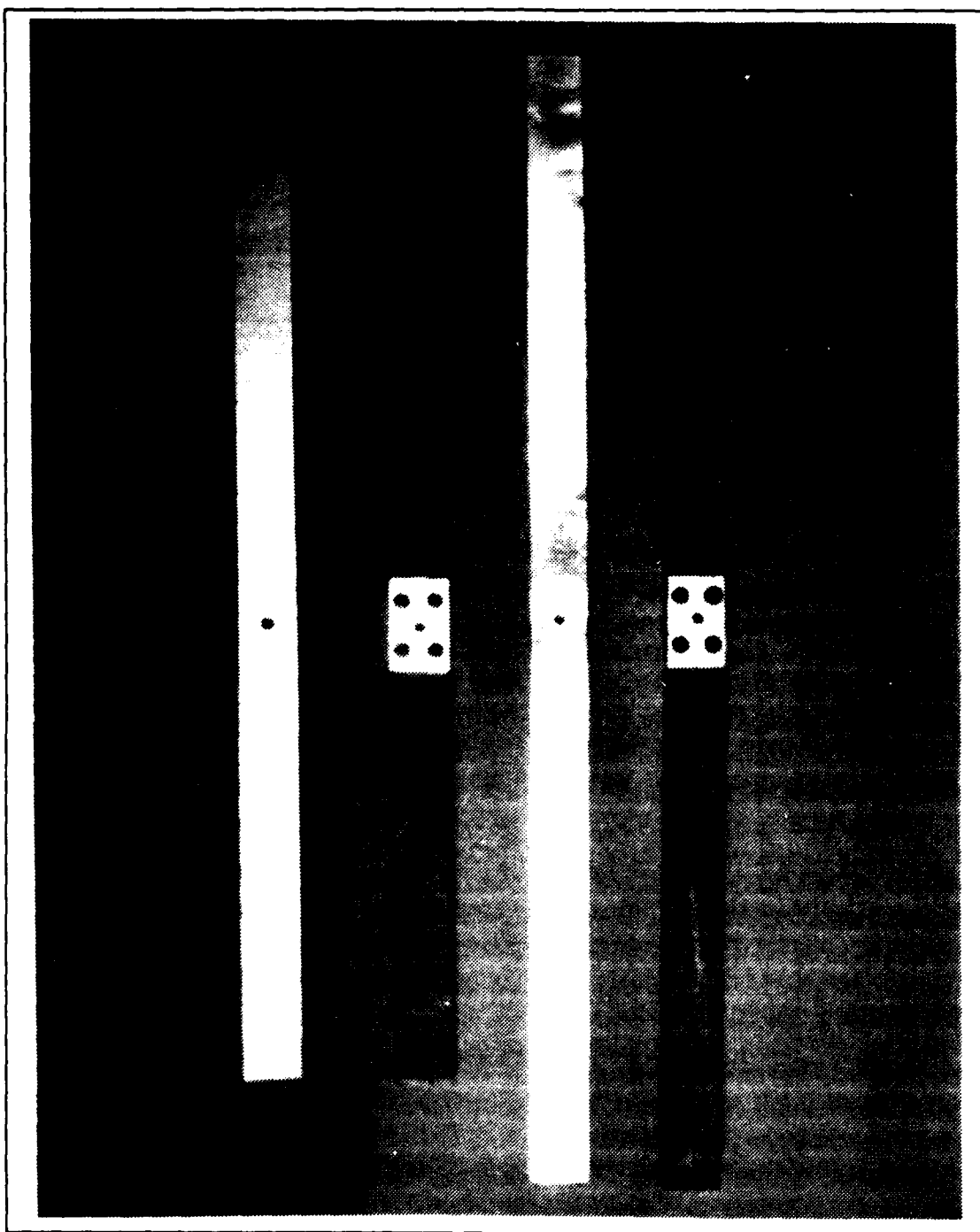


Figure 6. Viscoelastic and constrained layer beam waveguide absorbers.

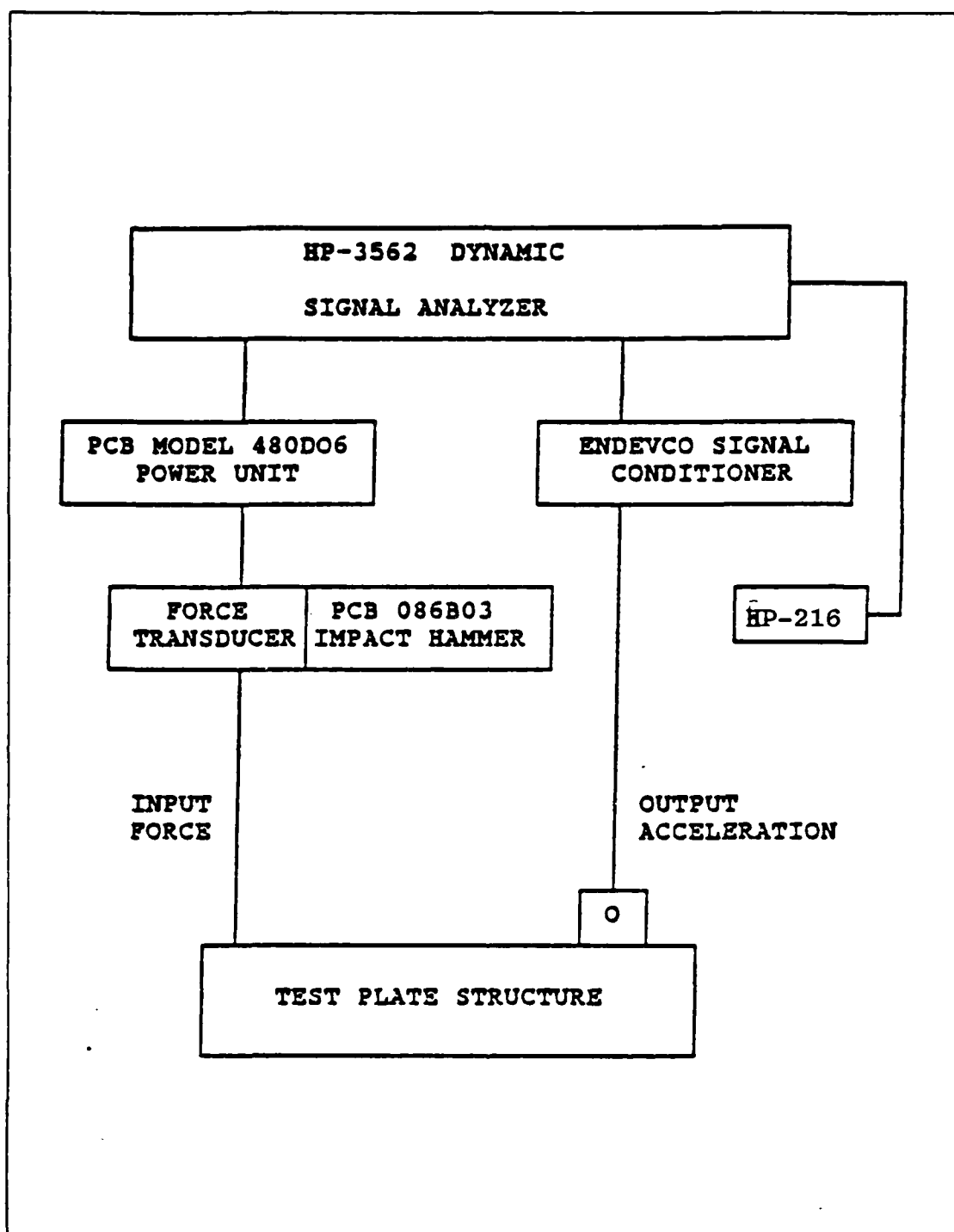


Figure 7. Modal survey test equipment arrangement.

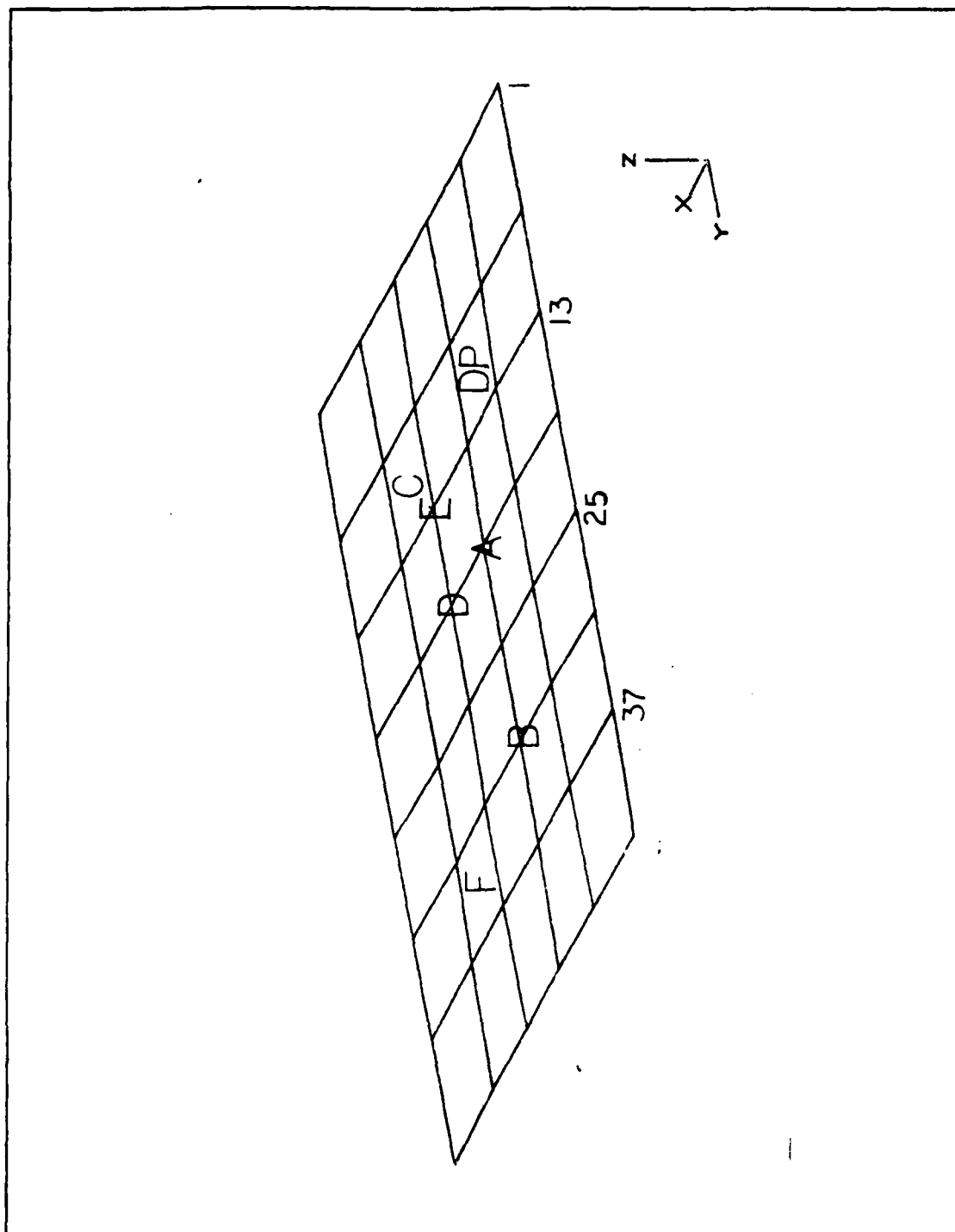


Figure 8. Modal survey undeformed shape and grid structure.

during this section of the investigation is shown in Figure 9. The input force was provided by a Wilcoxon Research F3 Vibration Generator mounted at grid point 21 (driving point). The vibration generator utilized a combination electromechanical and piezoelectric power amplifier which provided a controllable force output for the range of 10 to 15,000 Hz. An HP 3562A Dynamic Signal Analyzer provided a random noise control signal to the power amplifier. A force transducer and response accelerometer were mounted at the base of the vibration generator to measure the input excitation force and response signals. The input and output signals were amplified by a charge amplifier and fed into channel one and two, respectively, of the HP 3562A.

All structural measurements were performed with the HP 3562A Dynamic Signal Analyzer using 50 averages at each data point. The selection of the number of averages was based on providing good coherence for all measurements. The HP 3562A sampled, digitized, and filtered the analog input signals. With this data, the analyzer calculated the frequency response and coherence functions. These measurements were displayed, analyzed and saved for further comparisons.

3. Plate Impedance

The testing equipment arrangement used to determine the plate impedances was the same as shown in Figure 7 with the following exception. The locations A, B and C on the test plate were excited ten times and averaged. The input force and response signals were sampled, digitized and filtered by the HP3562A Dynamic Signal Analyzer. With this data, the analyzer calculated the impedances of the test plate locations. These measurements were displayed and saved for further comparisons.

C. GENERAL TEST PLAN

The experimentation was divided into five areas. First, a modal survey was conducted to determine the structural mode shapes and resonant frequencies. The modal survey was used to verify the theoretically predicted mode shapes and natural frequencies as well as determine the attachment points for the beam waveguide absorbers. In the second phase, the baseline frequency response function was determined for the plate without a waveguide absorber attached. Then, each type of beam waveguide absorber was attached to the test plate at: location A; locations A and B; and locations A, B and C. The waveguide absorbers during this phase were aligned parallel to the X axis. Frequency response measurements were performed at each step over the 2000 Hz frequency range to compare with the baseline frequency response. Based on these comparisons, the beam waveguide absorber which had the most pronounced effect

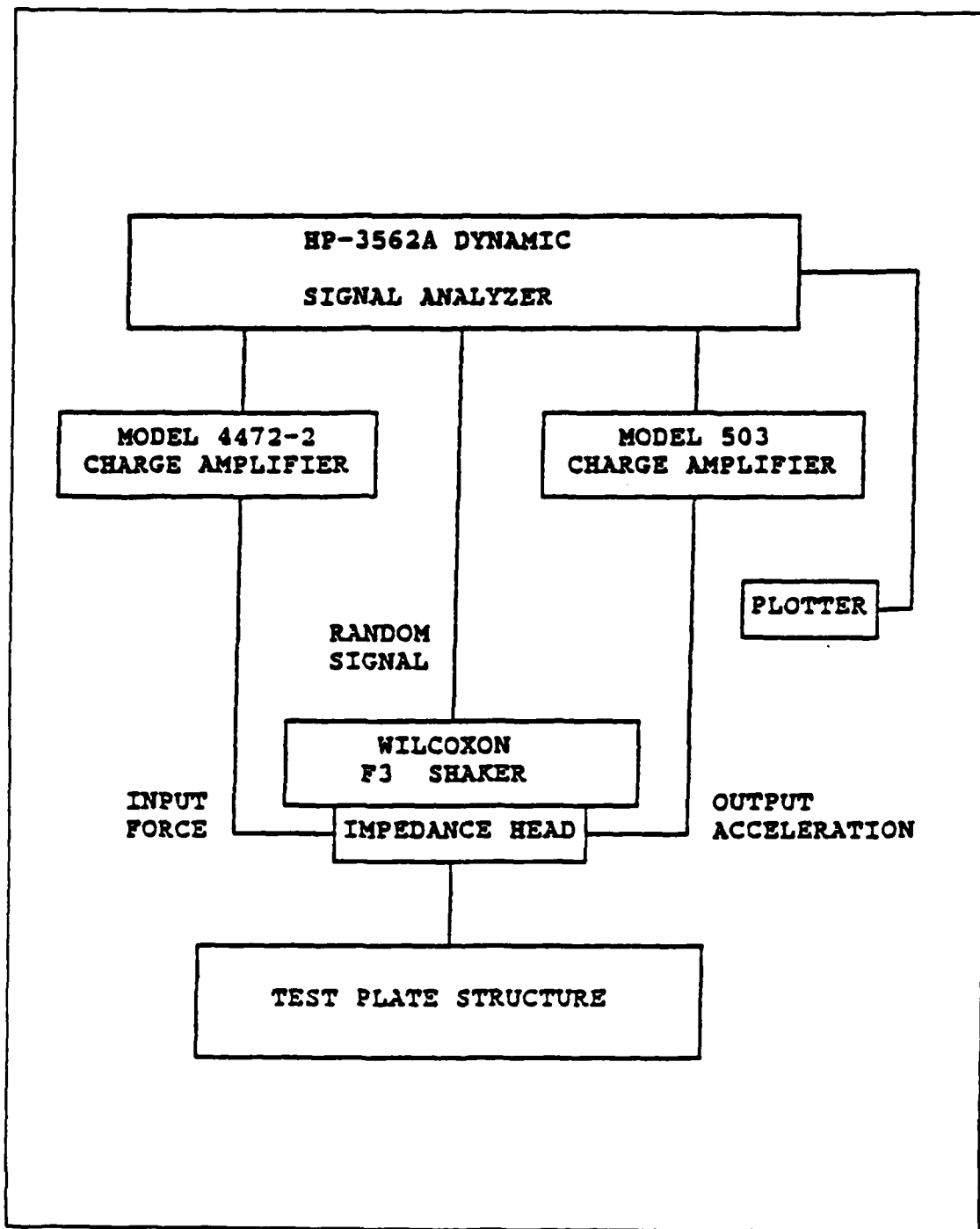


Figure 9. Equipment arrangement for the test plate frequency response measurements (with beam waveguide absorbers attached).

on the baseline frequency response was used in phases three and four. This beam waveguide absorber was later determined to be the 20 inch viscoelastic. The third phase studied the effects of attaching the most effective beam waveguide absorber at all the locations (A through F) of Figure 1. The fourth phase examined the effects of changing the orientation of the beam waveguide absorber. The final phase determined the impedances of the test plate at locations A, B and C. The impedances of each location and beam waveguide absorber were compared to explain the results of phase three and to understand the concept of impedance matching. The impedance values for each waveguide absorber was taken from Lee's experimental results [Ref. 5].

V. RESULTS

A. COMPARISONS

1. Theoretical and Experimental

The theoretically predicted modal frequencies are approximately 50 Hz higher than those determined by the modal survey with three exceptions. Three modal frequencies were not predicted by the finite element program, which were indicated by the modal survey. At 195 Hz, as shown in Figure 10, a twisting of the test model's outer corners is clearly visible while no deformation occurs at the center. Similar twisting of the test model occurs for the 338 and 499 Hz modes as shown in Figure 41 and Figure 43 of Appendix B. However, this twisting effect occurs along the model's edges vice corners. The twisting of the model is indicative of the test plate not having a "true" clamped boundary condition. Therefore, the test plate experiences the modified effects of having free boundaries. This would also explain why the predicted modal frequencies are slightly higher. The finite element program bases its predictions on the test plate having a clamped boundary condition. Since mechanical systems do not exhibit a true clamped boundary, an exact match between predicted and actual modal frequencies is not expected.

2. Viscoelastic and Constrained Layer

The frequency response functions for the test plate with waveguide absorbers attached at locations A, B and C are shown in Figure 11 and Figure 12. The solid lines for both figures represents the driving point (DP) baseline frequency response without waveguide absorbers attached. The dashed line of Figure 11 represents the frequency response function when a 20 inch viscoelastic beam waveguide absorber is attached at locations A, B and C, while the dashed line of Figure 12 represents a 20 inch constrained layer beam waveguide absorber at the same locations. In comparing Figure 11 and Figure 12, the frequency response amplitudes decreased for both beams in all the modes except at the 195 Hz mode. By examining the 195 Hz mode shape in Figure 10, attaching a waveguide near the corner of the test model would have affected this mode. Frequency shifts, upward in nature from the baseline, are clearly visible for the modal frequencies above 1500 Hz. Similar but opposite, frequency shifts occurred for modal frequencies below 1500 Hz. The frequency shifts result from the addition of the waveguide absorber which alters the mass, damping and stiffness matrices of the test

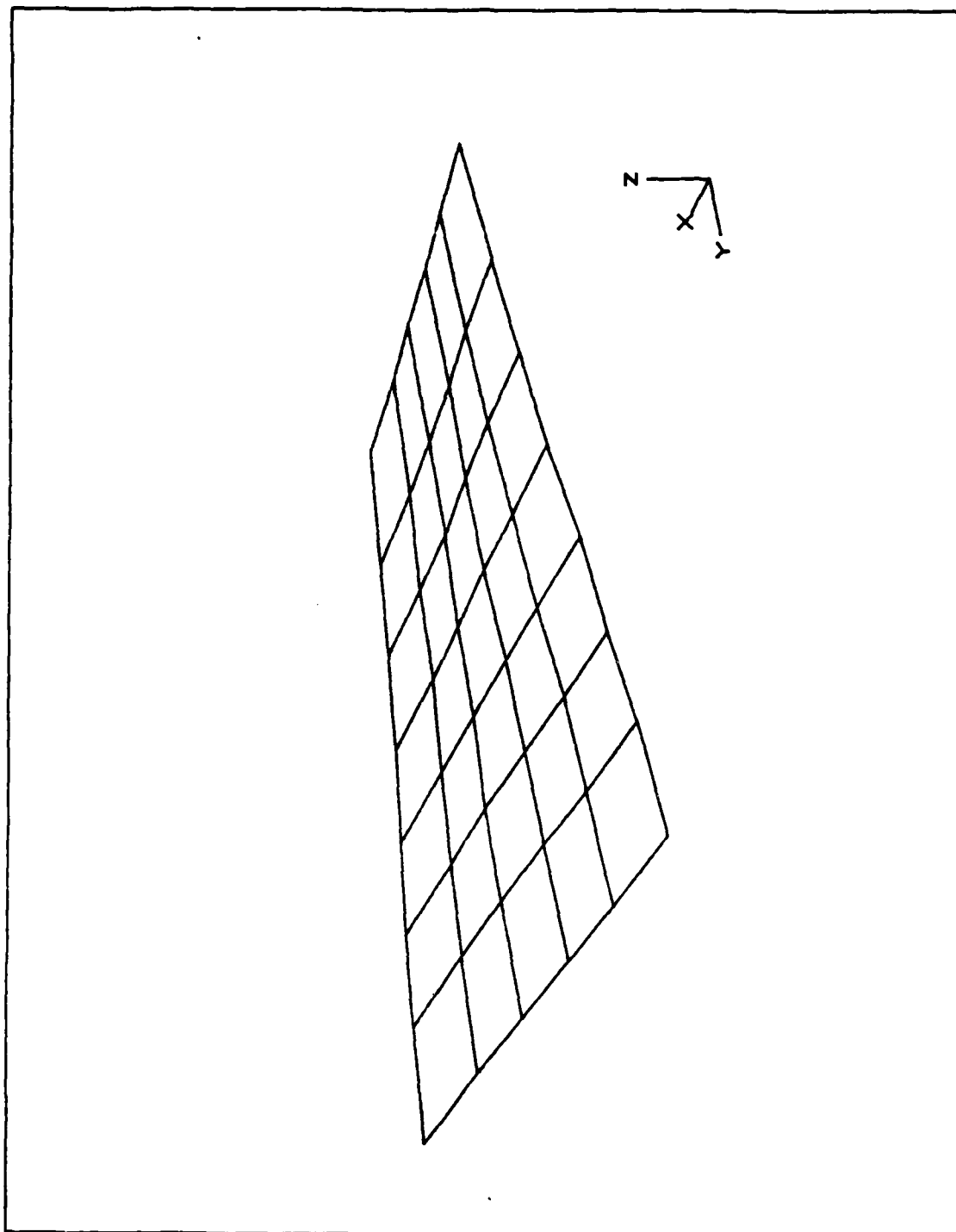


Figure 10. Modal survey perspective view - mode #1 (195.76 Hz).

plate. The viscoelastic beam had a more pronounced effect in decreasing the frequency response amplitudes. The viscoelastic material is a high damping material, whereas, the damping mechanism for the constrained layer beam is in the shear action between the constrained layers. The most significant decrease in frequency response amplitude occurred between 1300 and 1700 Hz of Figure 11. The response amplitude at 1400 Hz decreased by almost 12 decibels (dB). By examining the mode shapes for the frequency range as shown in Figure 22 through Figure 25 of Appendix A, all three locations contributed in decreasing the frequency response amplitudes as shown in the figures. At least two of locations were near or at points of maximum modal deformation. If the impedance matching concept were examined, the viscoelastic beam tends to more closely match the plate's impedance at each of the locations as shown in Figure 61 through Figure 67 of Appendix C.

Similar results are observed when a 16 inch constrained layer or viscoelastic beam waveguide absorber is attached at the same locations as shown in Figure 53 and Figure 60 of Appendix C. The decreases in the frequency response amplitudes and modal frequency shifts are less, with the shorter beam waveguide absorbers being more effective at higher frequencies.

B. ORIENTATION

The frequency response functions for the test plate with a 20 inch viscoelastic beam waveguide absorber attached at locations A, B and C are shown in Figure 13 and Figure 14. The solid line for both figures represents the baseline driving point (DP) frequency response. The dashed line of Figure 13 represents the frequency response when the three 20 inch viscoelastic beam waveguide absorbers are attached at locations A, B and C and aligned parallel to the *X* axis. The dashed line of Figure 14 represents alignment of the waveguide absorbers parallel to the *Y* axis. In comparing the two figures both orientations decreased the frequency response amplitudes for all modes when compared with the baseline except for the 195 Hz mode. The trend in frequency shifts are similar to those stated in Section 5.A.2. The *X* axis alignment has a more pronounced effect on the frequency response amplitudes for the modes above 900 Hz. Very little difference is noted between each orientation for the modes below 900 Hz. The important aspect to consider is how much effect does torsional waves have when the orientation of the waveguide absorber is changed. For the modes above 900 Hz, a measured change in the mode shapes occurs, indicating a significant increase in modal damping. This change in mode shape is more pronounced when the waveguide is aligned

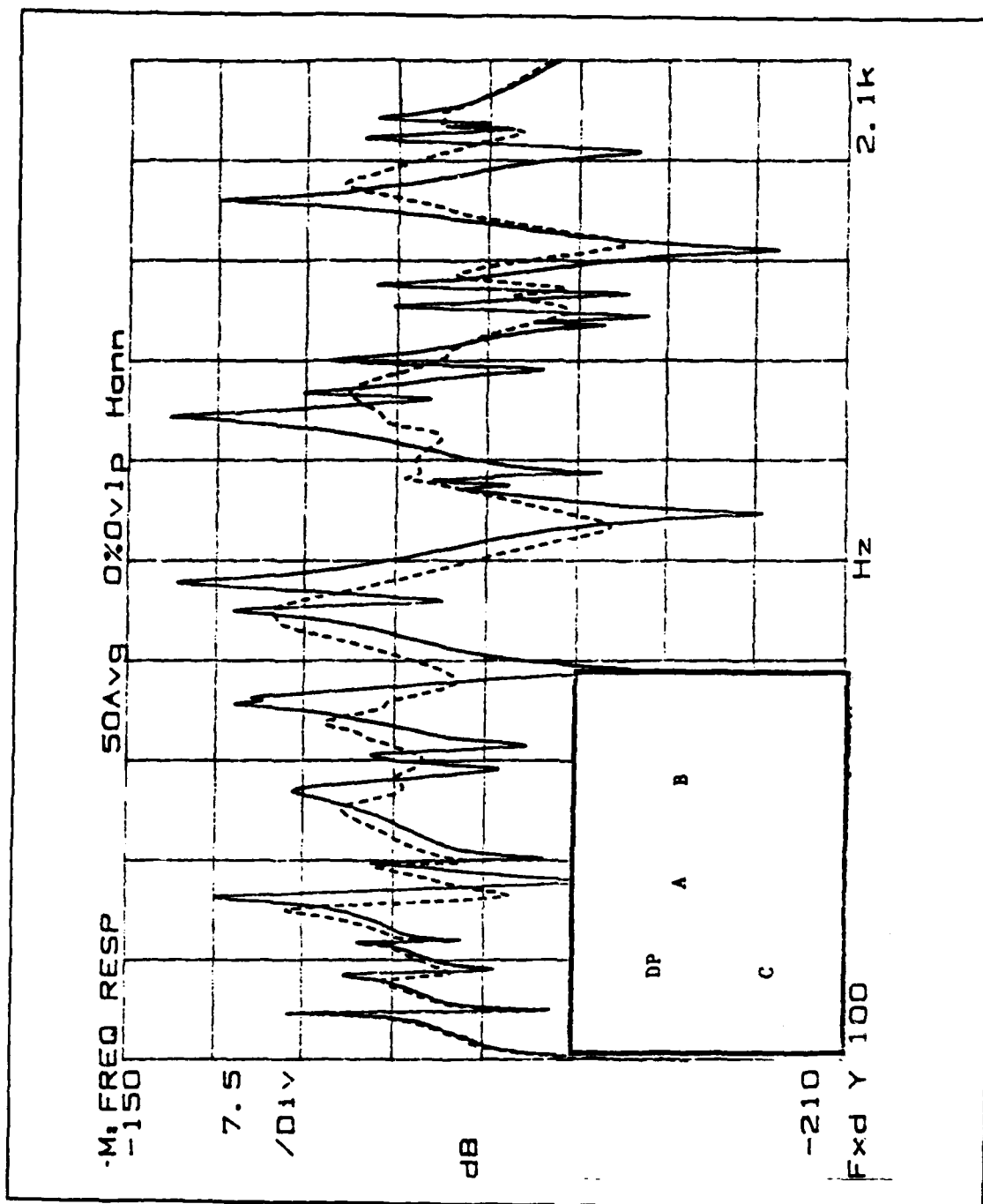


Figure 11. Baseline (DP) frequency response (solid); with a 20" viscoelastic waveguide (dashed) at locations A, B and C. Locations identified on insert.

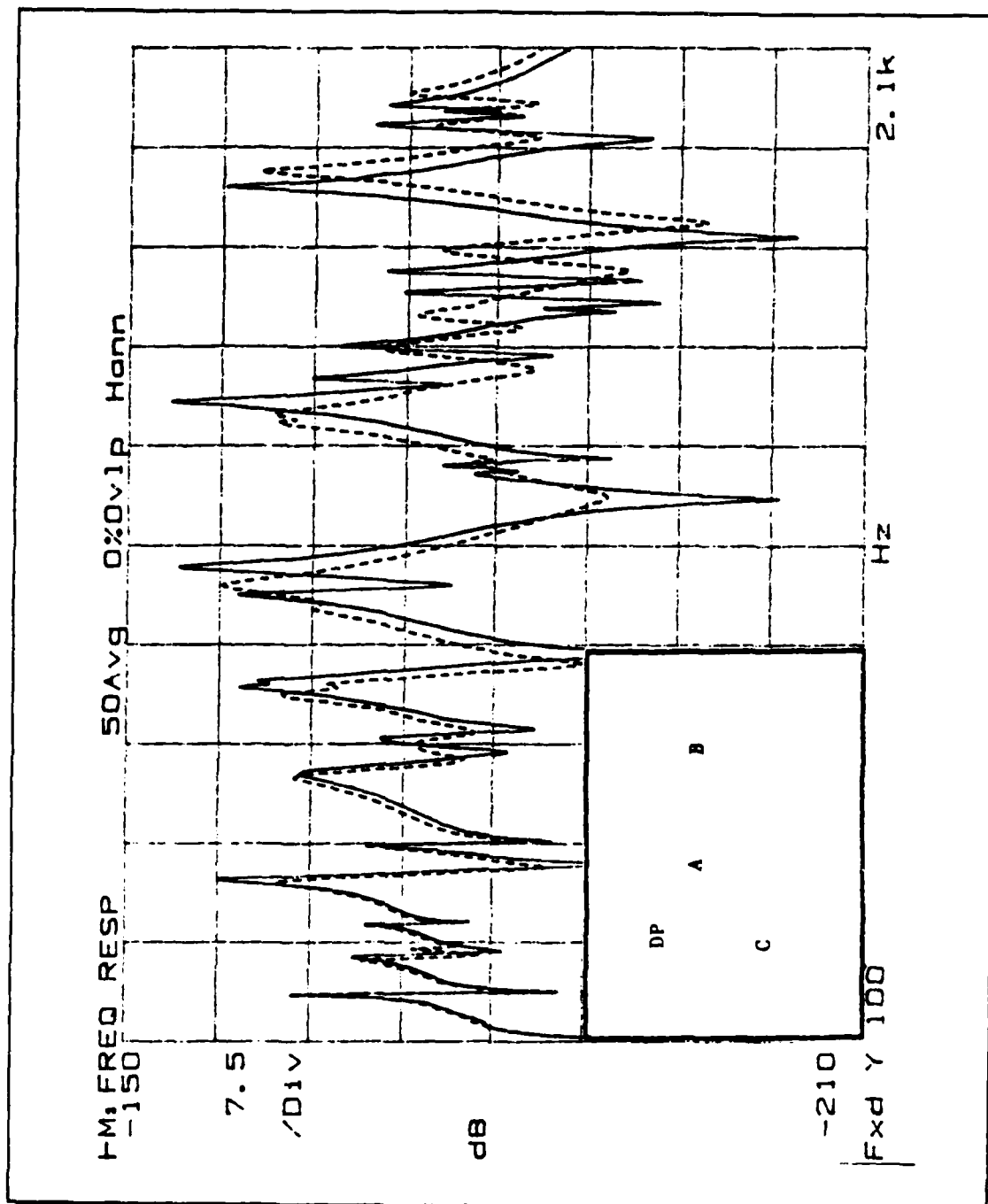


Figure 12. Baseline (DP) frequency response (solid); with a 20" constrained layer waveguide (dashed) at locations A, B and C. Locations shown in insert.

along the X axis. A possible explanation is that when aligned along the X axis the waveguide absorbers take more advantage of both torsional and flexural waves in dissipating the vibration energy. Examining the mode shapes for this frequency range, as shown in Figure 20 through Figure 27 of Appendix A, in each mode at least one of the waveguide absorbers experiences both torsion and bending when aligned parallel to the X axis. When aligned parallel to the Y axis, the waveguide absorbers predominately experience bending. Again, this effect seems mode dependent. Below 900 Hz, the beam waveguide absorbers will predominately experience bending with torsion having very little effect.

C. MULTIPLE WAVEGUIDE ABSORBERS

The frequency response functions of the test plate with a 20 inch viscoelastic waveguide attached at all six locations are shown in Figure 15. The solid line represents the driving point (DP) baseline frequency response, while the dashed line represents the frequency response with a viscoelastic waveguide absorber attached at locations A through F. The frequency response amplitudes show a drastic reduction for all modes except the 195 Hz mode. The response between 500 and 900 Hz is almost flat. Within this range the change in amplitude between resonant peaks and anti-resonant valleys is less than six dB, while the baseline's change in amplitude is over 25 dB. Likewise, significant changes in mode shape occurs between 1200 and 1600 Hz where the change in response amplitude is less than 10 dB; the baseline - approximately 30 dB. The most notable reduction of the frequency response amplitudes occurs within this range. At 1400 Hz, the response amplitude decreases by almost 20 dB.

With six 20 inch viscoelastic waveguide absorbers attached to the test plate, the changes in the response matrices are even more pronounced. Therefore, a significant change in mode shapes occur over the 2000 Hz frequency range. The 20 inch viscoelastic waveguide absorbers are aligned parallel to the X to take advantage of both torsional and flexural waves and again the impedances of the 20 inch viscoelastic beam waveguide absorber tends to more closely match the impedances of the attachment location.

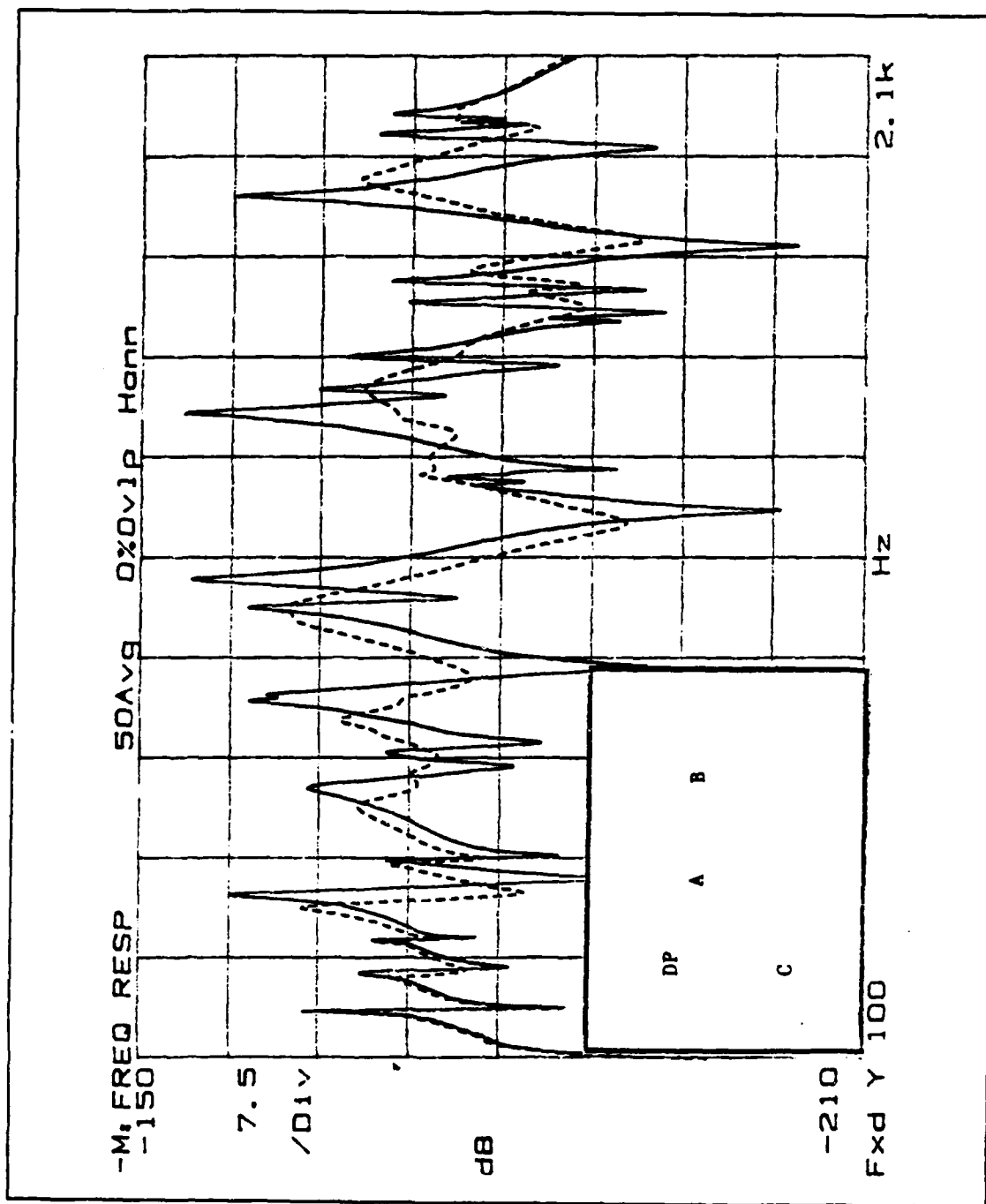


Figure 13. Baseline (DP) frequency response (solid); with a 20" viscoelastic waveguide parallel to the X axis (dashed) and attached at locations A, B and C. Locations indicated in insert.

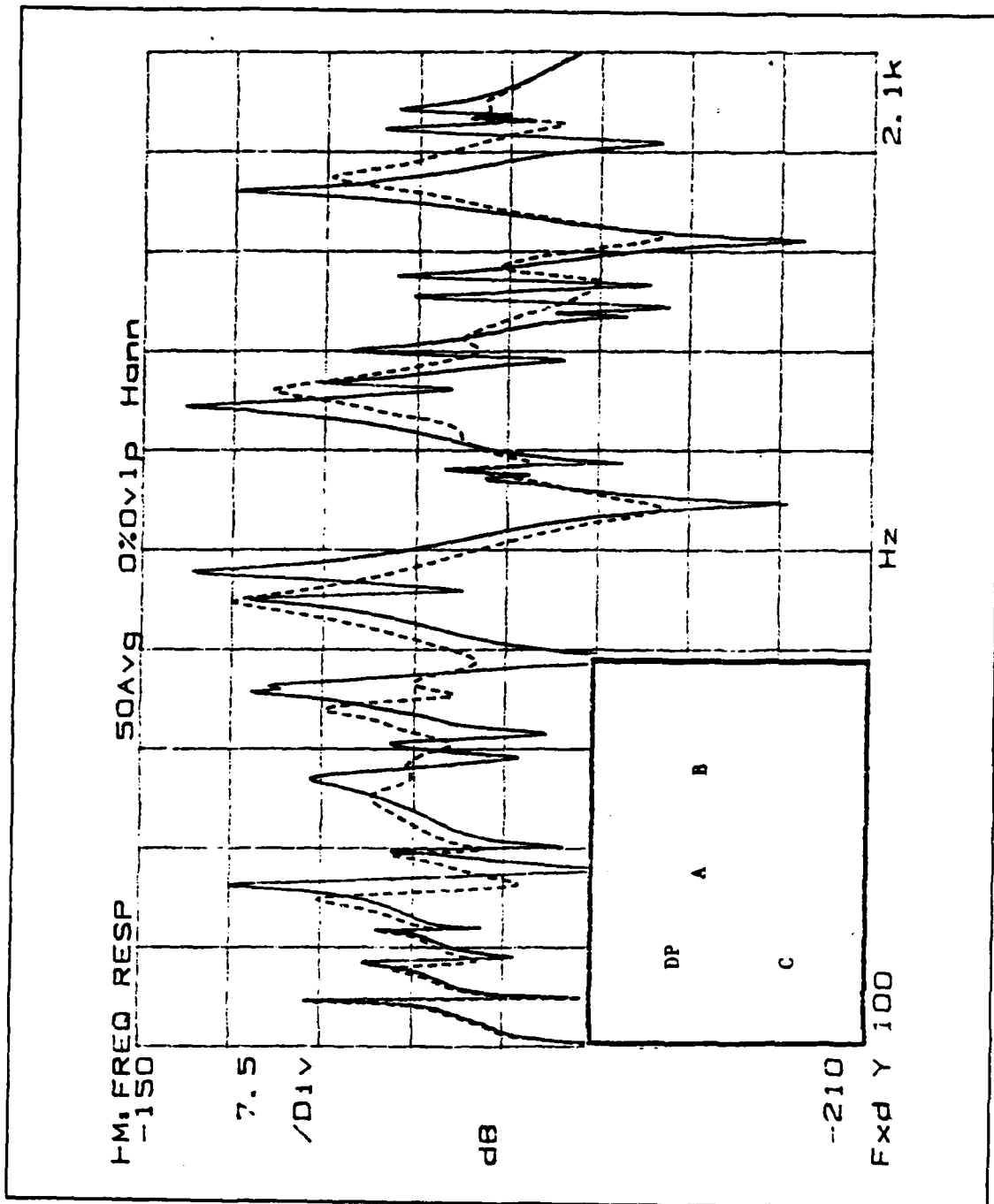


Figure 14. Baseline (DP) frequency response (solid); with a 20" viscoelastic waveguide parallel to the Y axis (dashed) and attached at locations A, B, and C. Locations indicated in insert.

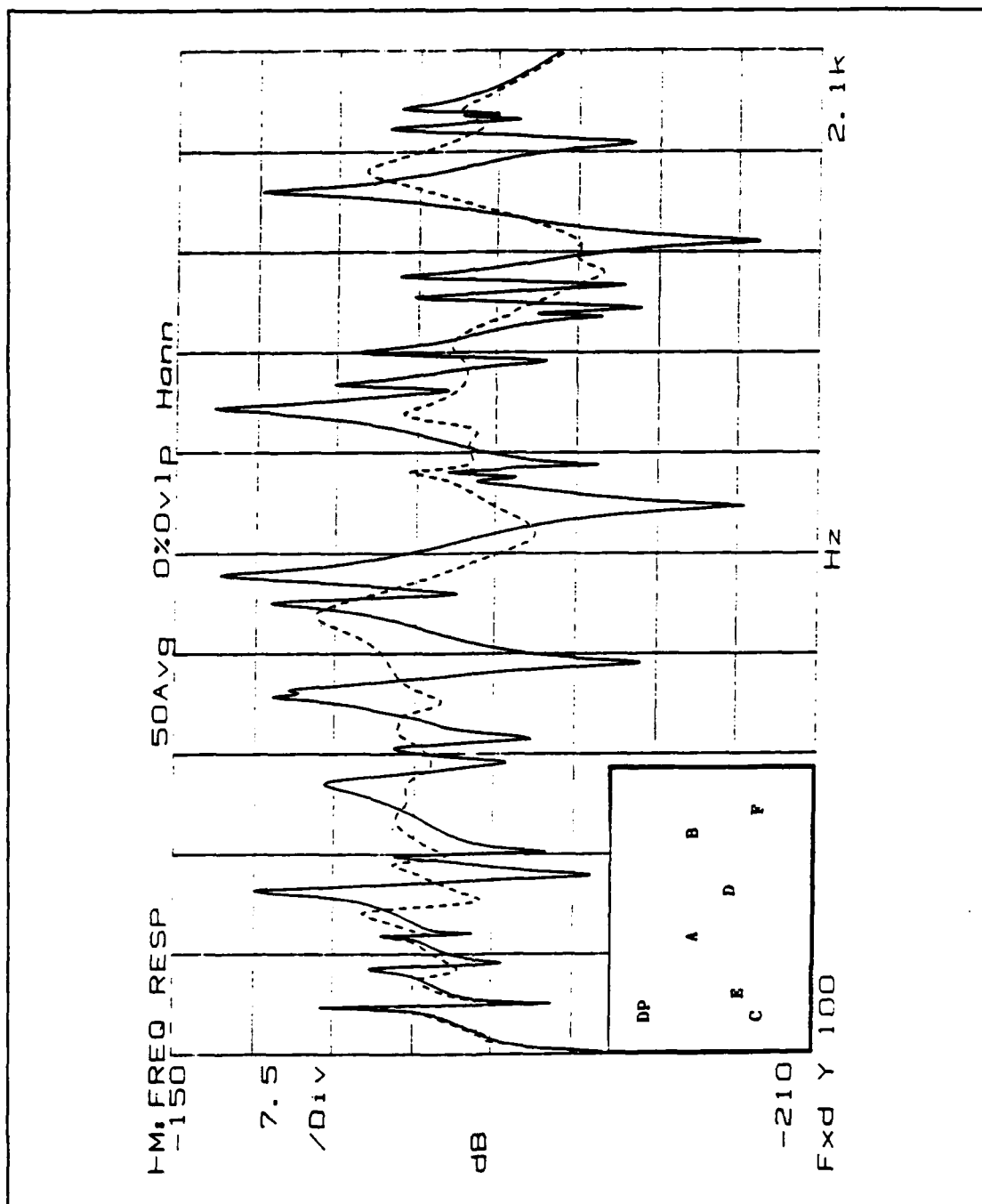


Figure 15. Baseline (DP) frequency response (solid); with a 20° viscoelastic waveguide absorber attached at locations A - F (dashed).

VI. CONCLUSIONS

The purpose of this investigation was to examine the effects of the location, number and orientation of light weight, multiple waveguide absorbers in reducing the driving point frequency response amplitude over a broad frequency range. Several theoretical concepts are still not fully understood. The reduction of the frequency response amplitudes is a direct result of the interaction between the waveguide absorber and the test plate at the attachment point. As previously discussed, this interaction affects both the attachment point velocity and the average spatial velocity of the test plate. Trying to predict this interaction in equation form is quite difficult. By using a finite element approach, however this task can be accomplished.

The NASTRAN finite element analysis program was used to calculate the test plate's modal frequencies and shapes. The predicted modal frequencies were higher than those determined experimentally. The difference between the predicted and actual modal frequencies was due to the the boundary conditions of the test plate. The plate's boundary conditions did not exhibit a "true" clamped condition. With this, the test plate's stiffness was less than theoretically predicted, causing lower modal frequencies. This condition did not affect the quantitative results.

The viscoelastic waveguide absorber was more effective than the constrained layer. The longer waveguides generally were more effective at lower frequencies, while the shorter waveguide was more effective at higher frequencies. At lower frequencies, the shift in modal frequency was effected more by the mass addition of the waveguide absorber, whereas at higher frequencies, the effects from the imaginary part of the waveguide absorber's impedance caused the upward shift of the modal frequencies. The increase in structural damping was mode dependent. Those modes which had significant increases in structural damping, were affected by all three factors; location, number and orientation. Modal damping was increased when the waveguide absorber's location coincided with the mode's area of highest strain energy, when all of the waveguide absorbers attached to the structure contributed to the increase in modal damping, or if the waveguide absorber's orientation took both torsional and flexural effects into account. With each addition of a waveguide absorber, the effect was more than just additive. The waveguide absorber was interacting with a structure that was more highly damped.

Using multiple beam waveguide absorbers to increase structural damping is highly effective only if an optimization approach is used. More than just the location, number and orientation should be optimized. The waveguide absorber's design must be included within this approach. However, before the optimization approach can be attempted, a better theoretical understanding of the interaction between the waveguide absorbers and the test plate at the attachment point is in order.

VII. RECOMMENDATIONS

The interaction between the waveguide absorber and the structure at the attachment point is complex. It is difficult to theoretically predict how this interaction effects the structural damping characteristics. It is known that the interaction is a function of the impedance of the waveguide absorber and the structure at the attachment point. The waveguide absorber alters the structure's mass, damping and stiffness matrices at the attachment point, therefore a finite element analysis approach can be effective in predicting the effects of the interaction and should be investigated.

For a waveguide absorber to be effective in increasing the structural damping over a desired frequency range, many complex factors are involved. A frequency response analysis of the structure must be performed to identify the frequency range of concern. Using a modal analysis package, the mode shapes of the structure can also be determined. Once the structure's motion and impedances are known, the waveguide absorber can be designed. This is probably the most difficult step, in that many variables have to be considered. Based on this investigation, a viscoelastic material should be chosen for the design. The physical properties of the waveguide absorber such as length and cross sectional area are determined by the structure's impedance and the frequency range of concern. Once the design is completed, the location, number and orientation of the beam waveguide absorber with respect to the structure is determined based on the mode shapes of the structure. To correlate this process, an optimization approach should be investigated to design the waveguide absorber and determine its location, number and orientation to effectively increase structural damping.

APPENDIX A.
THEORETICAL PERSPECTIVE VIEWS AND Z - PLANE DEFORMATION
CONTOURS

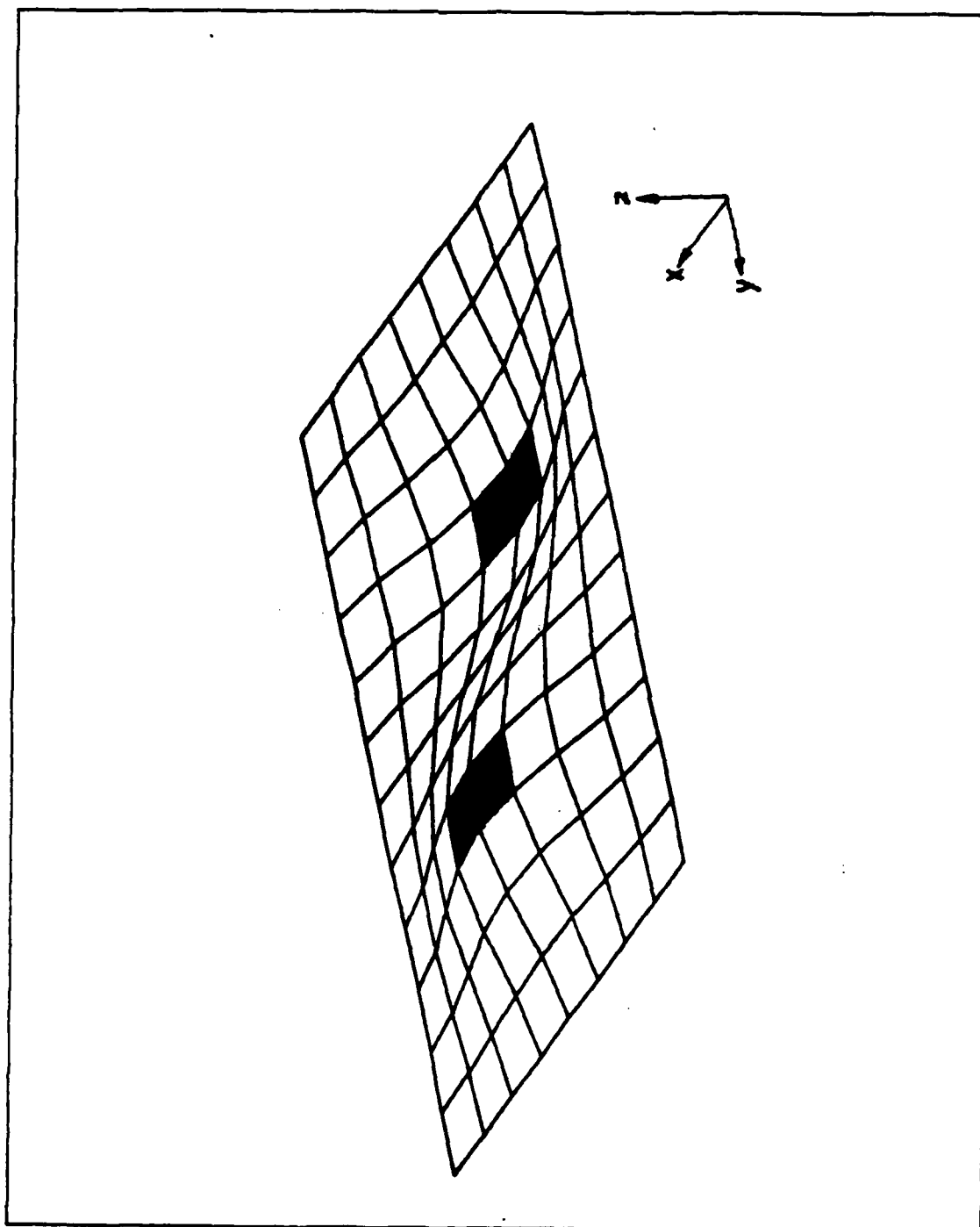


Figure 16. Theoretical perspective view - mode #2 (475.25 Hz): Shaded elements
- area of highest strain energy.

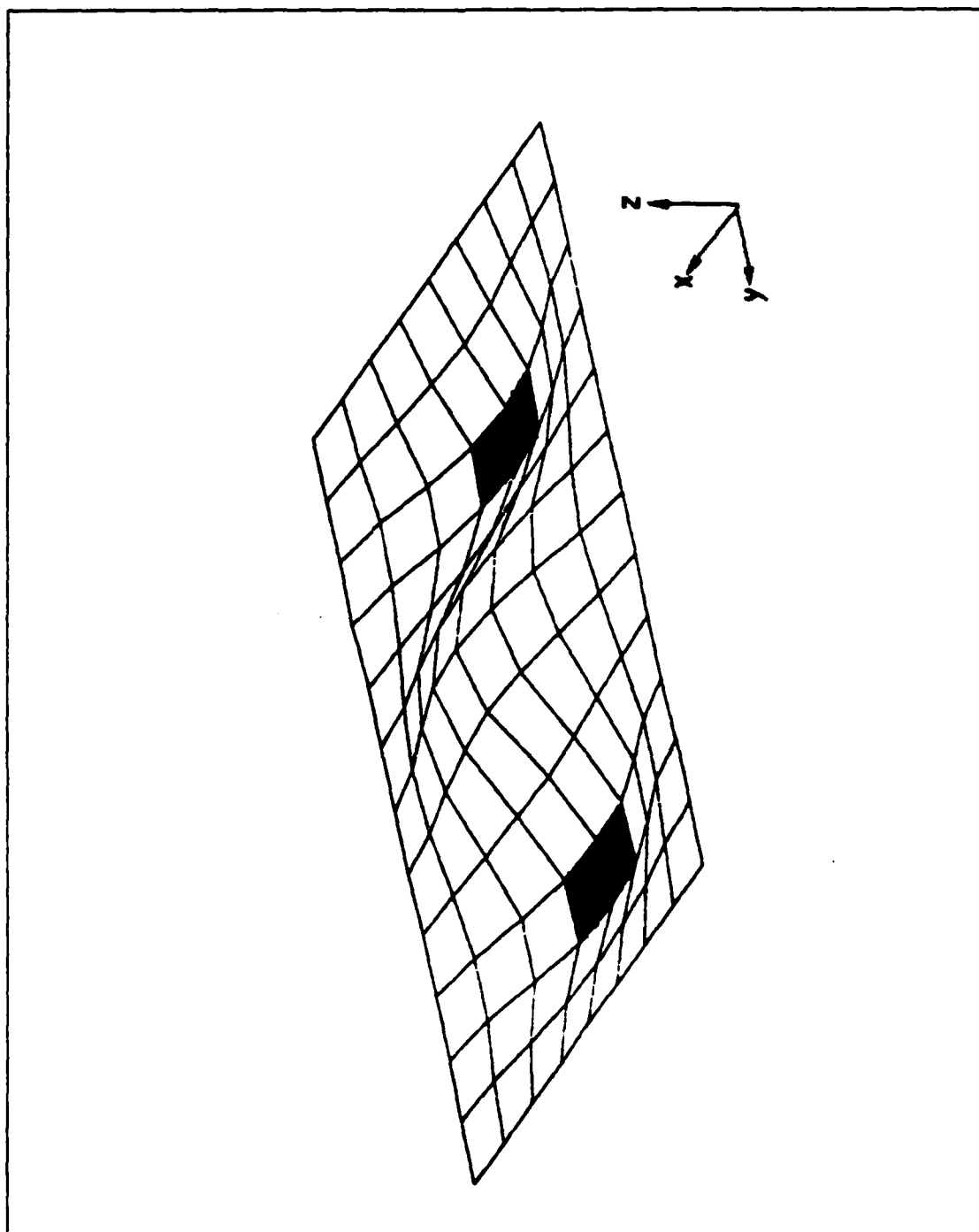


Figure 17. Theoretical perspective view - mode #3 (755.67 Hz): Shaded elements
- area of highest strain energy.

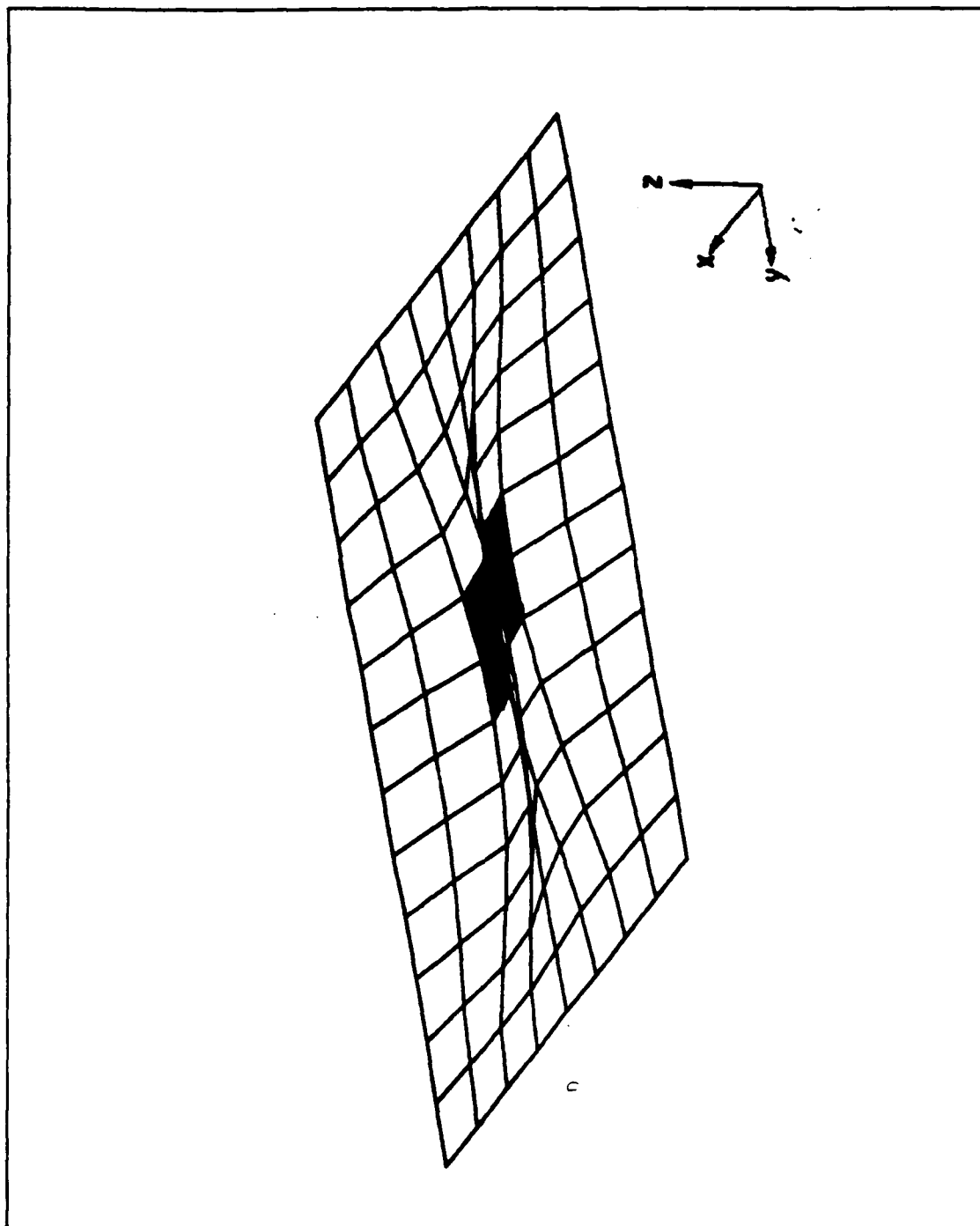


Figure 18. Theoretical perspective view - mode #4 (762.99 Hz): Shaded elements
- area of highest strain energy.

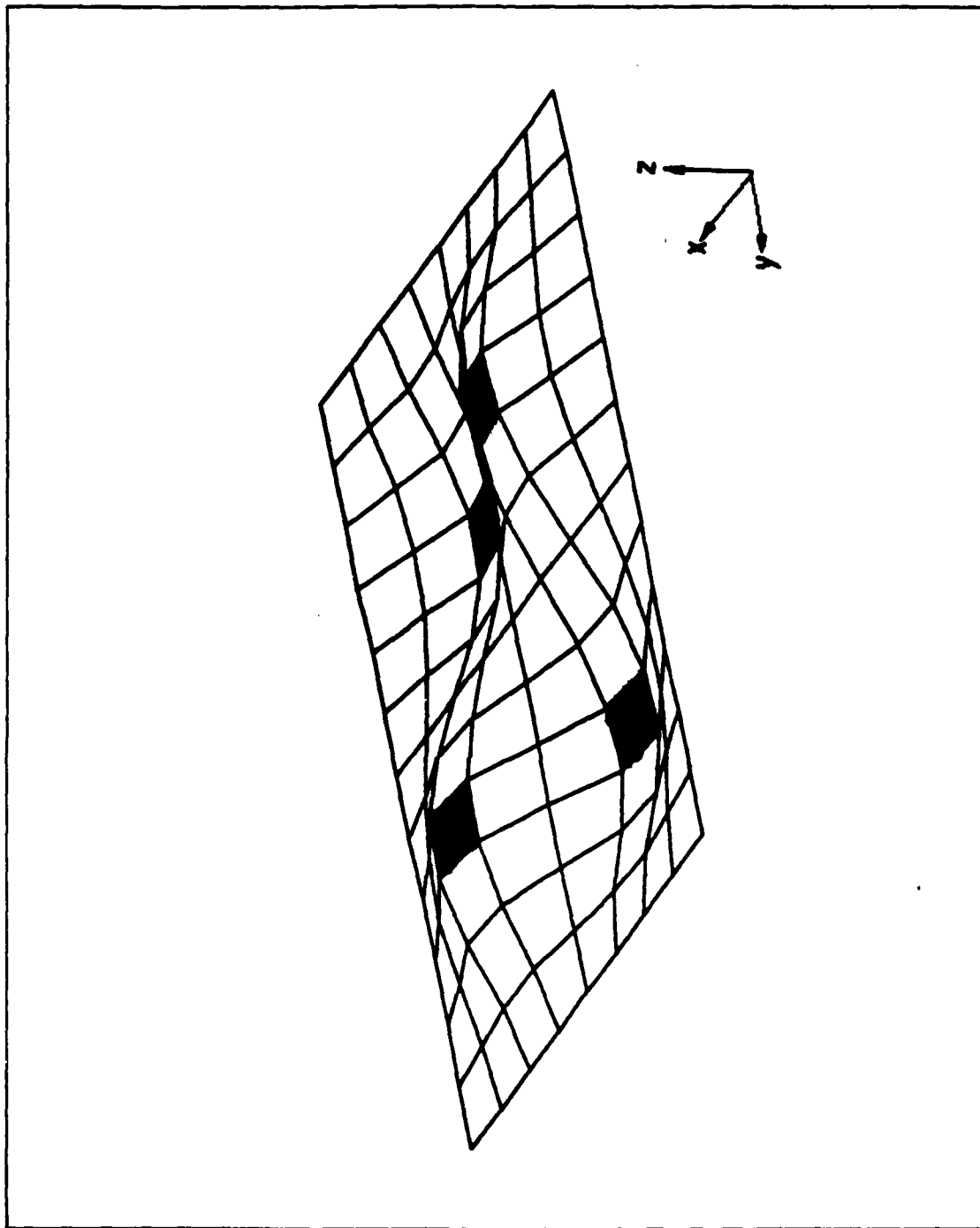


Figure 19. Theoretical perspective view - mode #5 (897.72 Hz): Shaded elements
- area of highest strain energy.

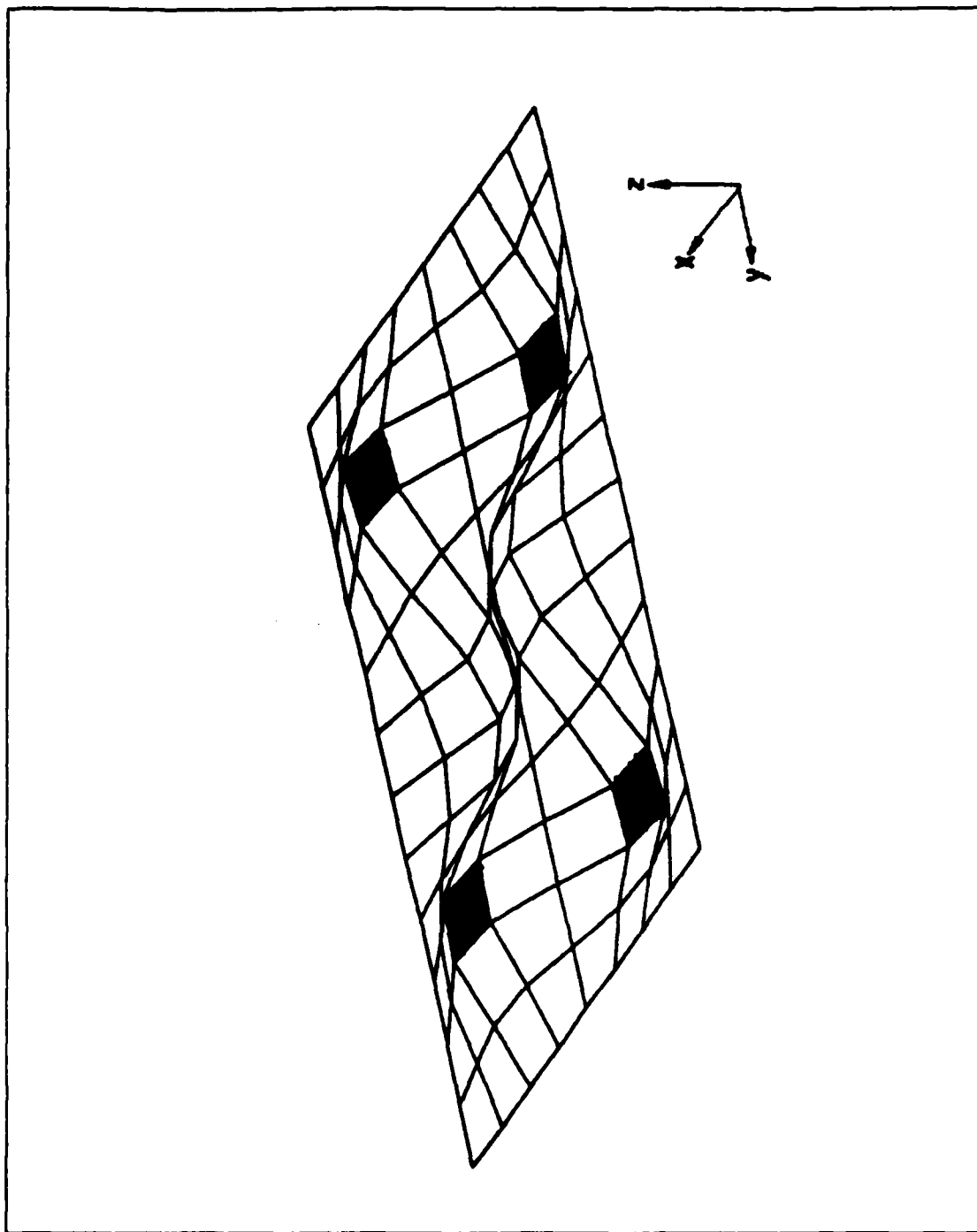


Figure 20. Theoretical perspective view - mode #6 (1136.16 Hz): Shaded elements - area of highest strain energy.

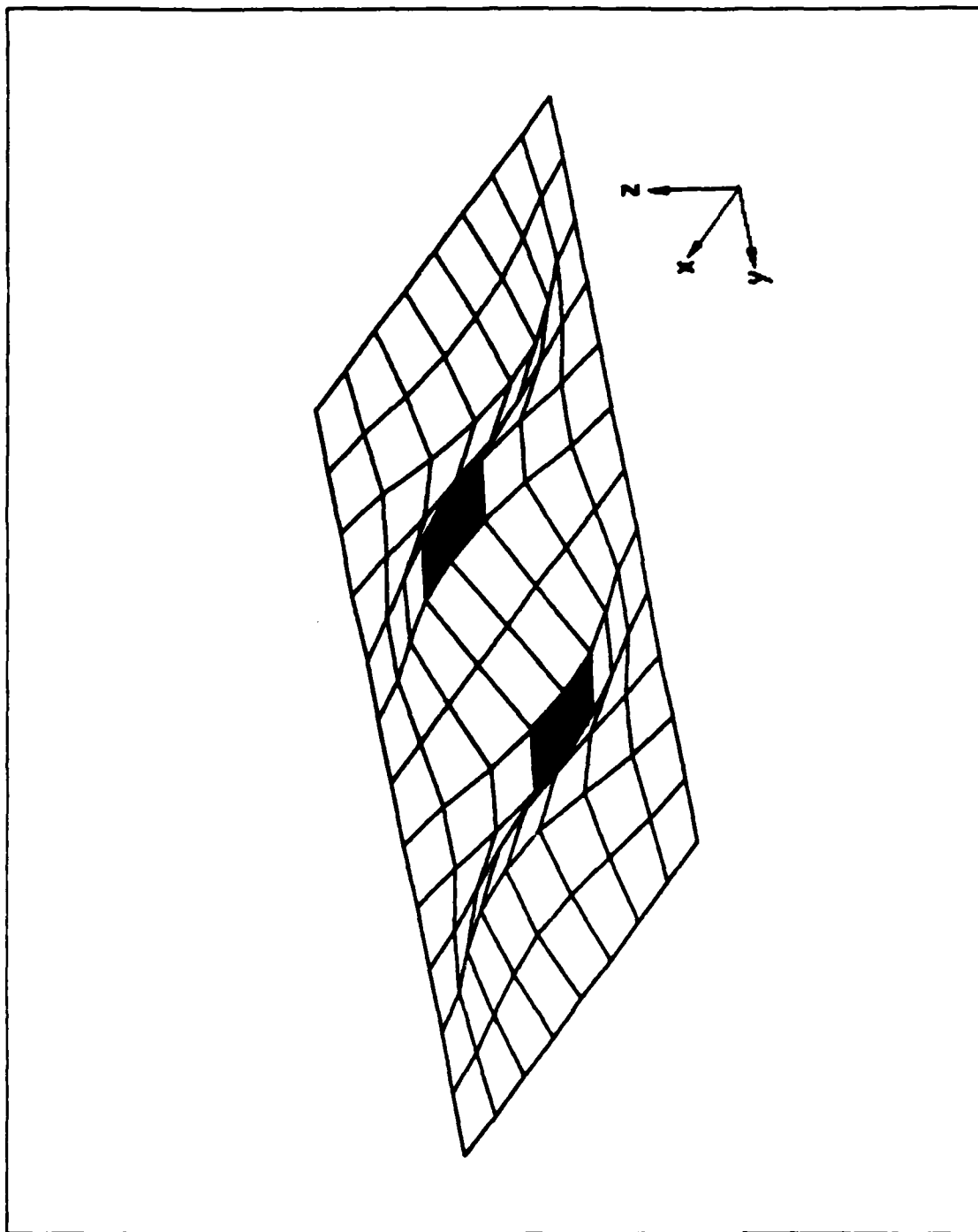


Figure 21. Theoretical perspective view - mode #7 (1145.22 Hz): Shaded elements - area of highest strain energy.

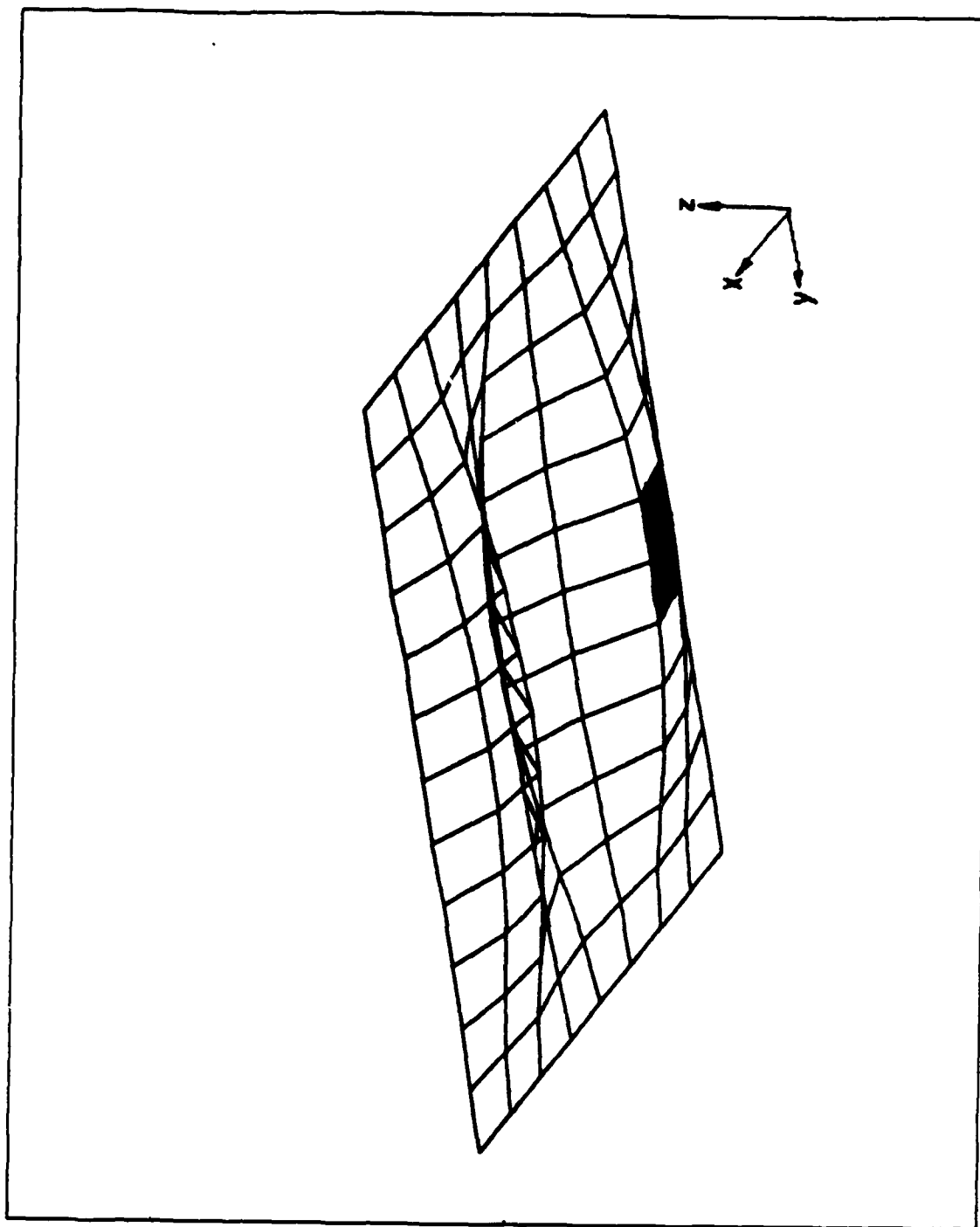


Figure 22. Theoretical perspective view - mode #8 (1438.39 Hz): Shaded elements - area of highest strain energy.

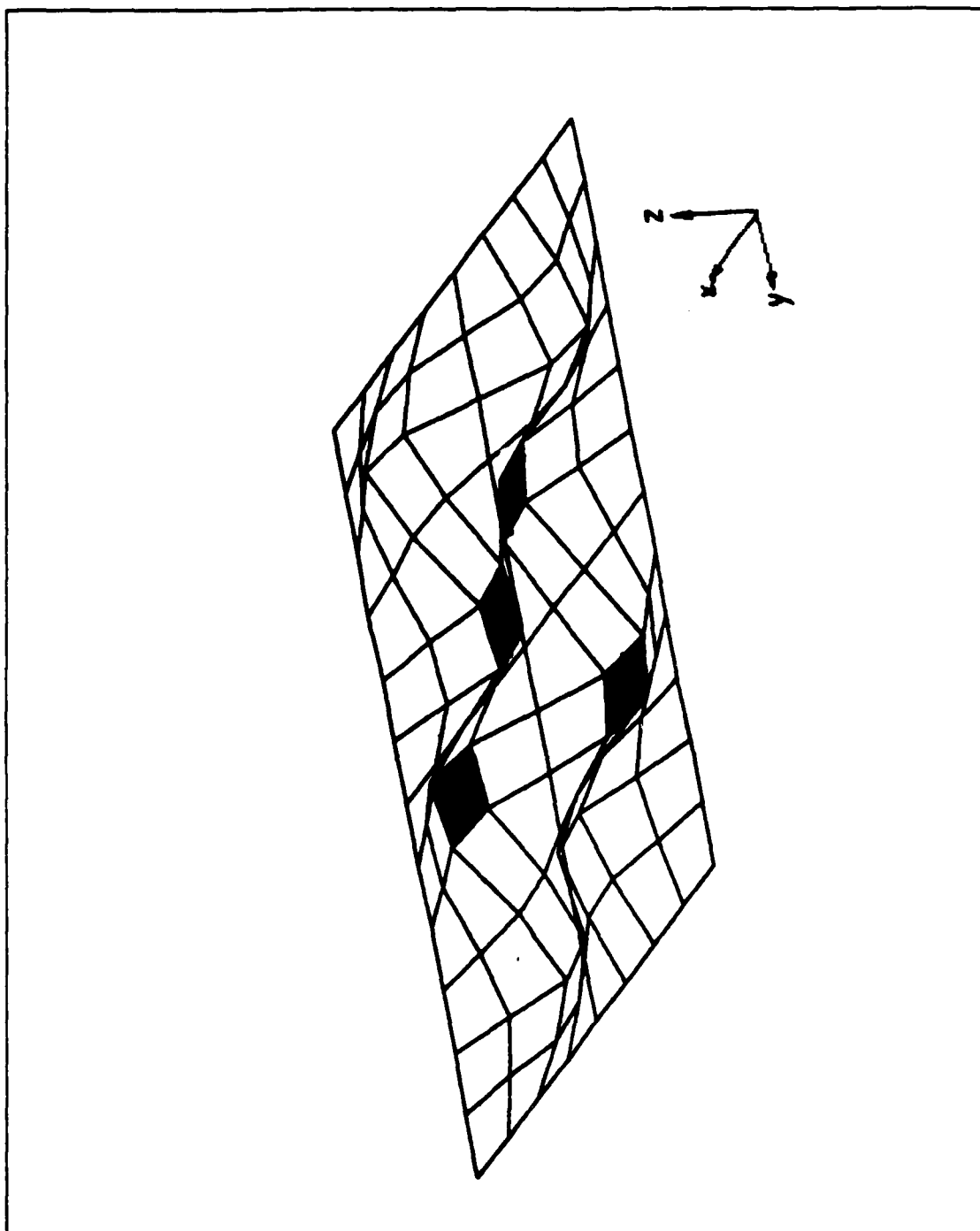


Figure 23. Theoretical perspective view - mode #9 (1484.84 Hz): Shaded elements - area of highest strain energy.

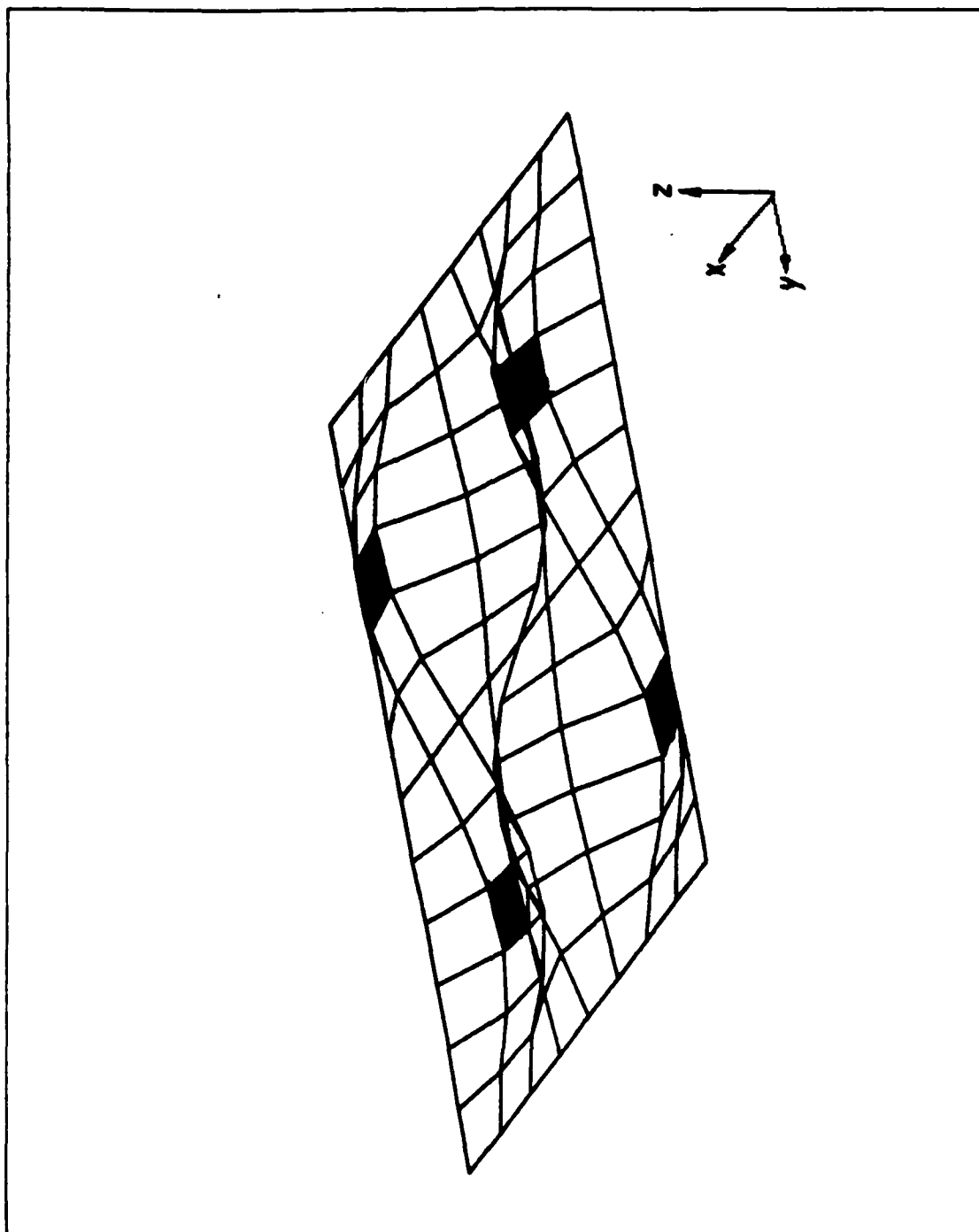


Figure 24. Theoretical perspective view - mode #10 (1558.78 Hz): Shaded elements - area of highest strain energy.

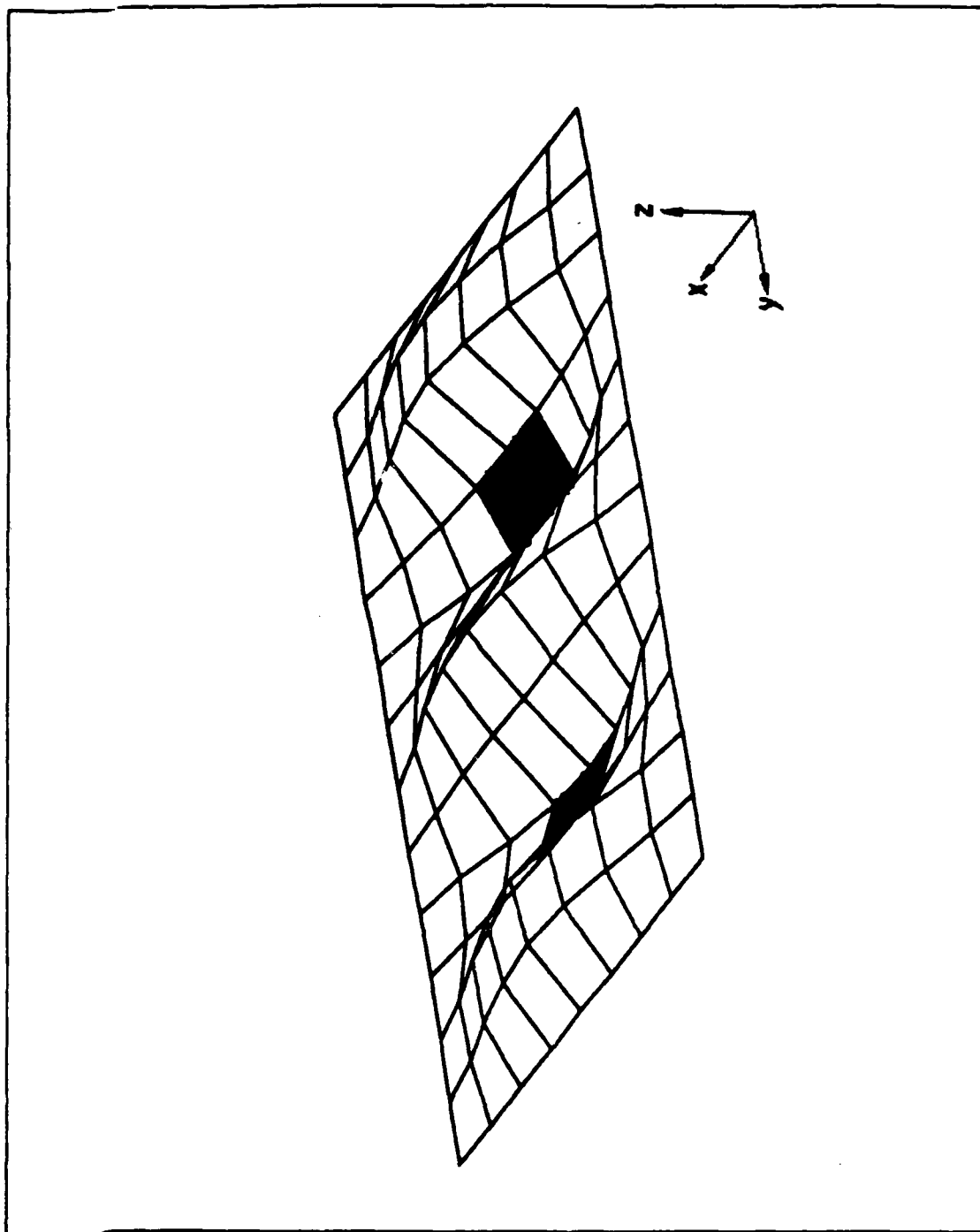


Figure 25. Theoretical perspective view - mode #11 (1636.15 Hz): Shaded elements - area of highest strain energy.

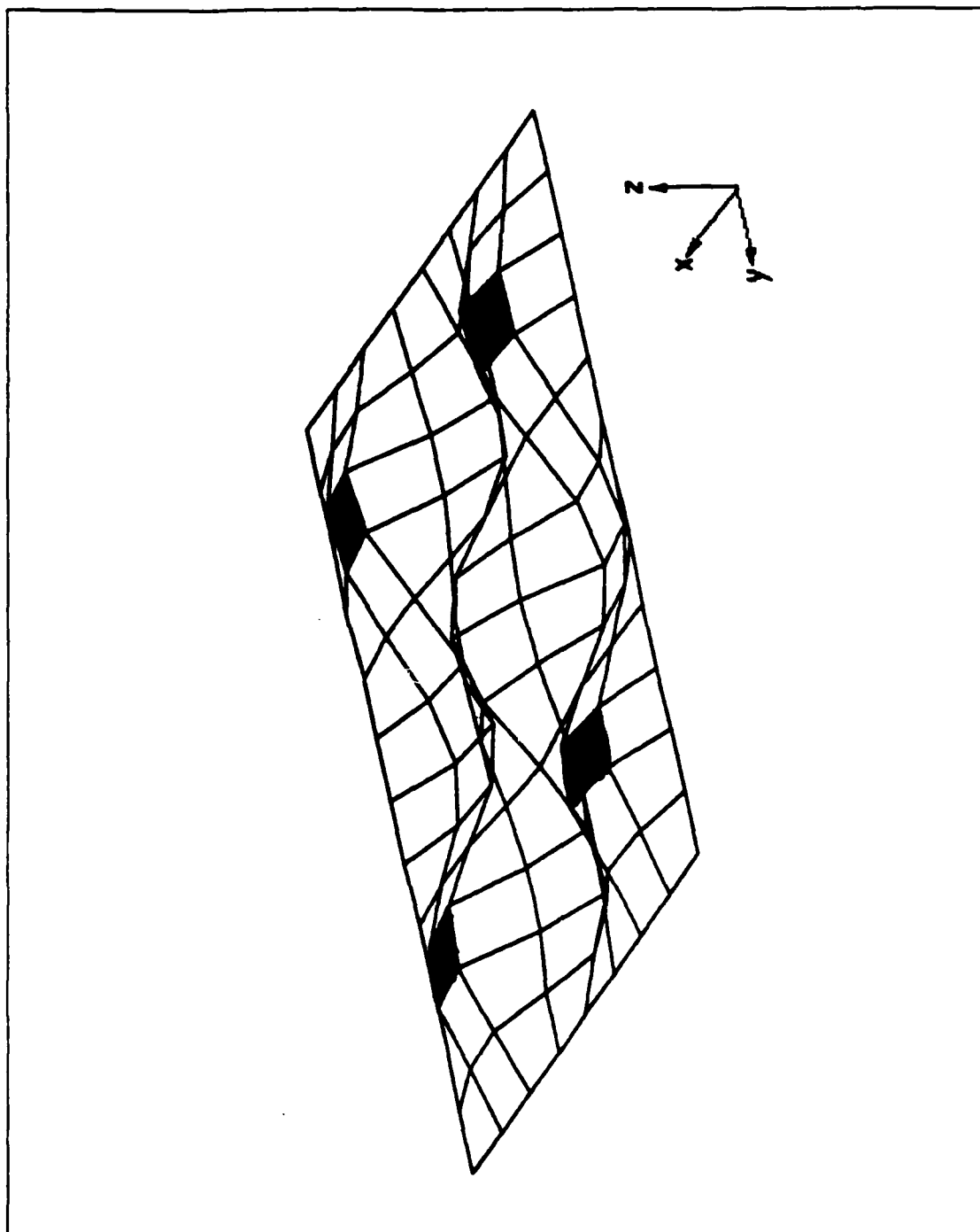


Figure 26. Theoretical perspective view - mode #12 (1766.34 Hz): Shaded elements - area of highest strain energy.

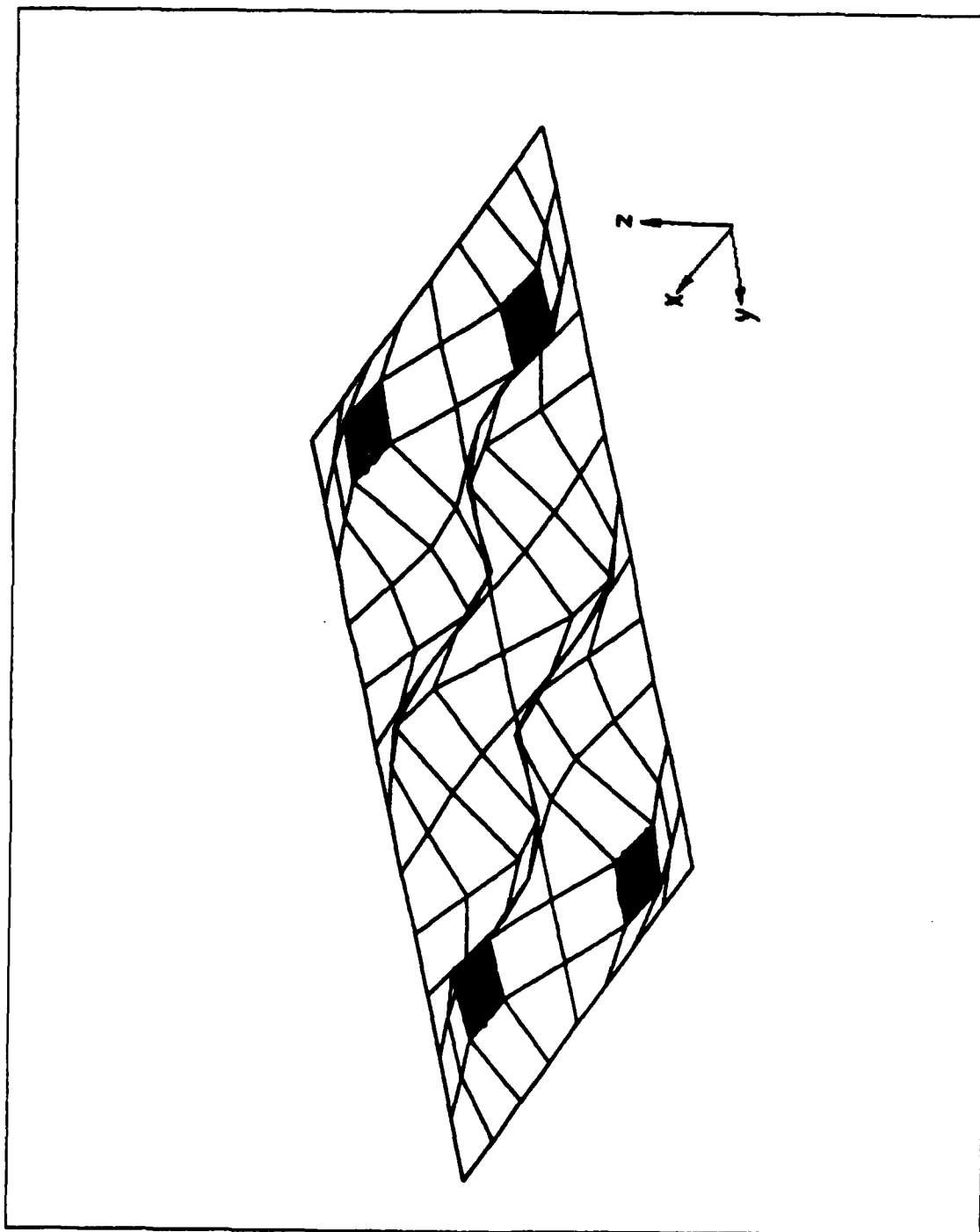


Figure 27. Theoretical perspective view - mode #13 (1945.23 Hz): Shaded elements - area of highest strain energy.

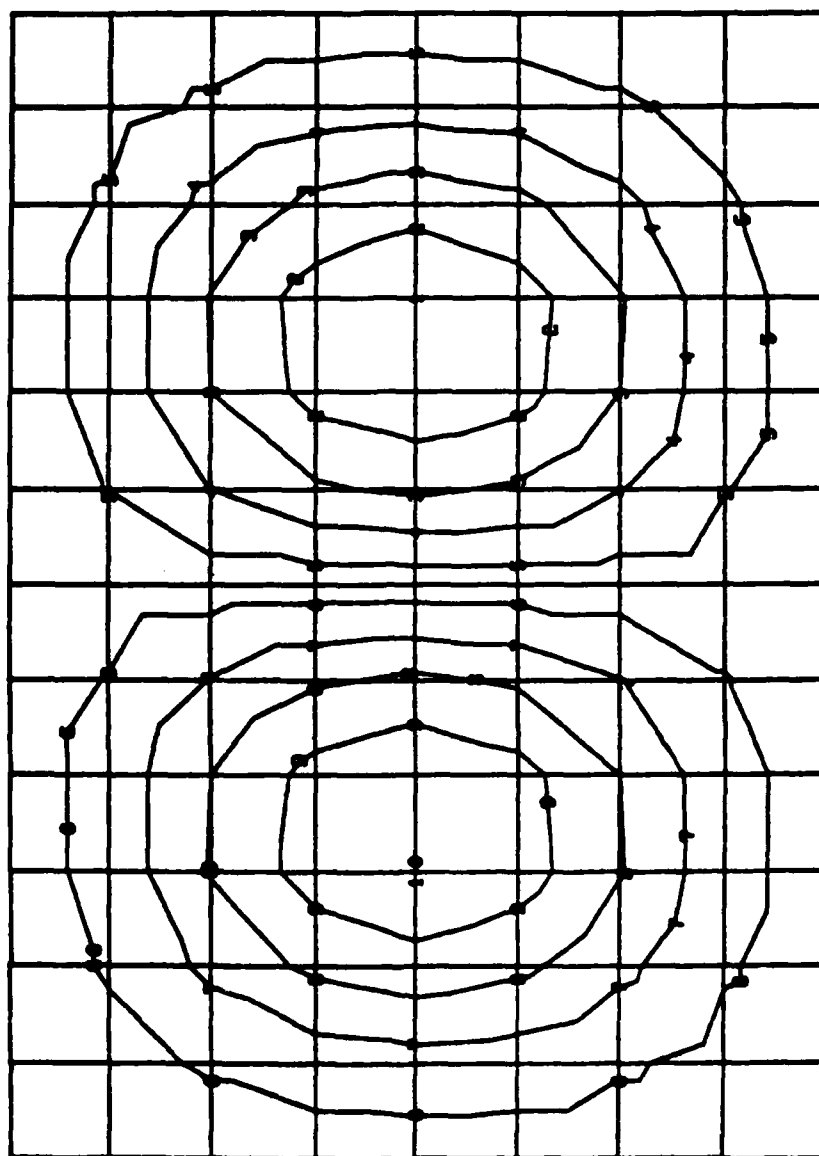


Figure 28. Theoretical z-plane deformation contour - mode #2.

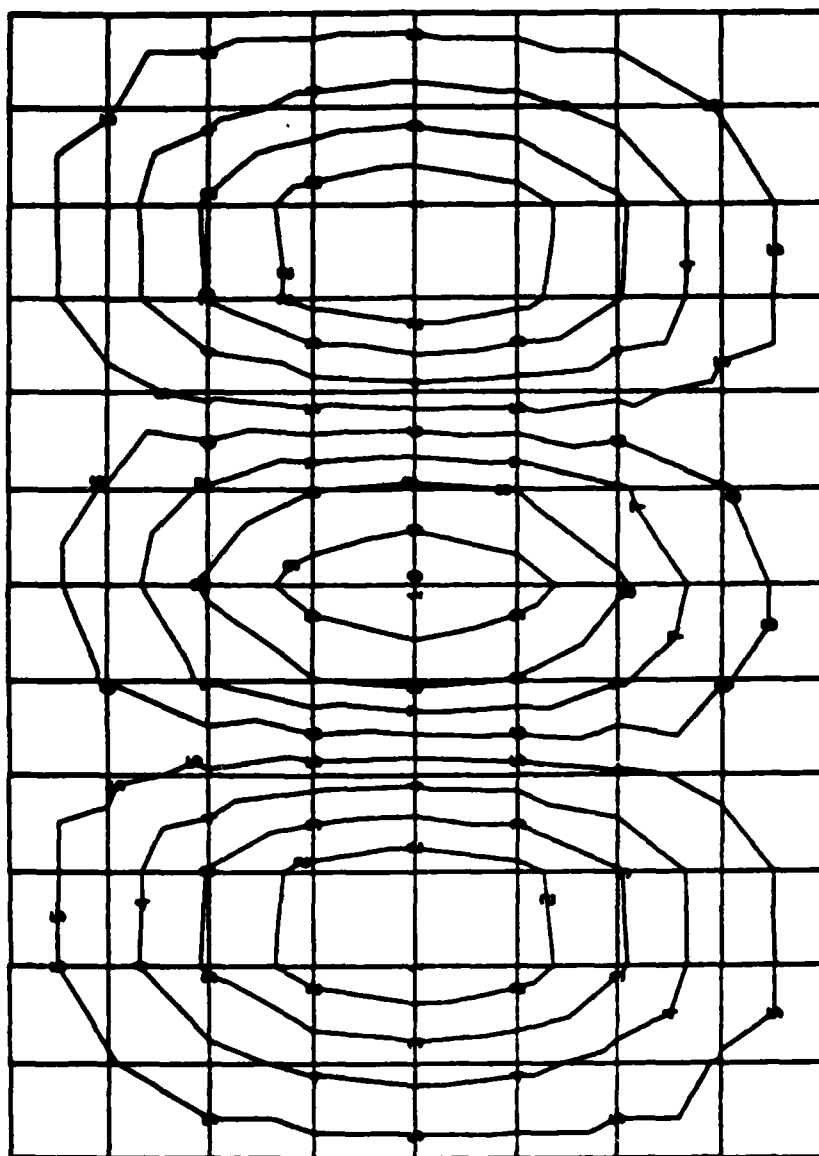


Figure 29. Theoretical z-plane deformation contour - mode #3.

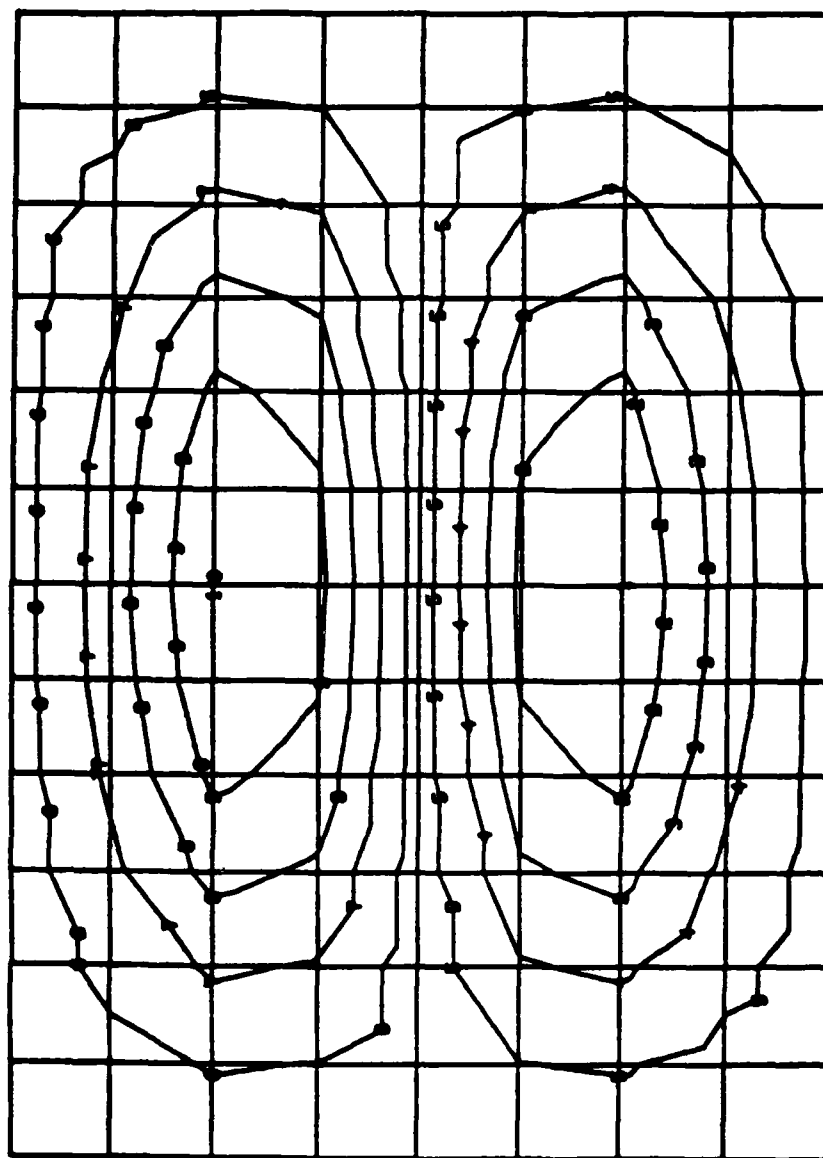


Figure 30. Theoretical z-plane deformation contour - mode #4.

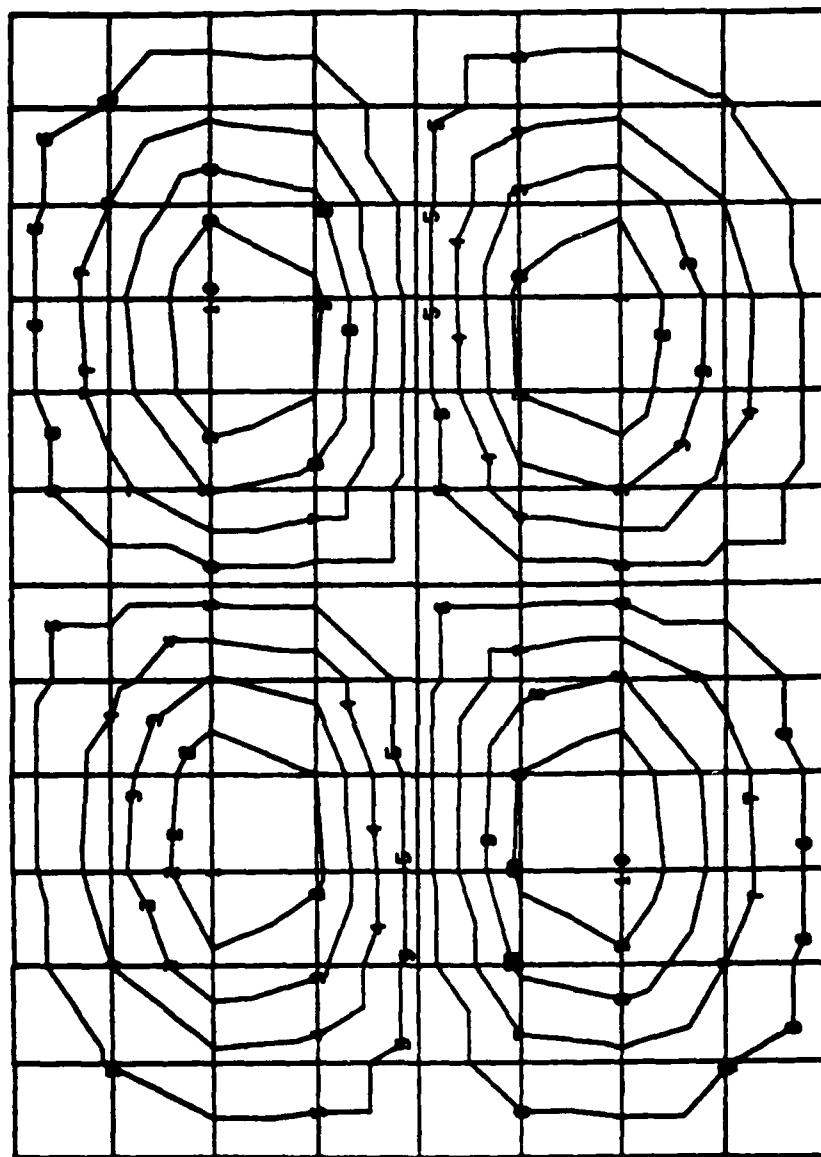


Figure 31. Theoretical z-plane deformation contour - mode #5.

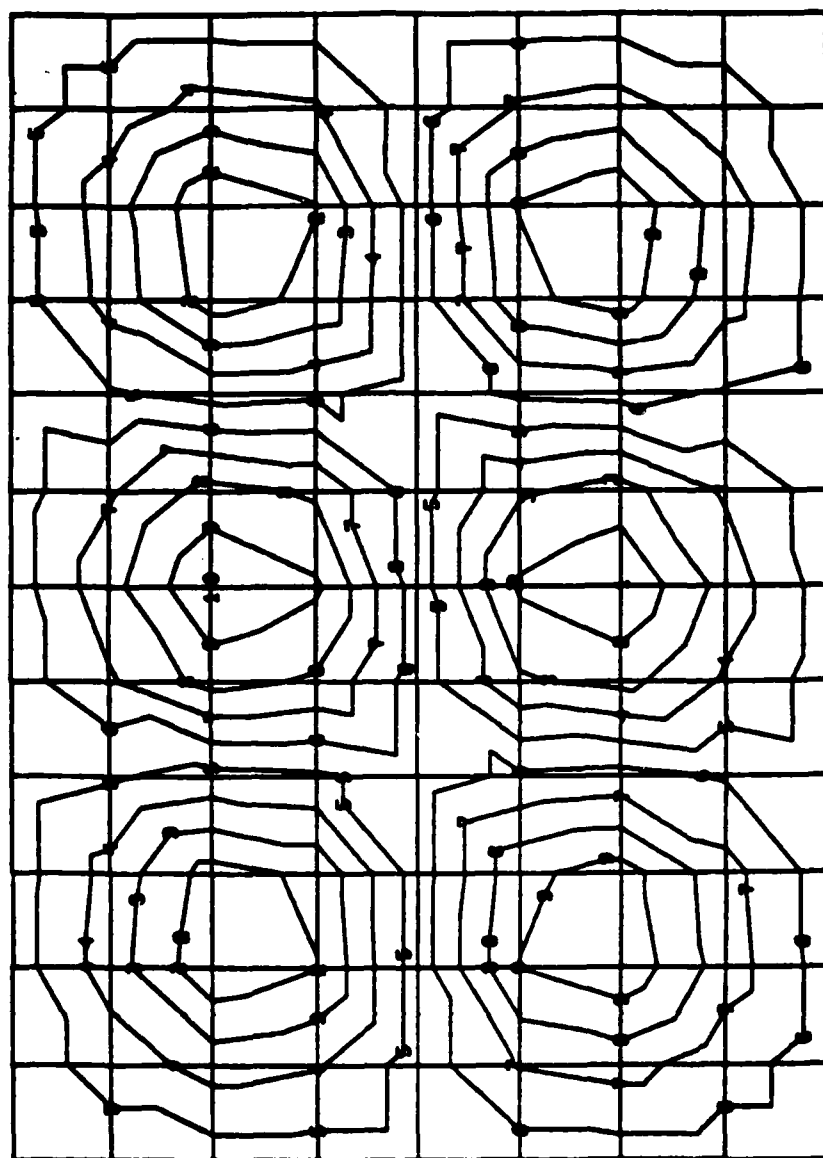


Figure 32. Theoretical z-plane deformation contour - mode #6.

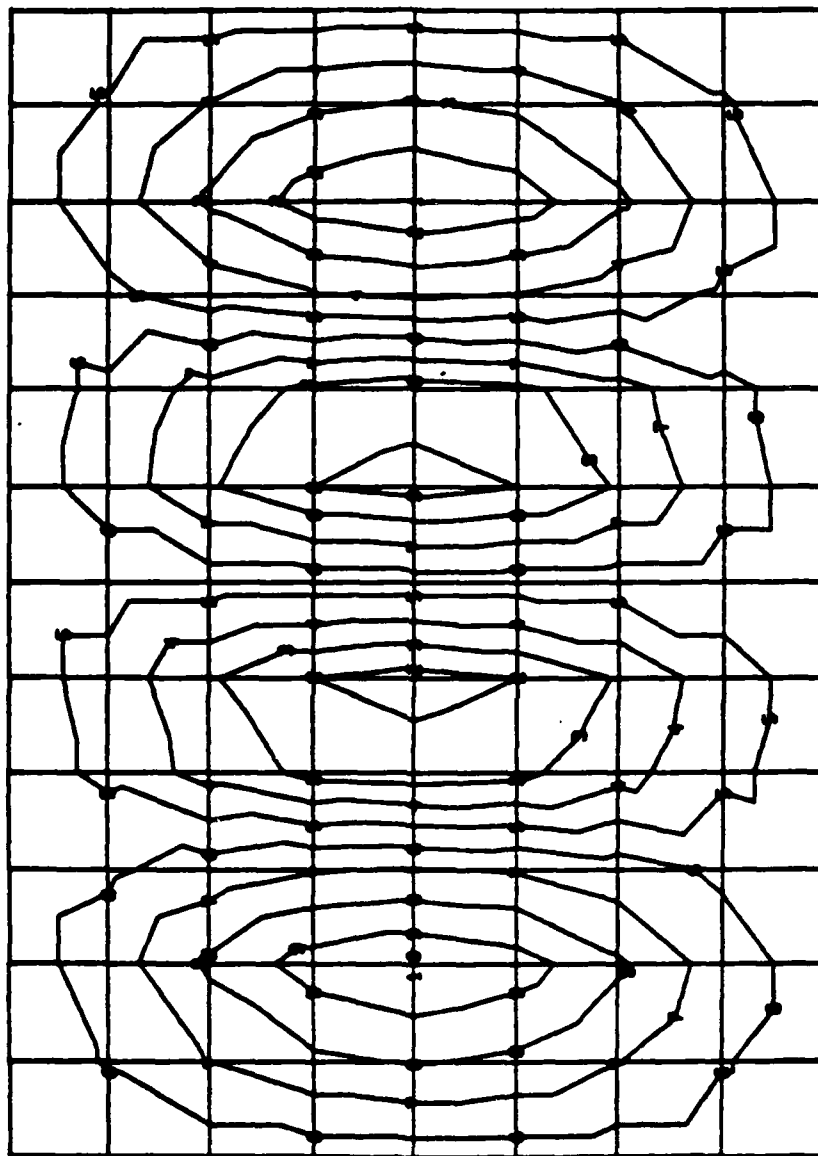


Figure 33. Theoretical z-plane deformation contour - mode #7.

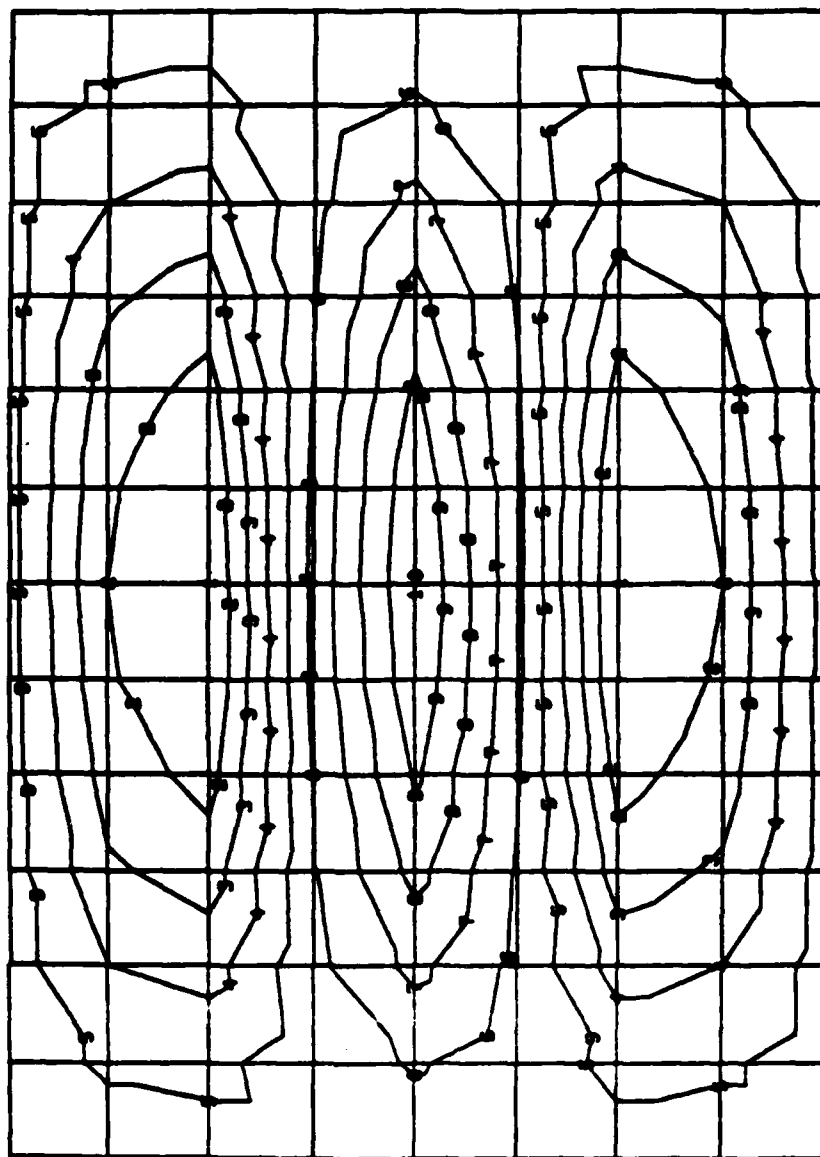


Figure 34. Theoretical z-plane deformation contour - mode #8.

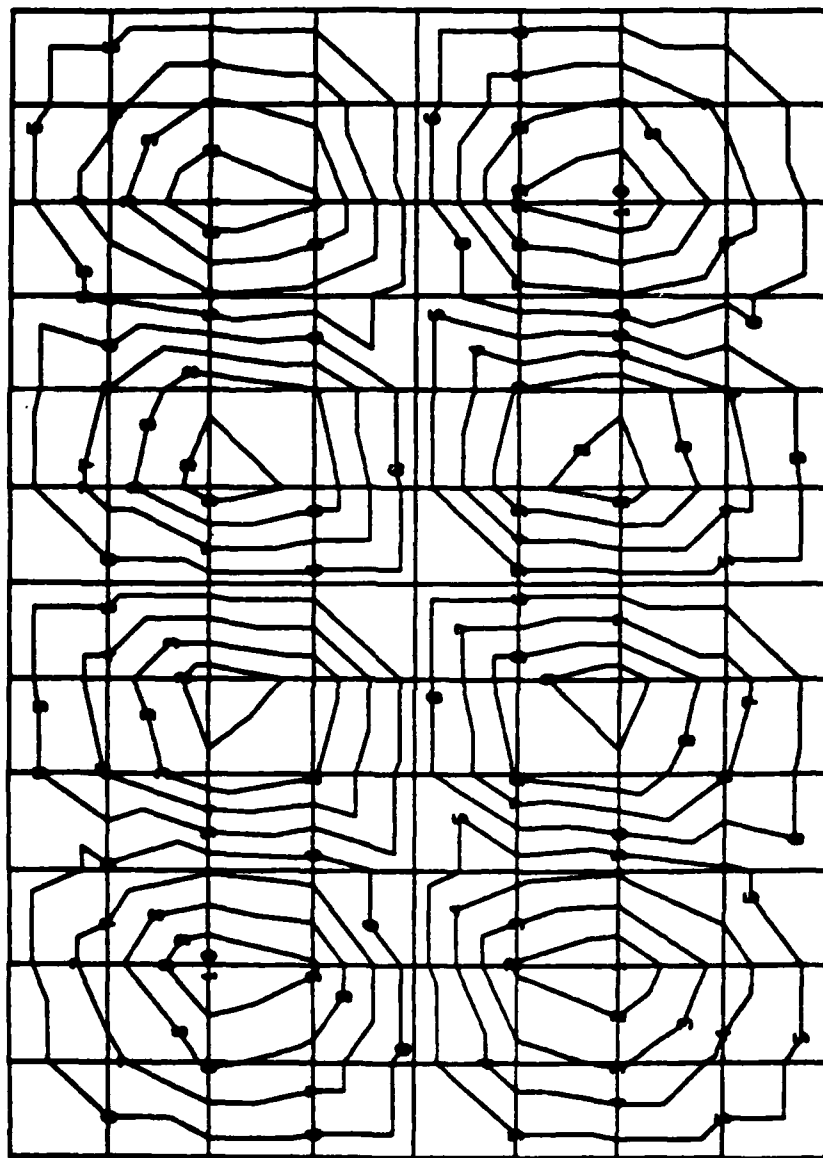


Figure 35. Theoretical z-plane deformation contour - mode #9.

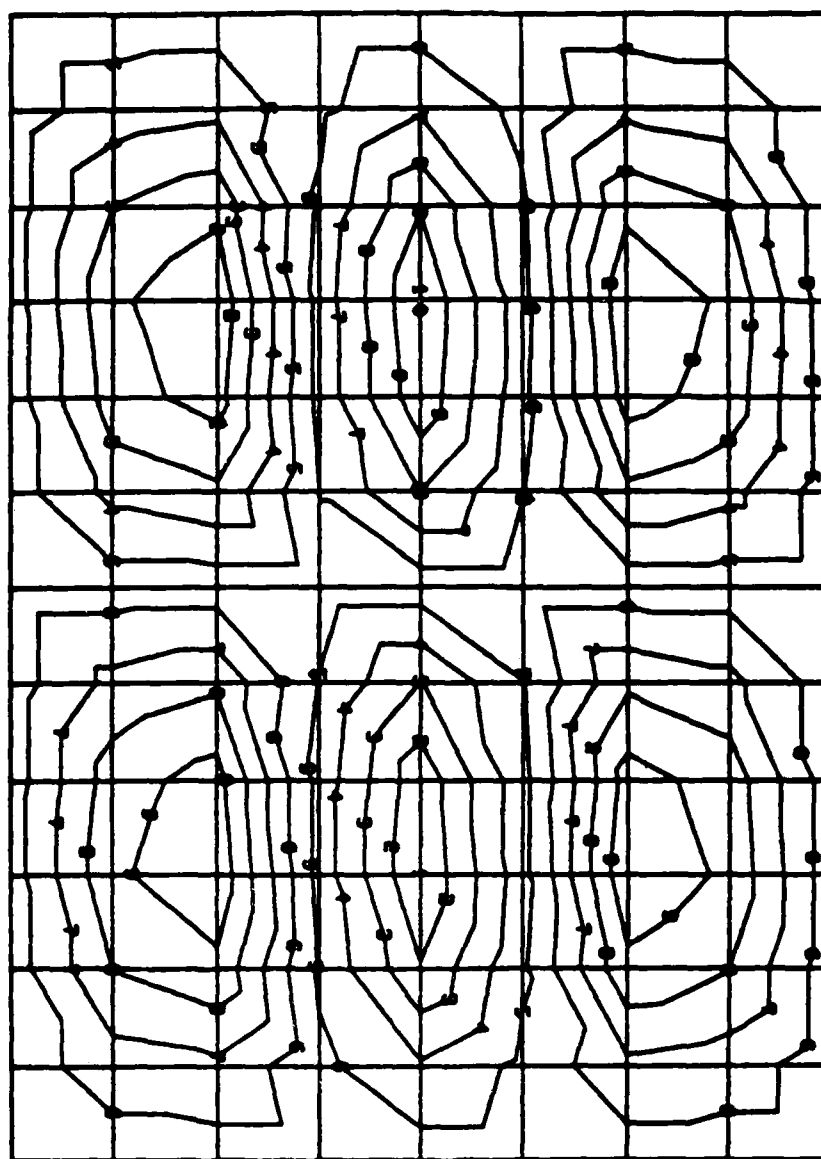


Figure 36. Theoretical z-plane deformation contour - mode #10.

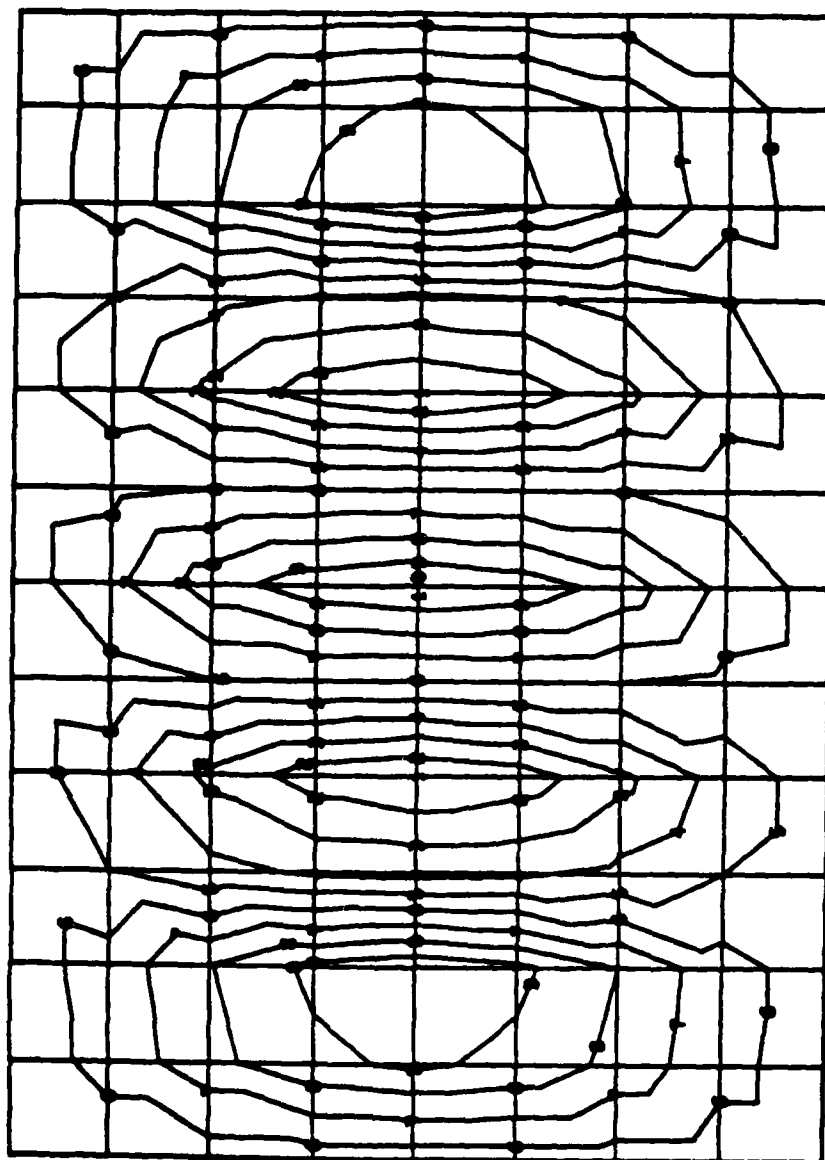


Figure 37. Theoretical z-plane deformation contour - mode #11.

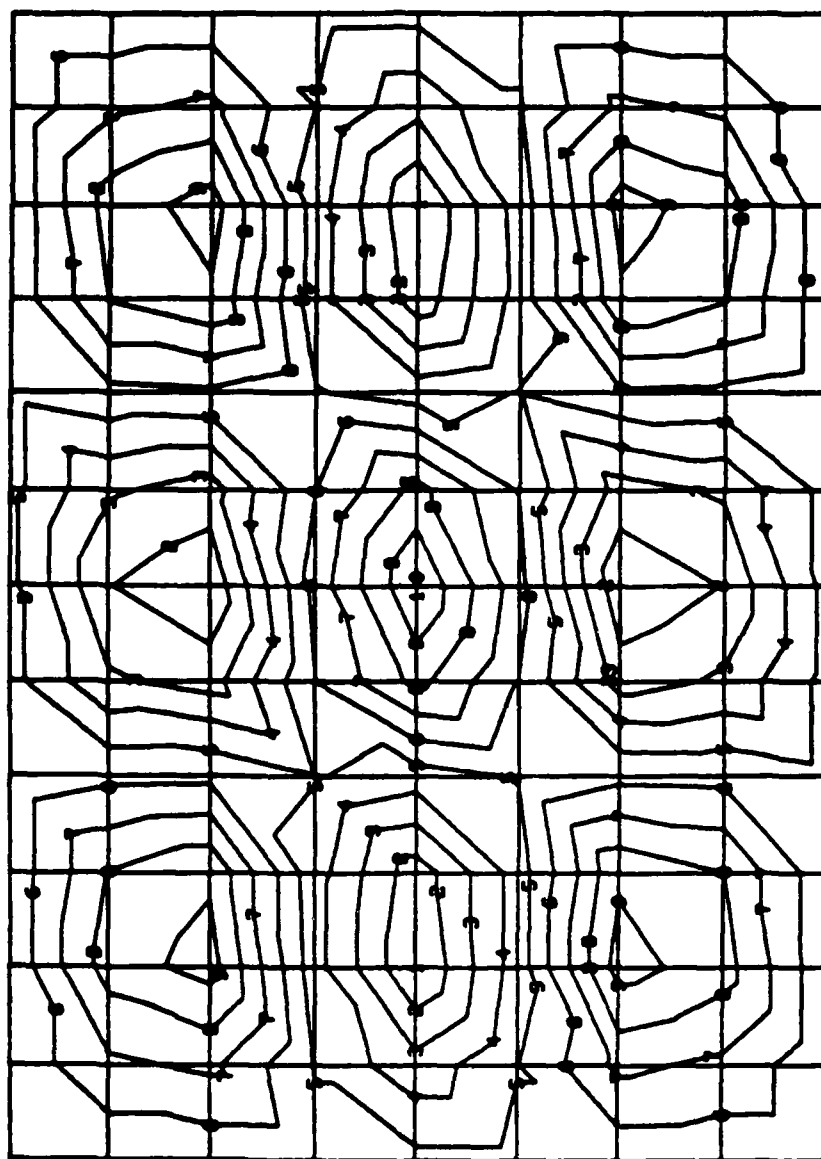


Figure 38. Theoretical z-plane deformation contour - mode #12.

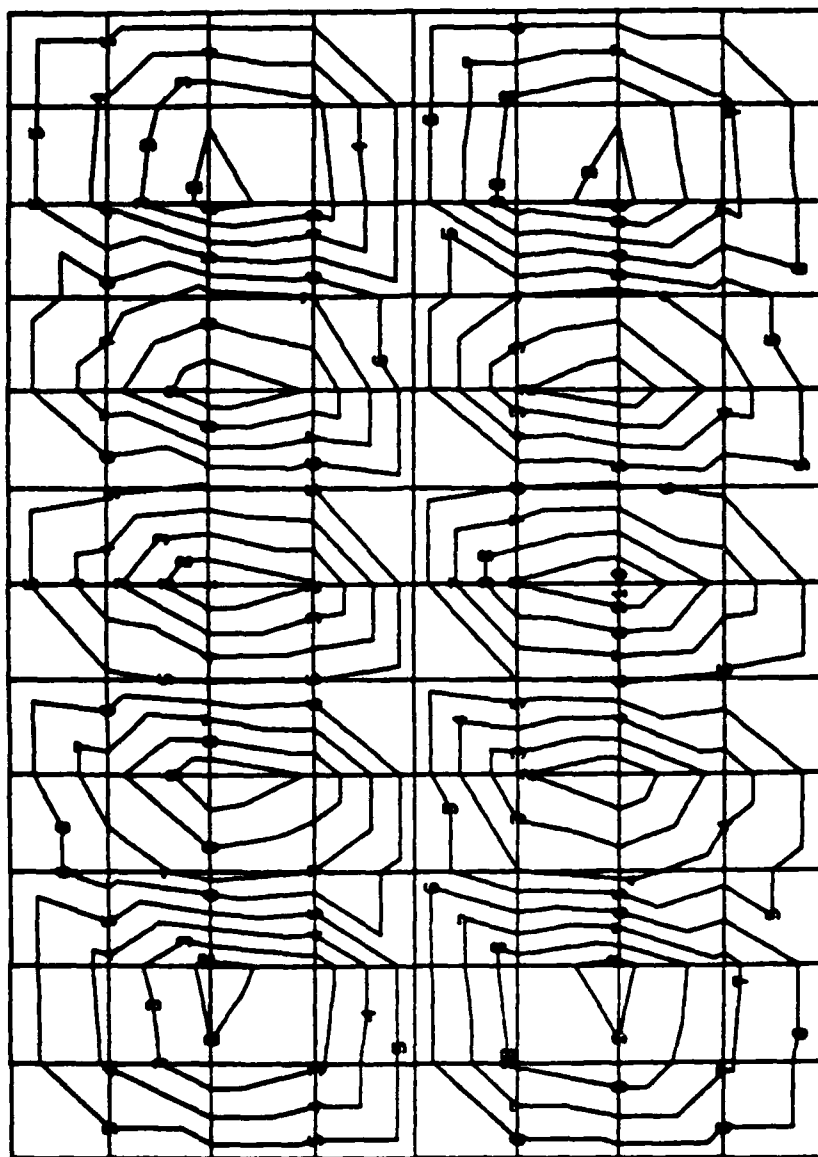


Figure 39. Theoretical z-plane deformation contour - mode #13.

APPENDIX B.
MODAL SURVEY PERSPECTIVE VIEWS

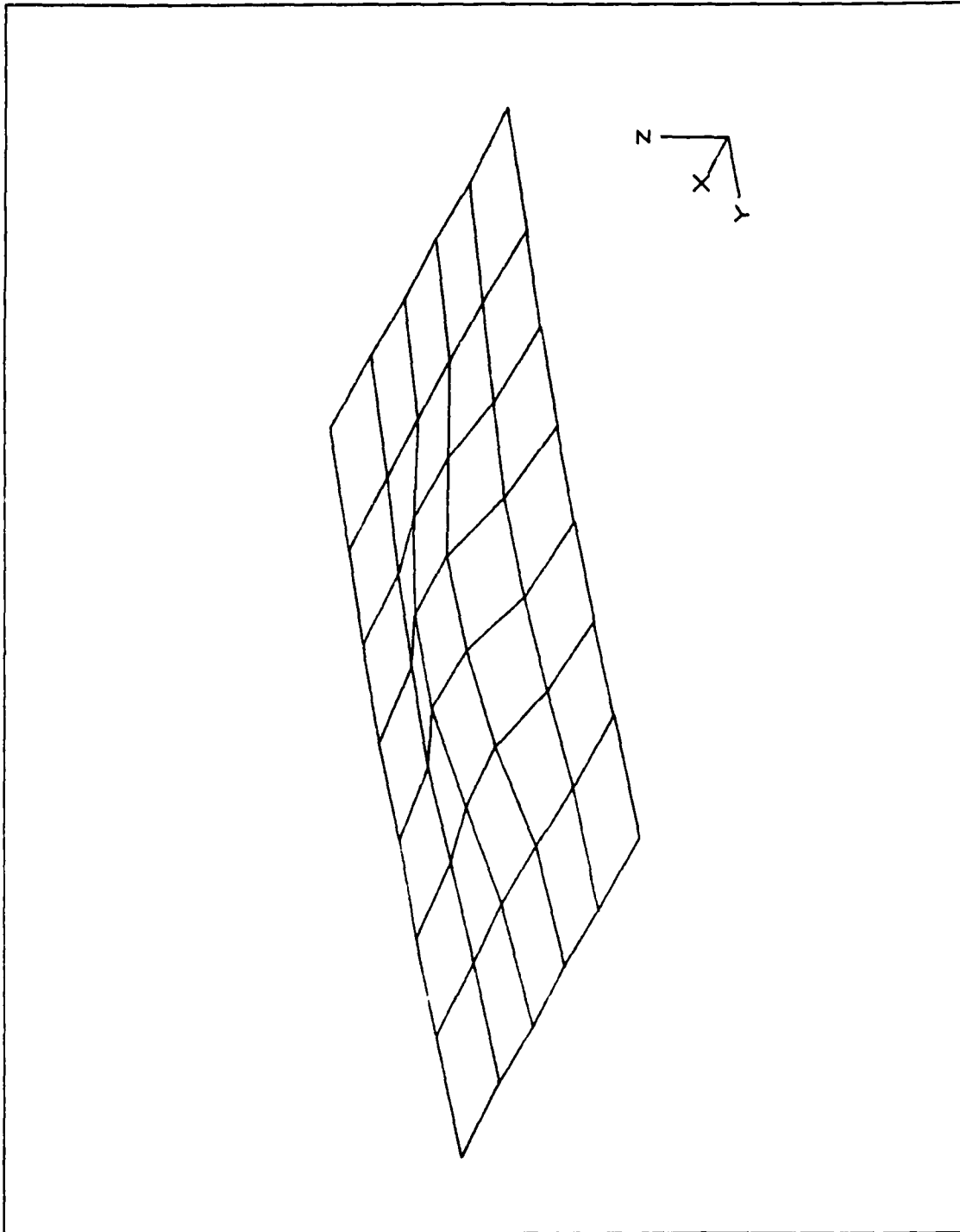


Figure 40. Modal survey perspective view - mode #2 (276.04 Hz).

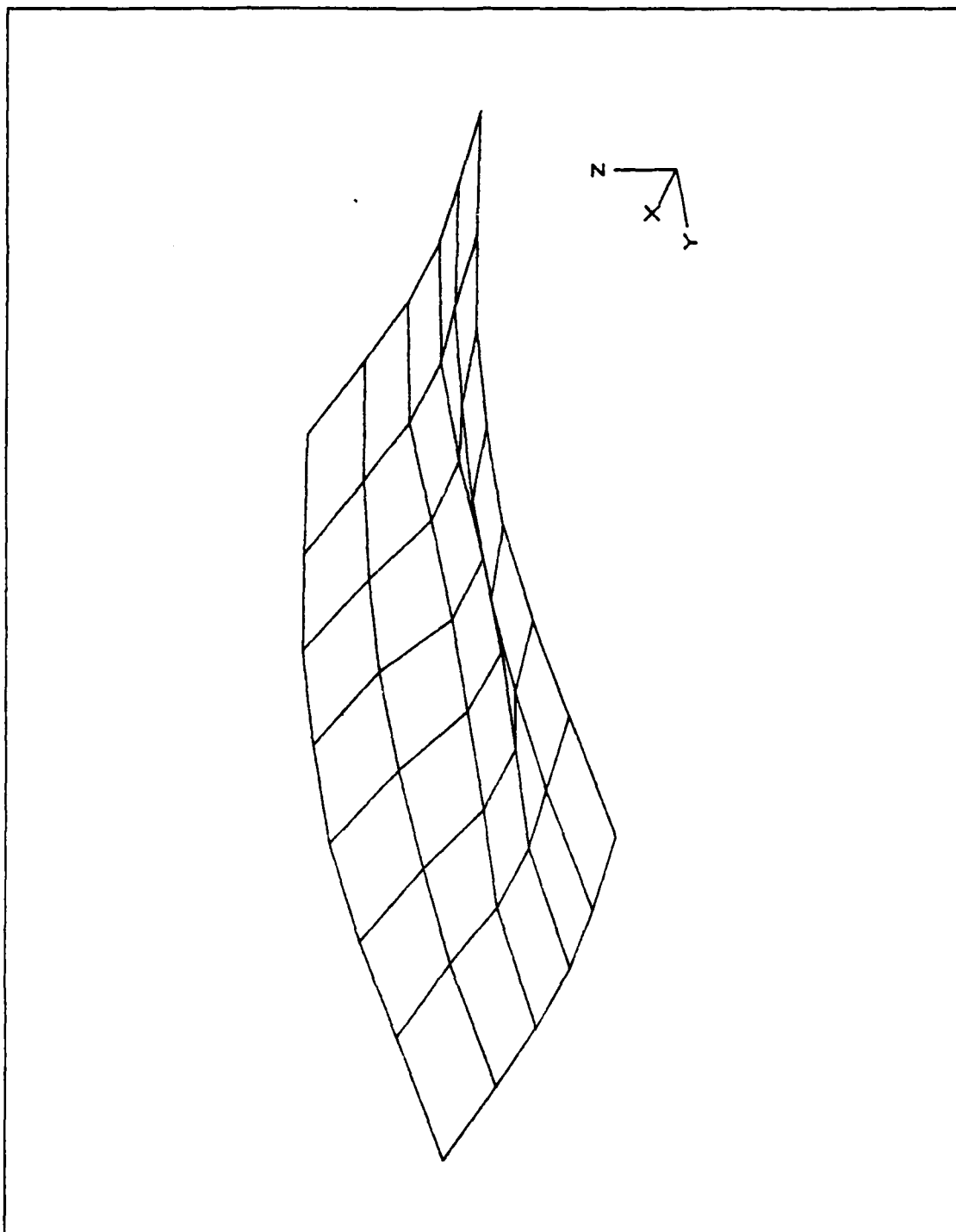


Figure 41. Modal survey perspective view - mode #3 (338.71 Hz).

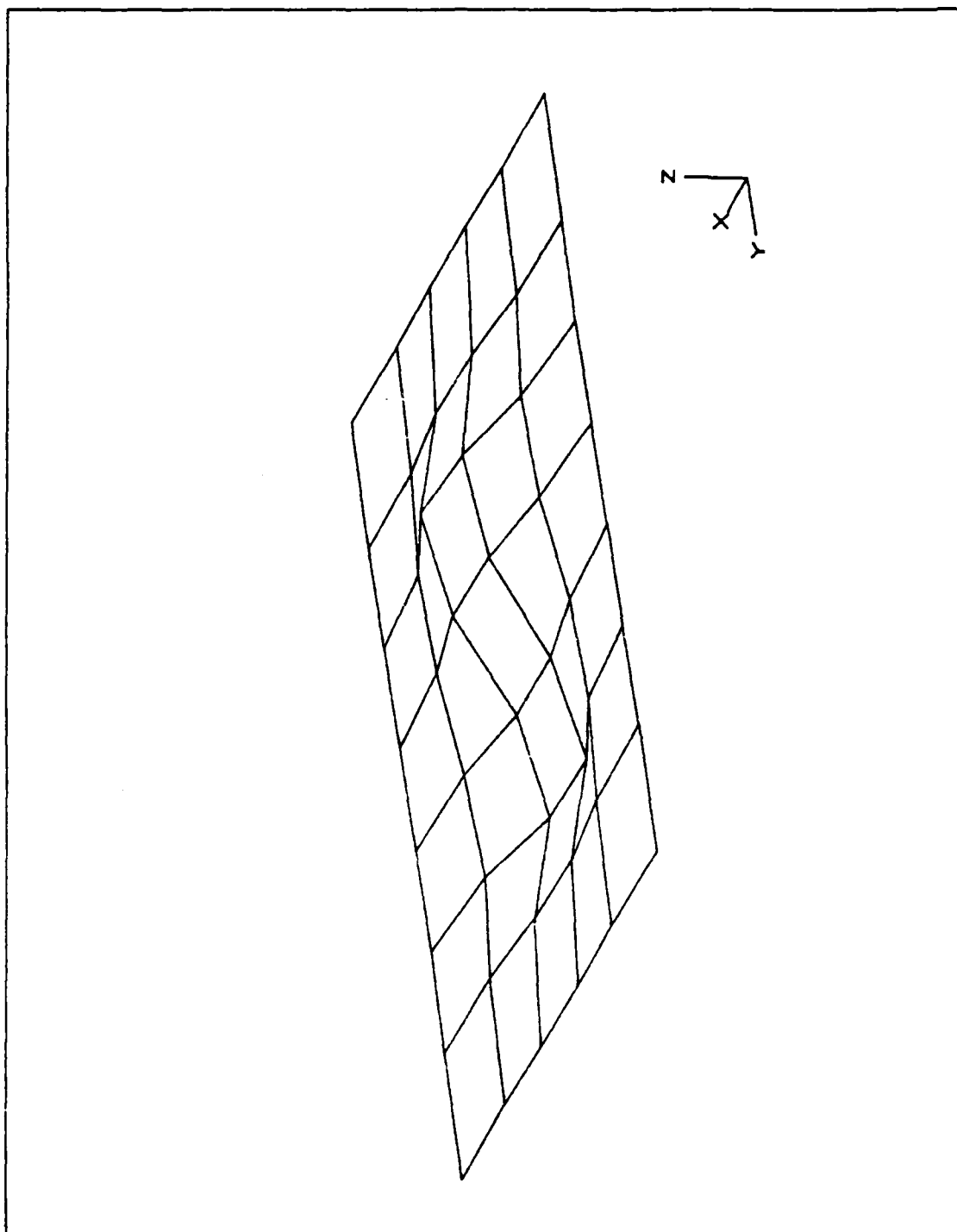


Figure 42. Modal survey perspective view - mode #4 (429.66 Hz).

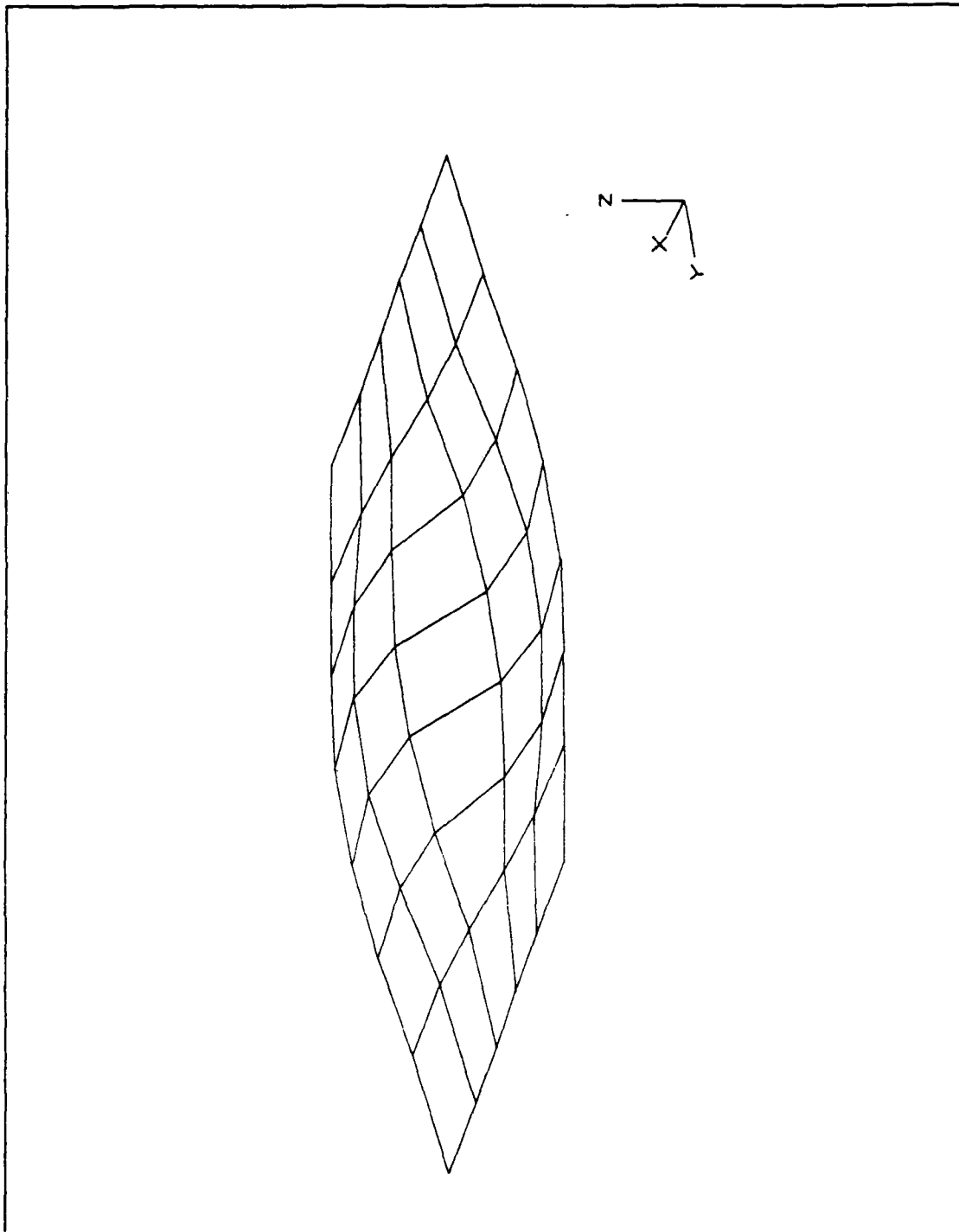


Figure 43. Modal survey perspective view - mode #5 (499.84 Hz).

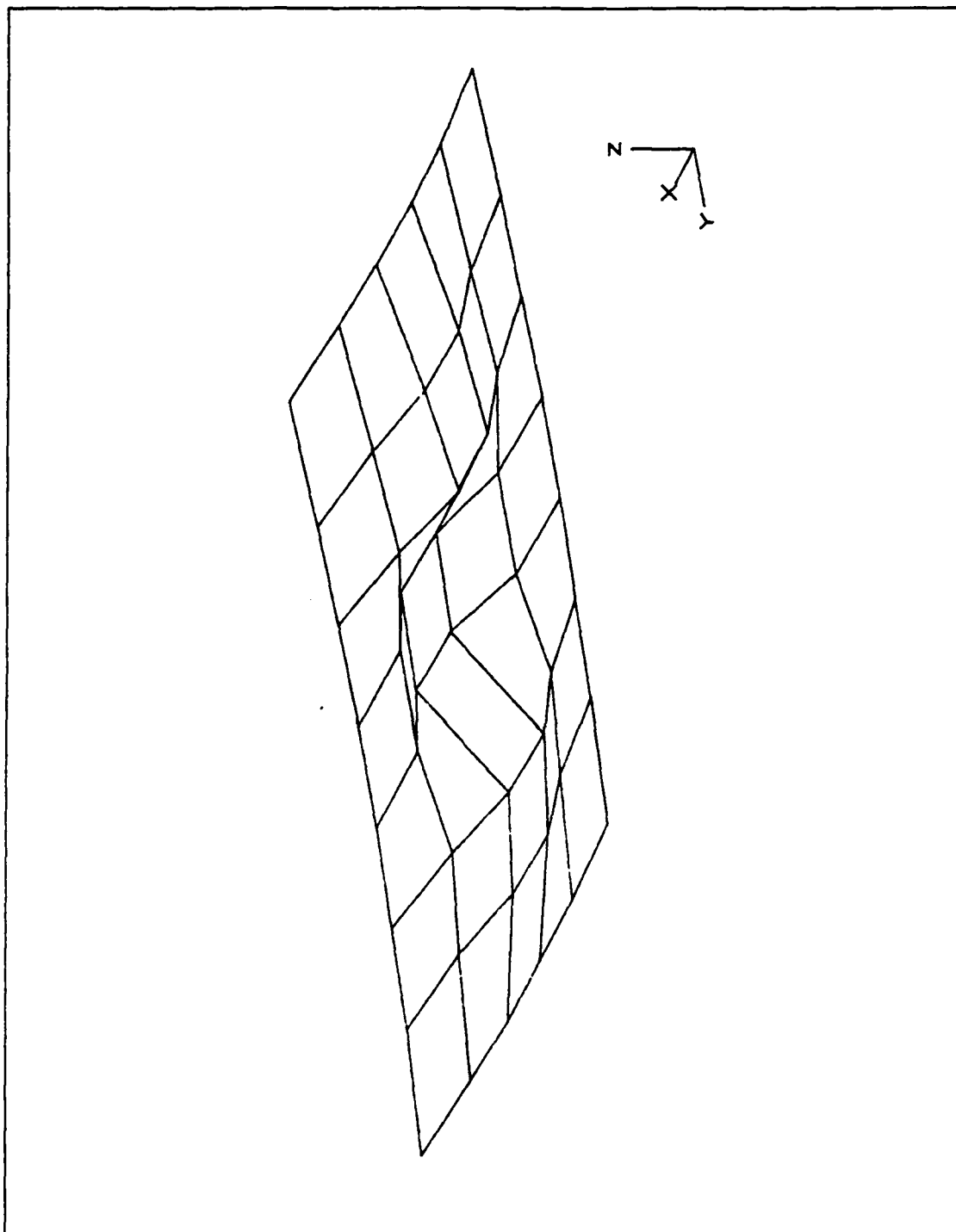


Figure 44. Modal survey perspective view - mode #6 (665.73 Hz).

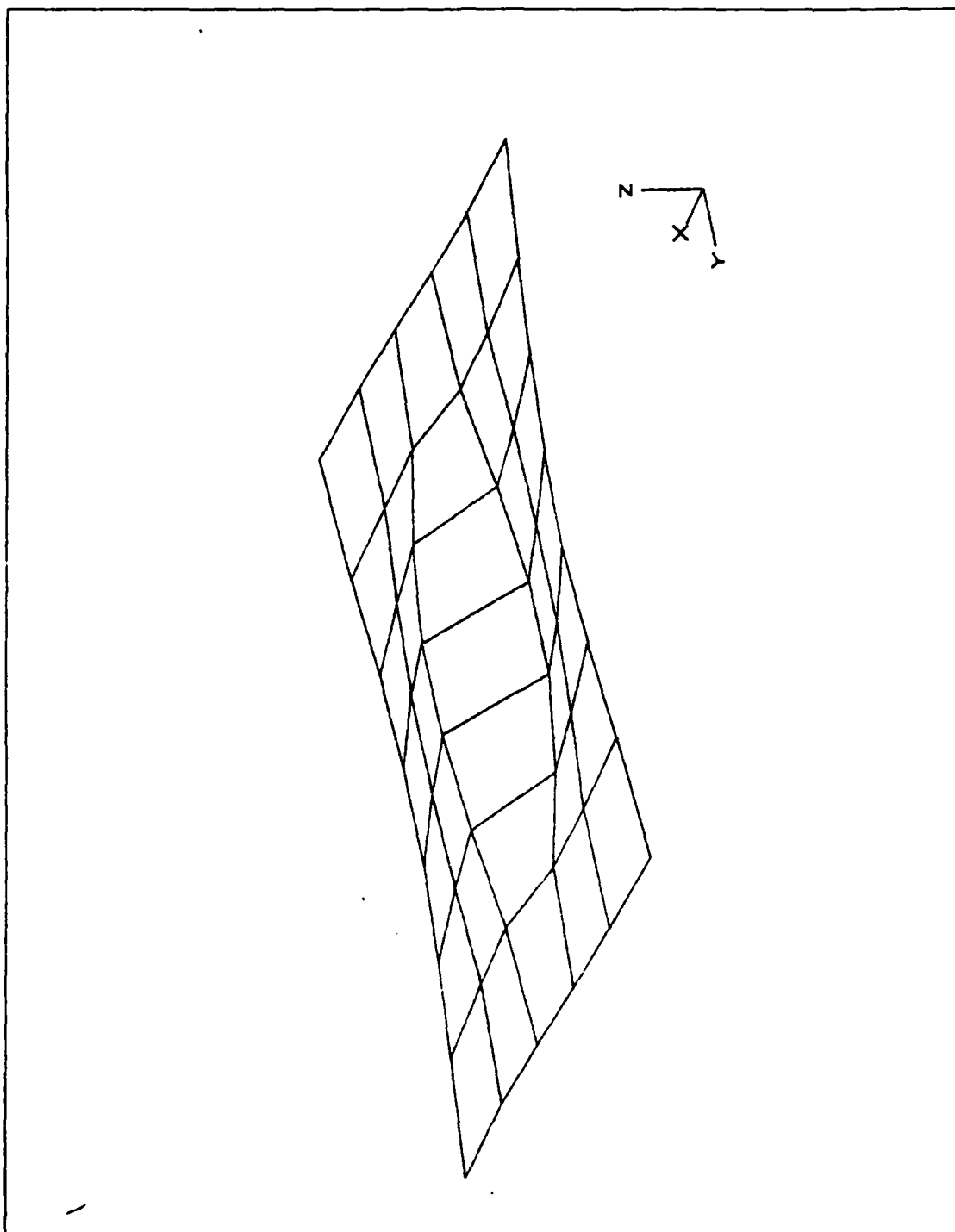


Figure 45. Modal survey perspective view - mode #7 (708.52 Hz).

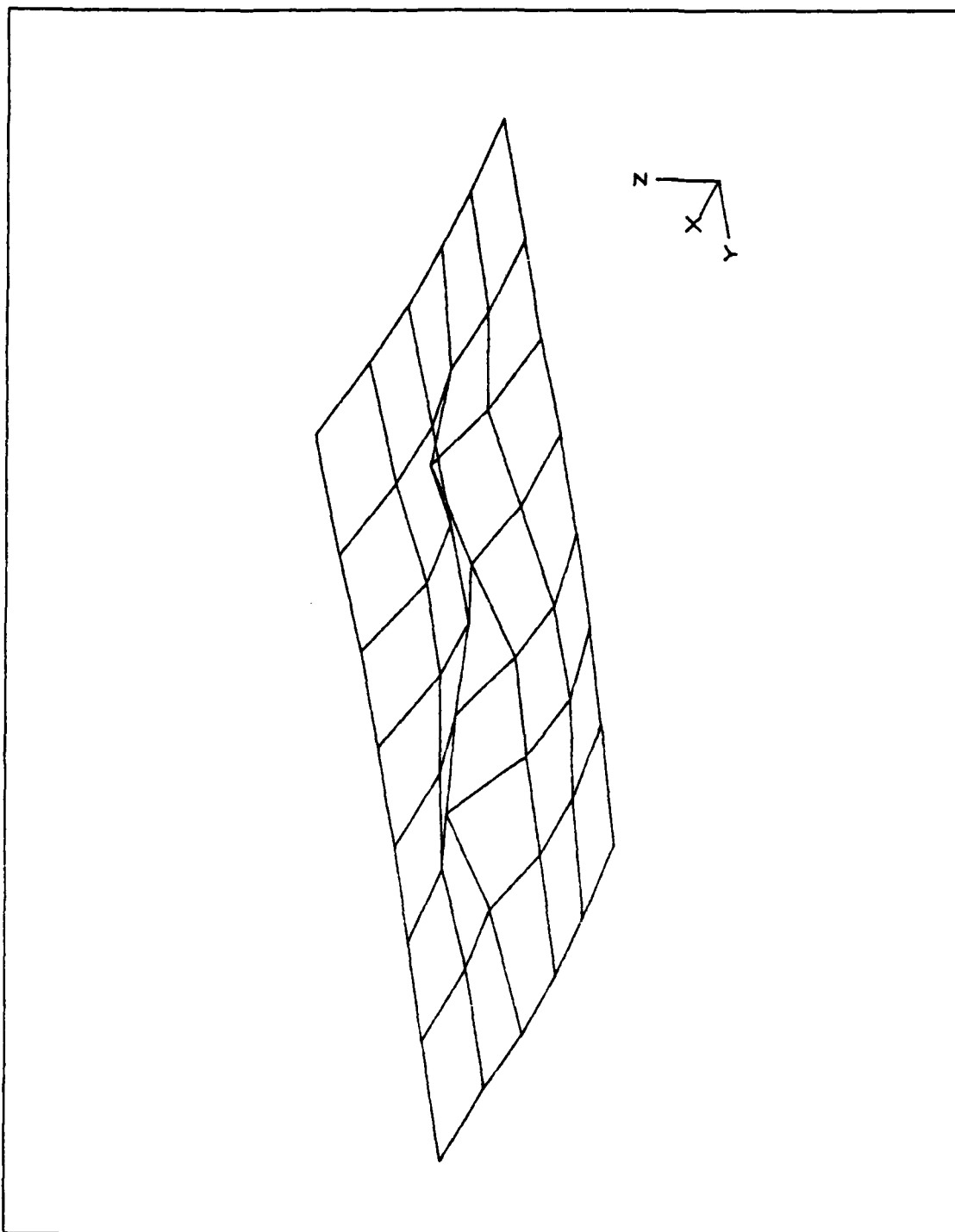


Figure 46. Modal survey perspective view - mode #8 (815.66 Hz).

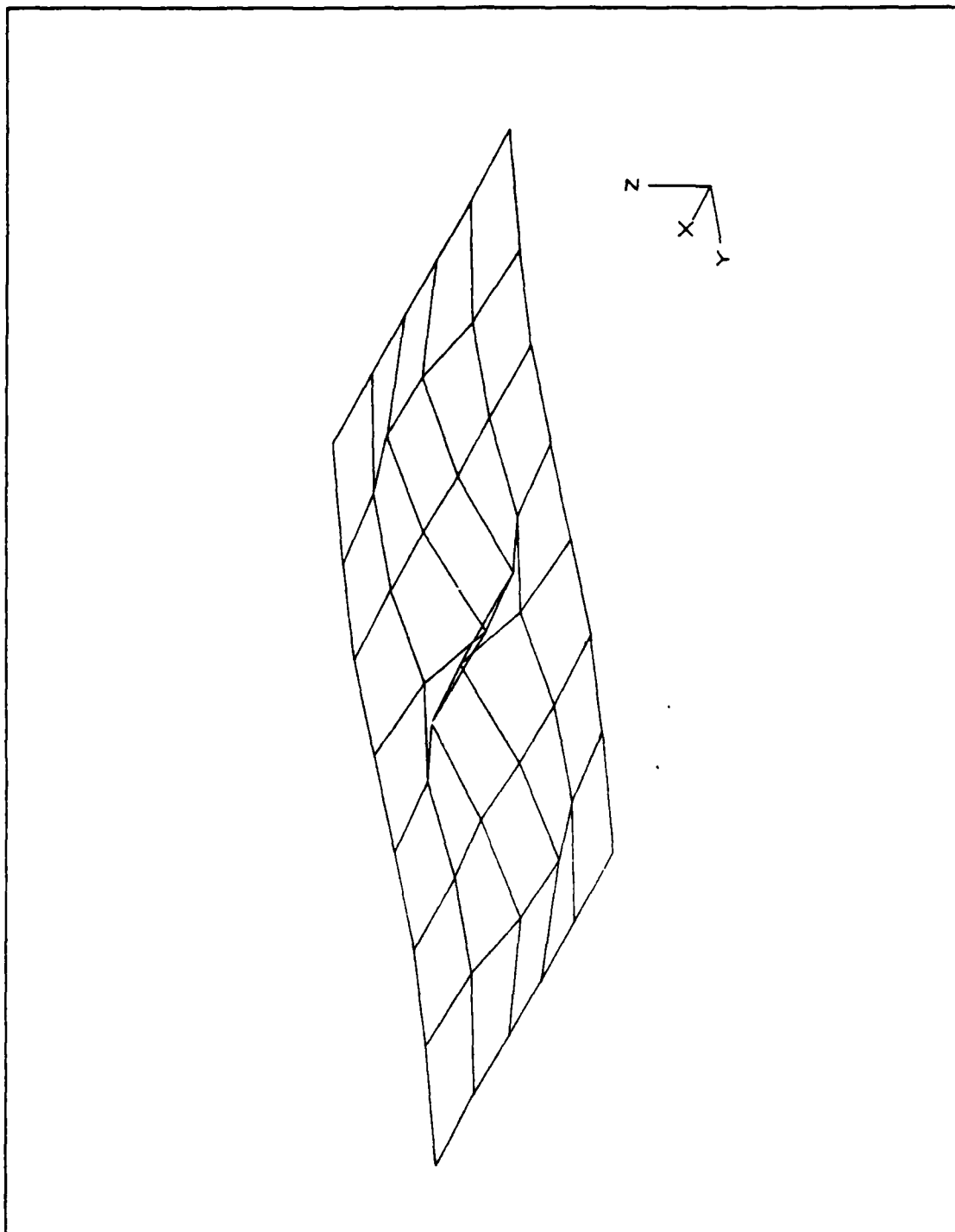


Figure 47. Modal survey perspective view - mode #9 (1005.73 Hz).

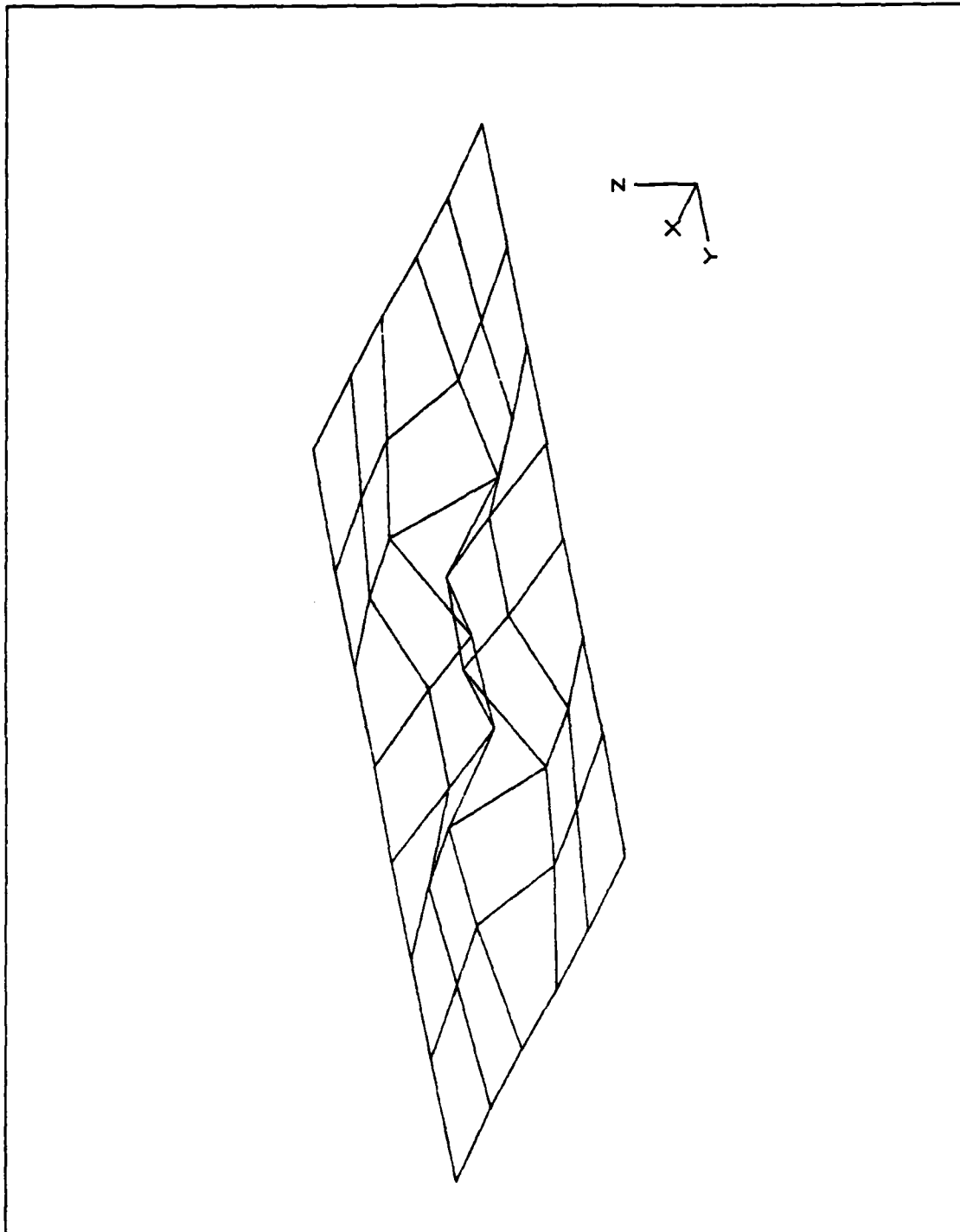


Figure 48. Modal survey perspective view - mode #10 (1062.31 Hz).

APPENDIX C.

FREQUENCY RESPONSE FUNCTIONS OF THE TEST PLATE WITH BEAM WAVEGUIDE ABSORBERS ATTACHED

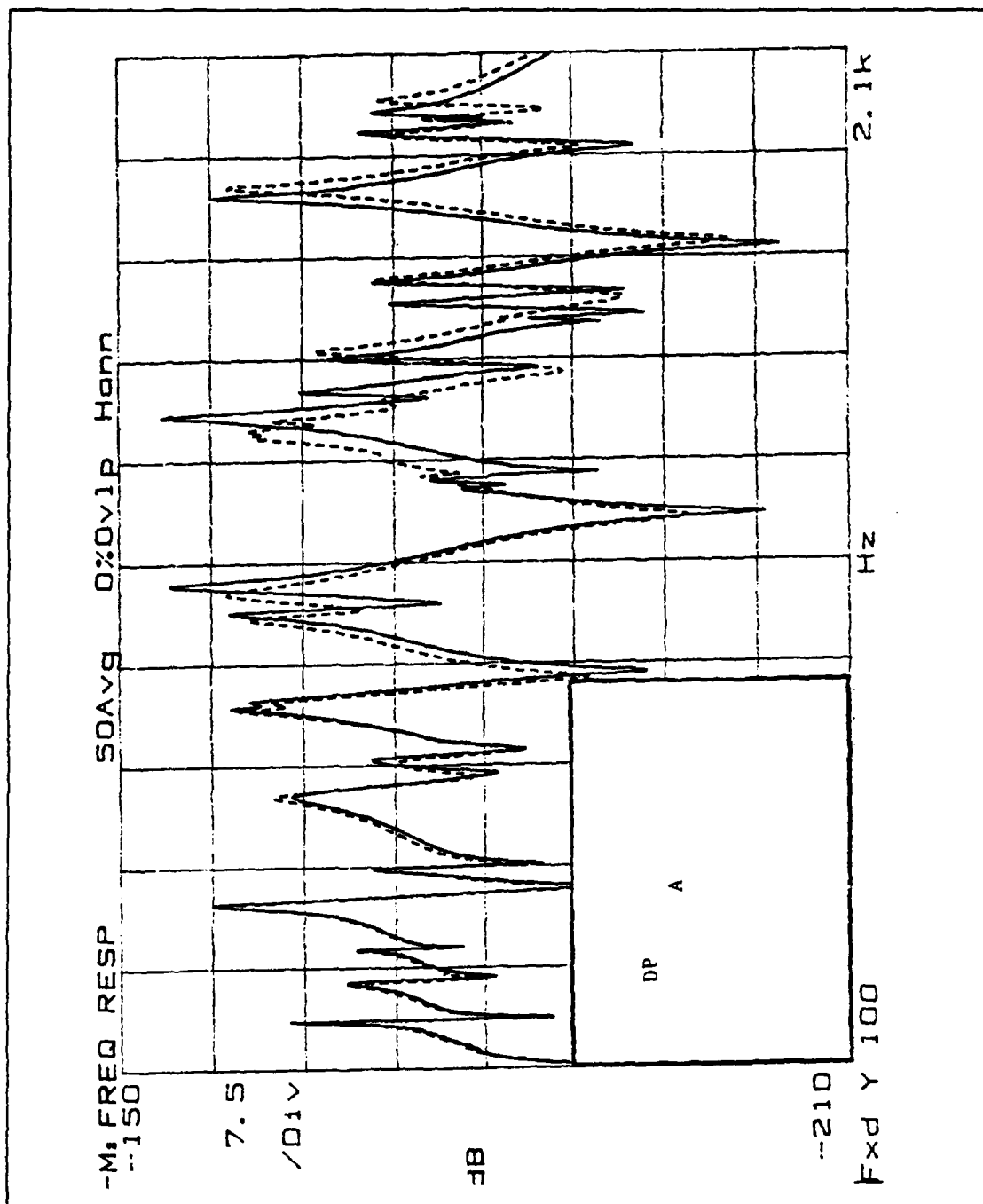


Figure 49. Baseline (DP) frequency response (solid); with a 20" constrained layer waveguide attached at location A (dashed): Locations shown in insert.

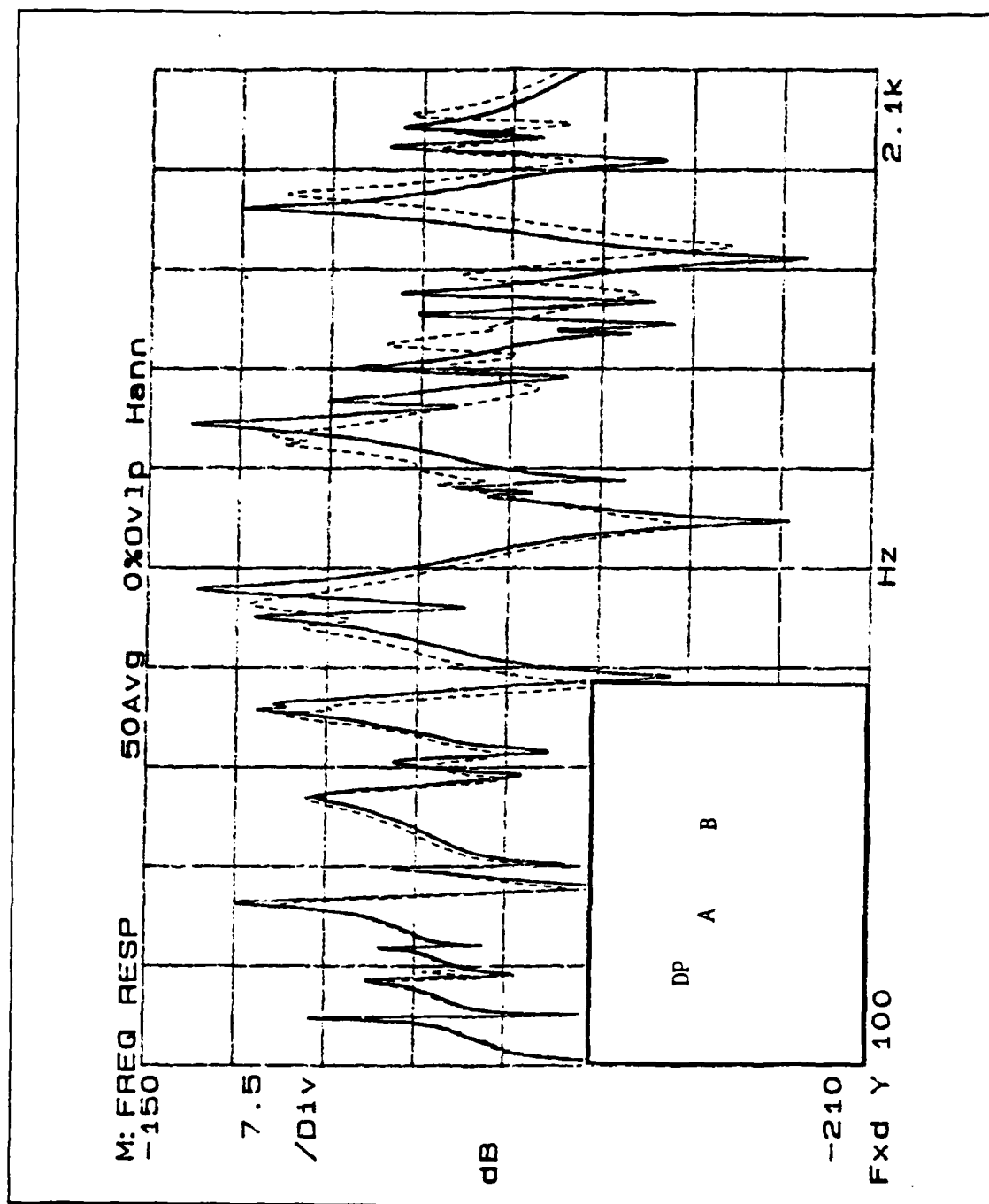


Figure 50. Baseline (DP) frequency response (solid); with a 20" constrained layer waveguide attached at locations A and B (dashed): Locations shown in insert.

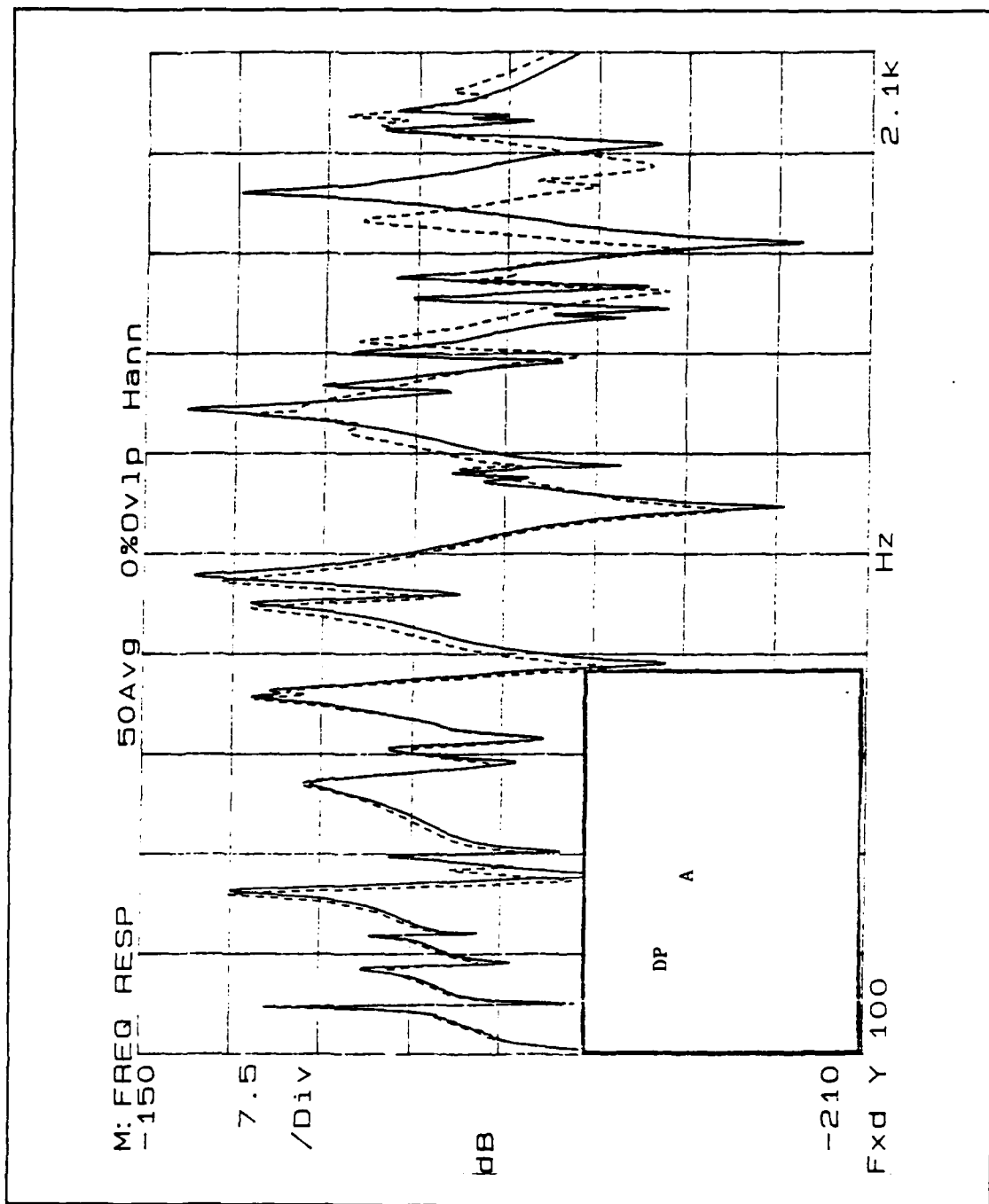


Figure 51. Baseline (DP) frequency response (solid); with a 16" constrained layer waveguide absorber at location A (dashed): Locations shown in insert.

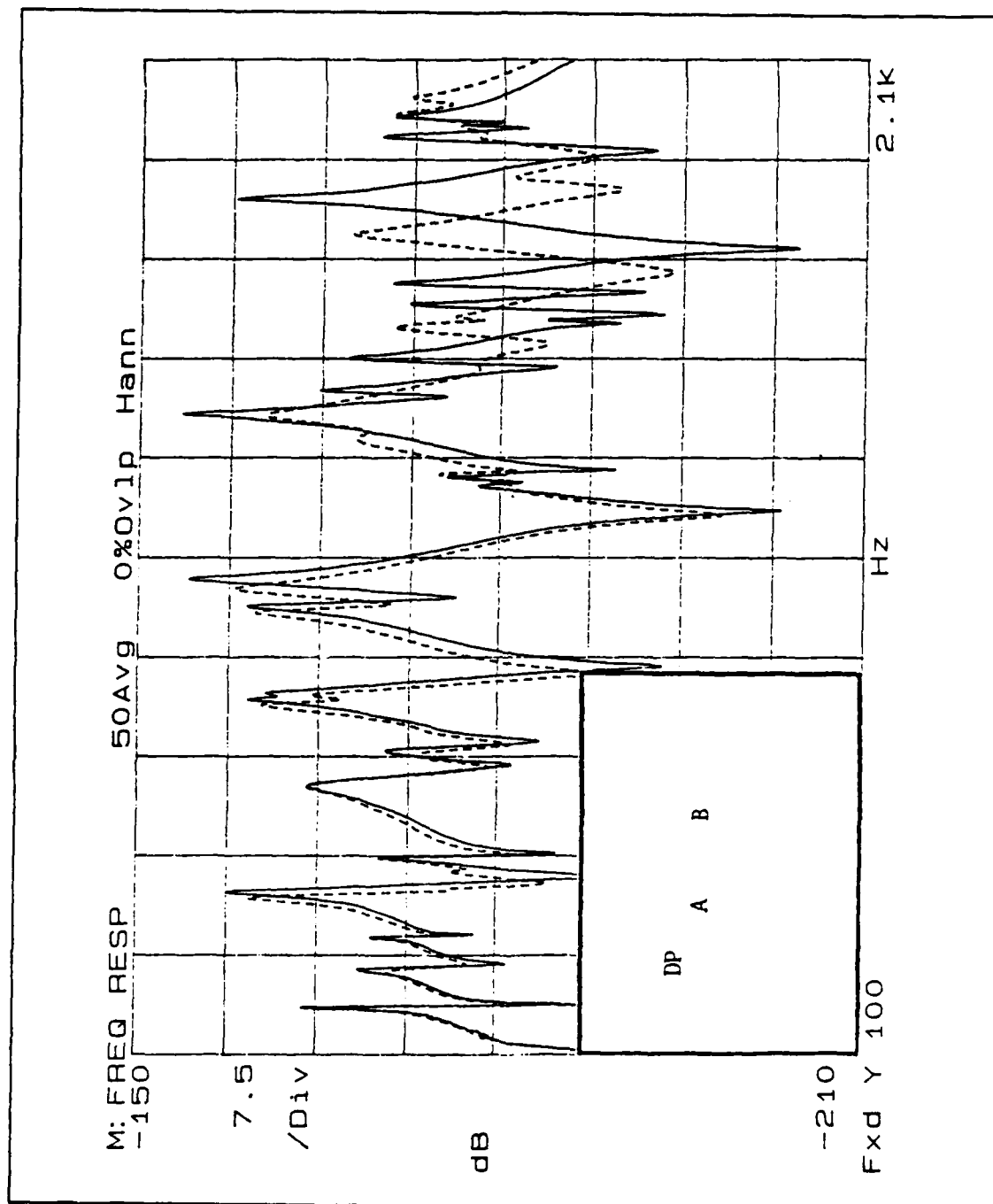


Figure 52. Baseline (DP) frequency response (solid); with a 16" constrained layer waveguide absorber at locations A and B (dashed): Locations shown in insert.

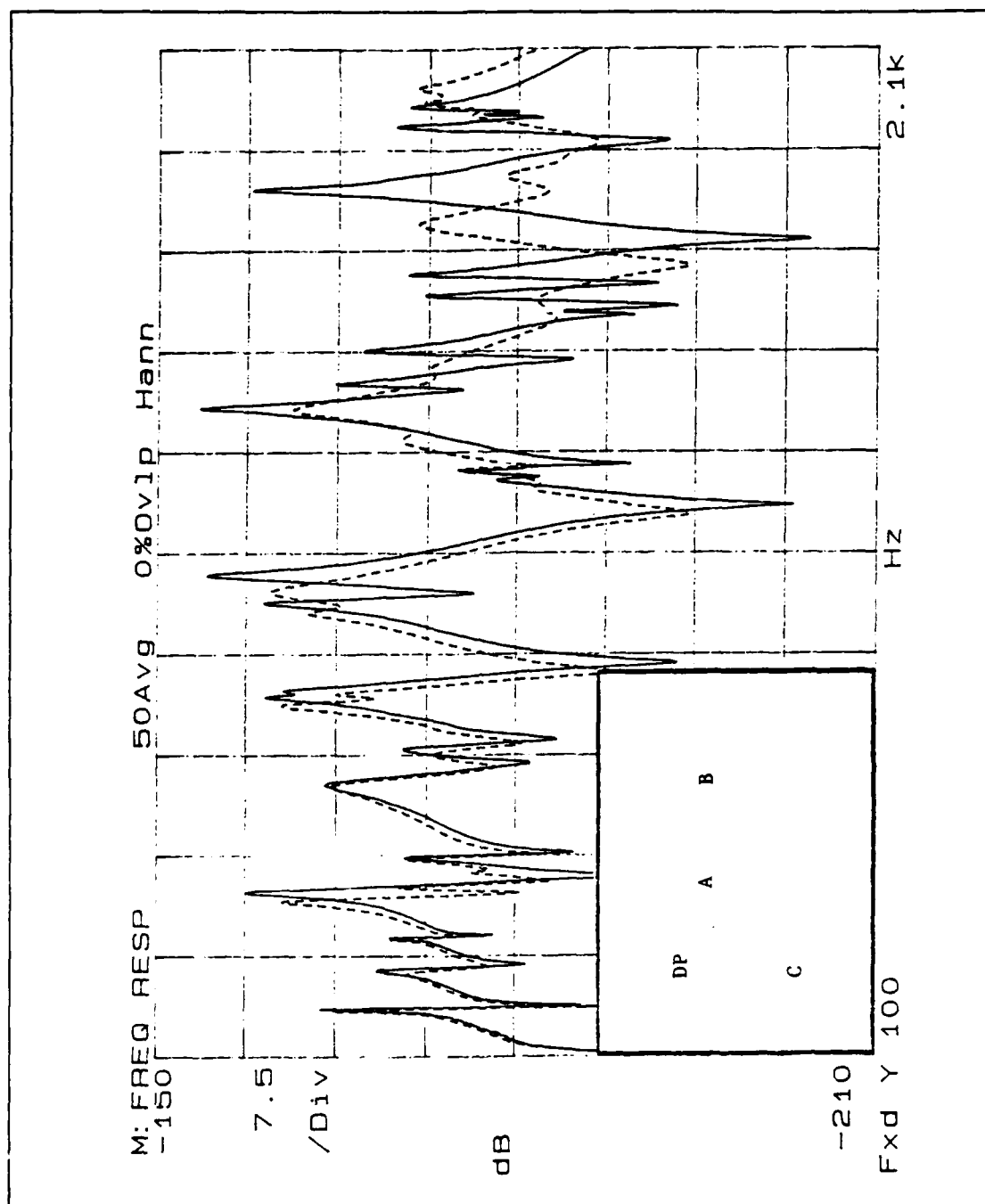


Figure 53. Baseline (DP) frequency response (solid); with a 16" constrained layer waveguide absorber at locations A, B and C (dashed): Locations shown in insert.

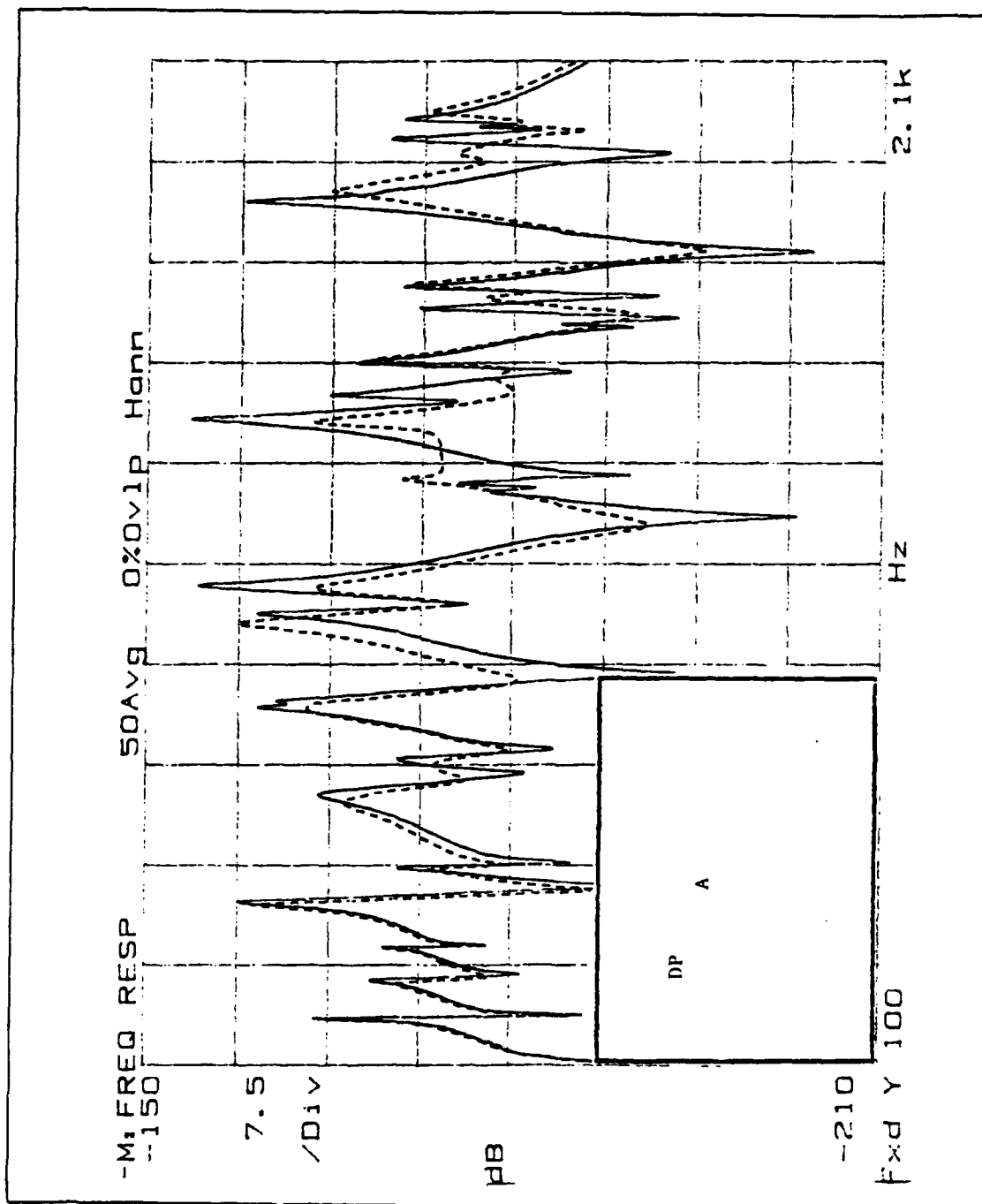


Figure 54. Baseline (DP) frequency response (solid); with a 20" viscoelastic waveguide absorber attached at location A (dashed): Locations shown in insert.

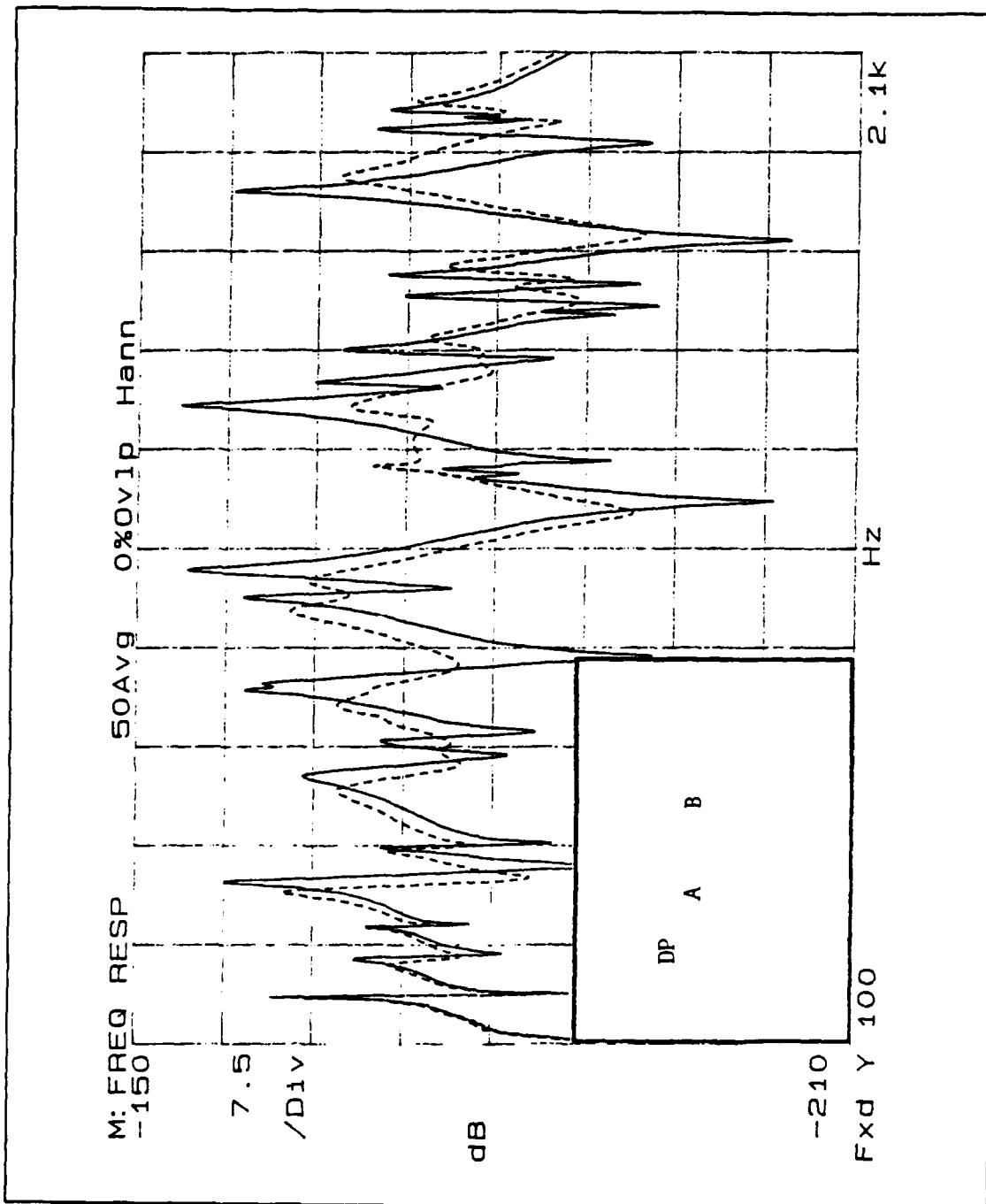


Figure 55. Baseline (DP) frequency response (solid); with a 20" viscoelastic waveguide absorber at locations A and B (dashed): Locations shown in insert.

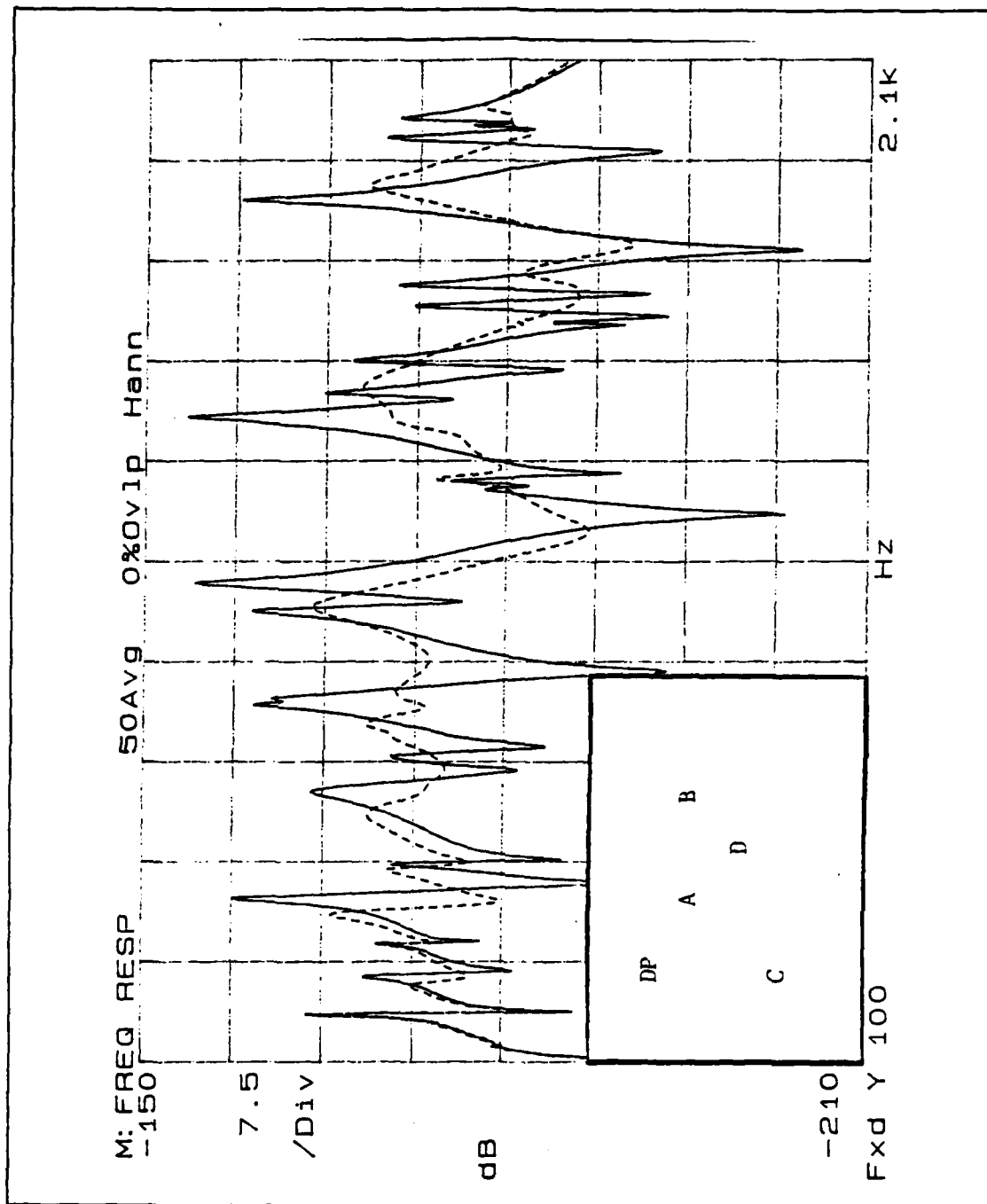


Figure 56. Baseline (DP) frequency response (solid); with a 20~ viscoelastic waveguide absorber at locations A, B, C and D (dashed): Locations shown in insert.

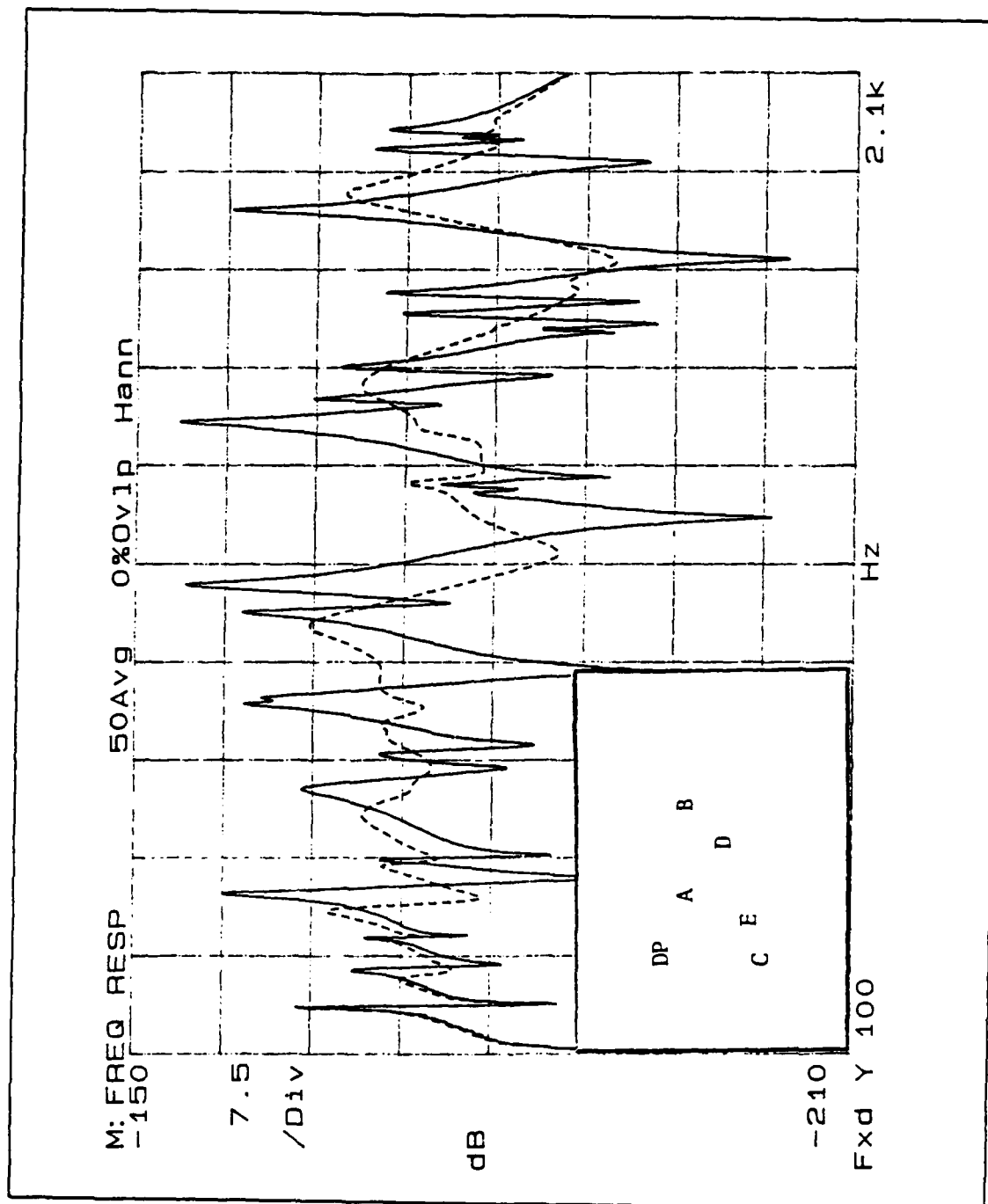


Figure 57. Baseline (DP) frequency response (solid); with a 20~ viscoelastic waveguide absorber at locations A, B, C, D and E (dashed): Locations shown in insert.

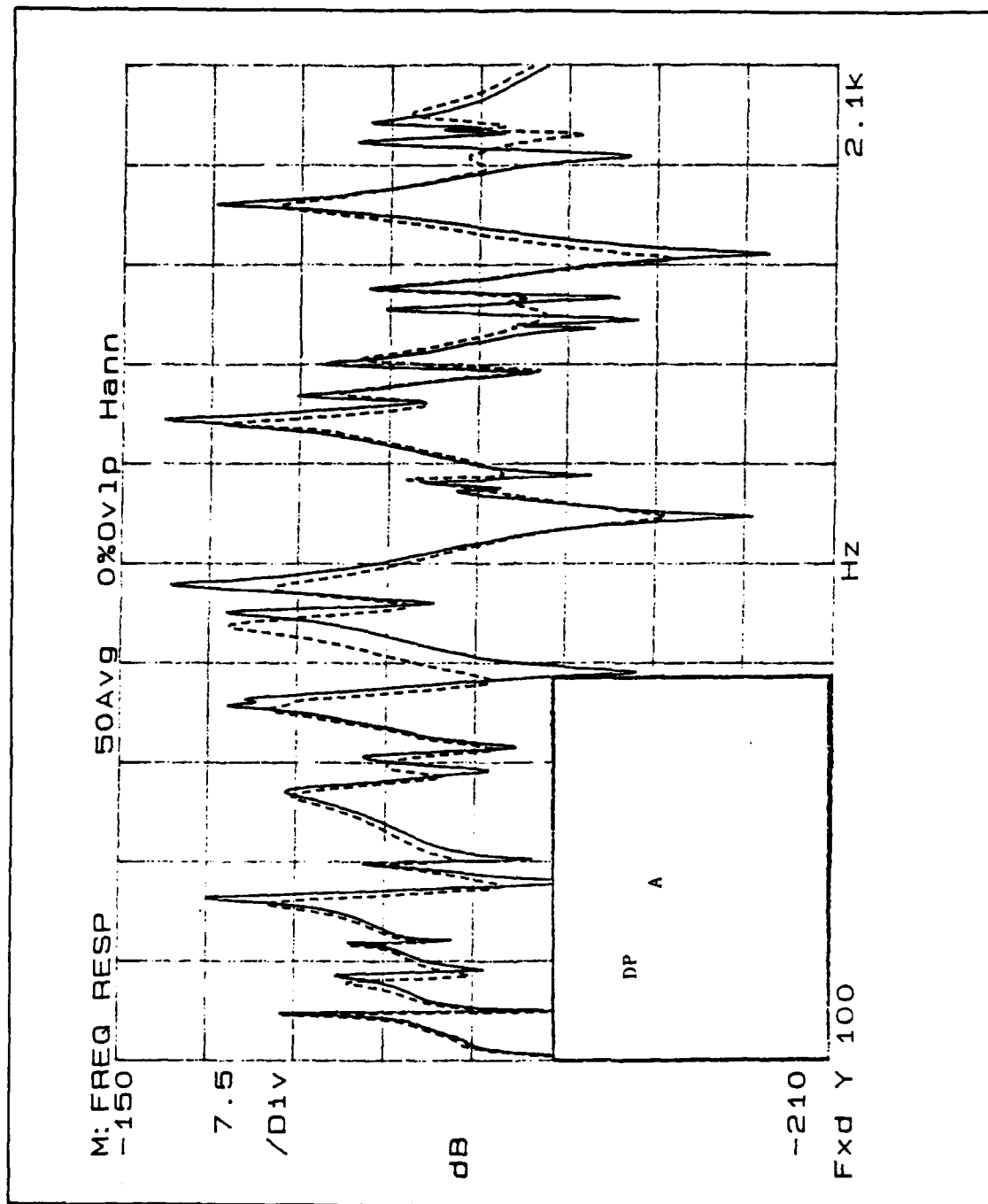


Figure 58. Baseline (DP) frequency response (solid); with a 16" viscoelastic waveguide absorber at location A (dashed): Locations shown in insert.

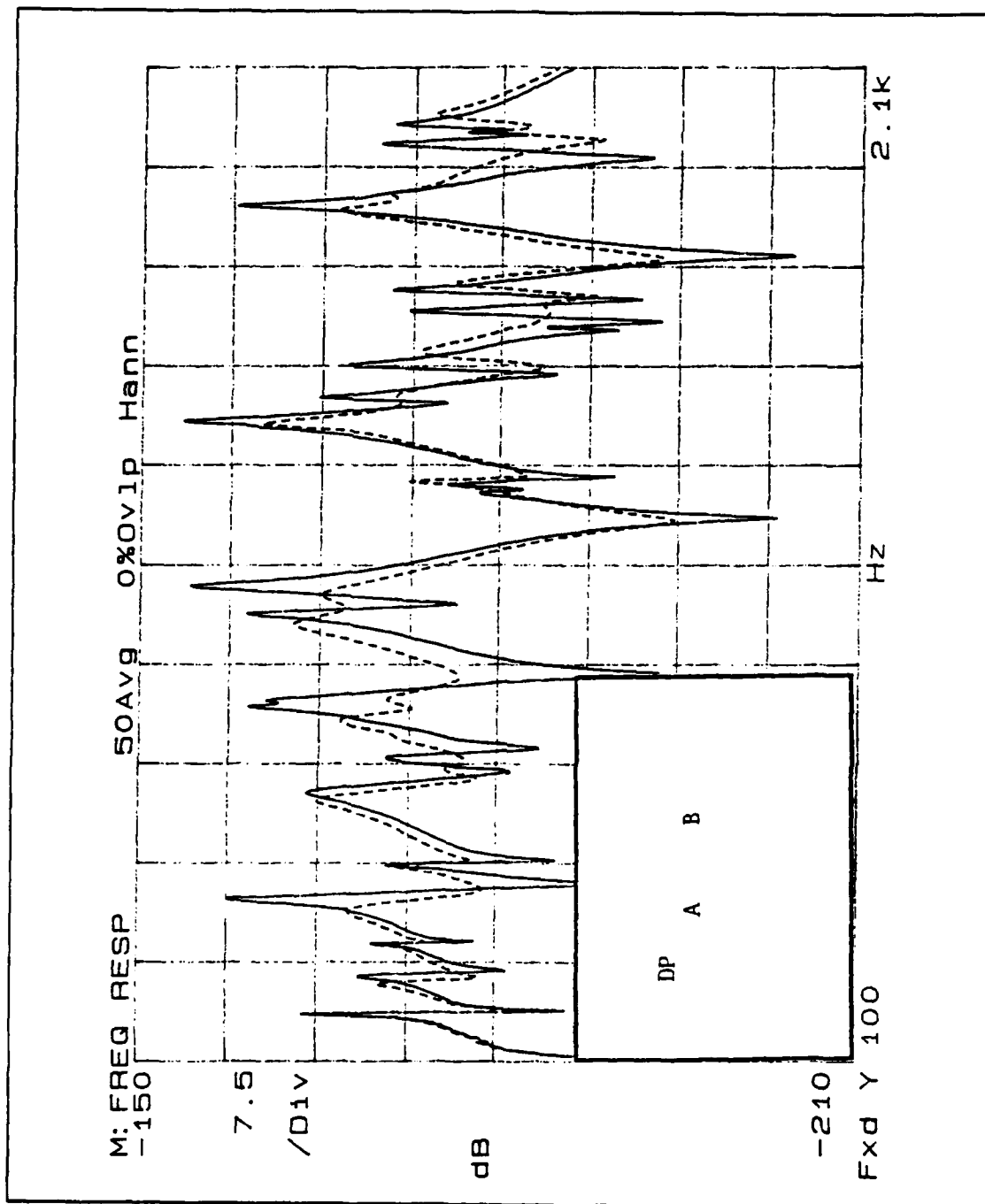


Figure 59. Baseline (DP) frequency response (solid); with a 16" viscoelastic waveguide absorber at locations A and B (dashed): Locations shown in insert.

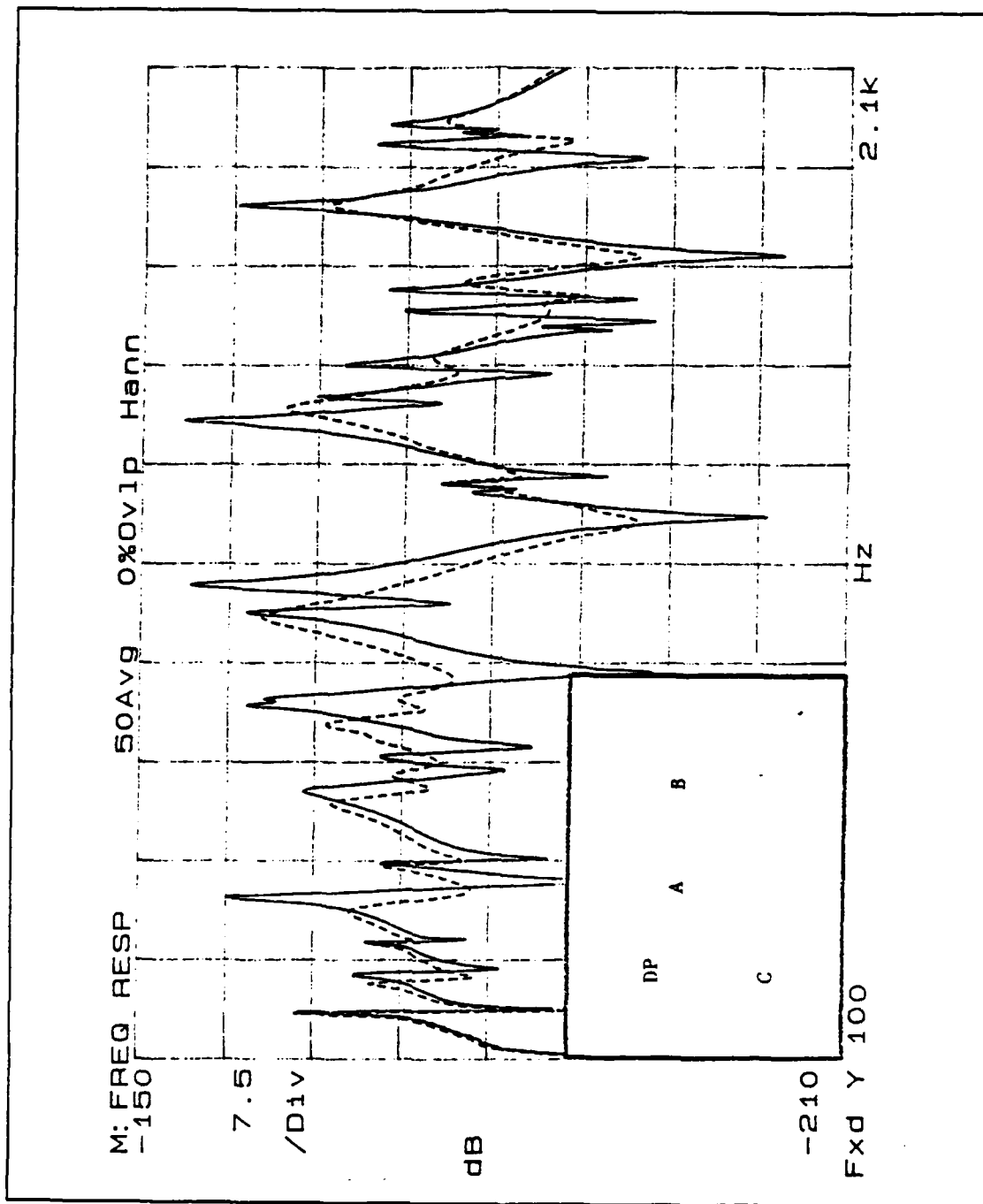


Figure 60. Baseline (DP) frequency response (solid); with a 16" viscoelastic waveguide absorber at locations A, B and C (dashed): Locations shown in insert.

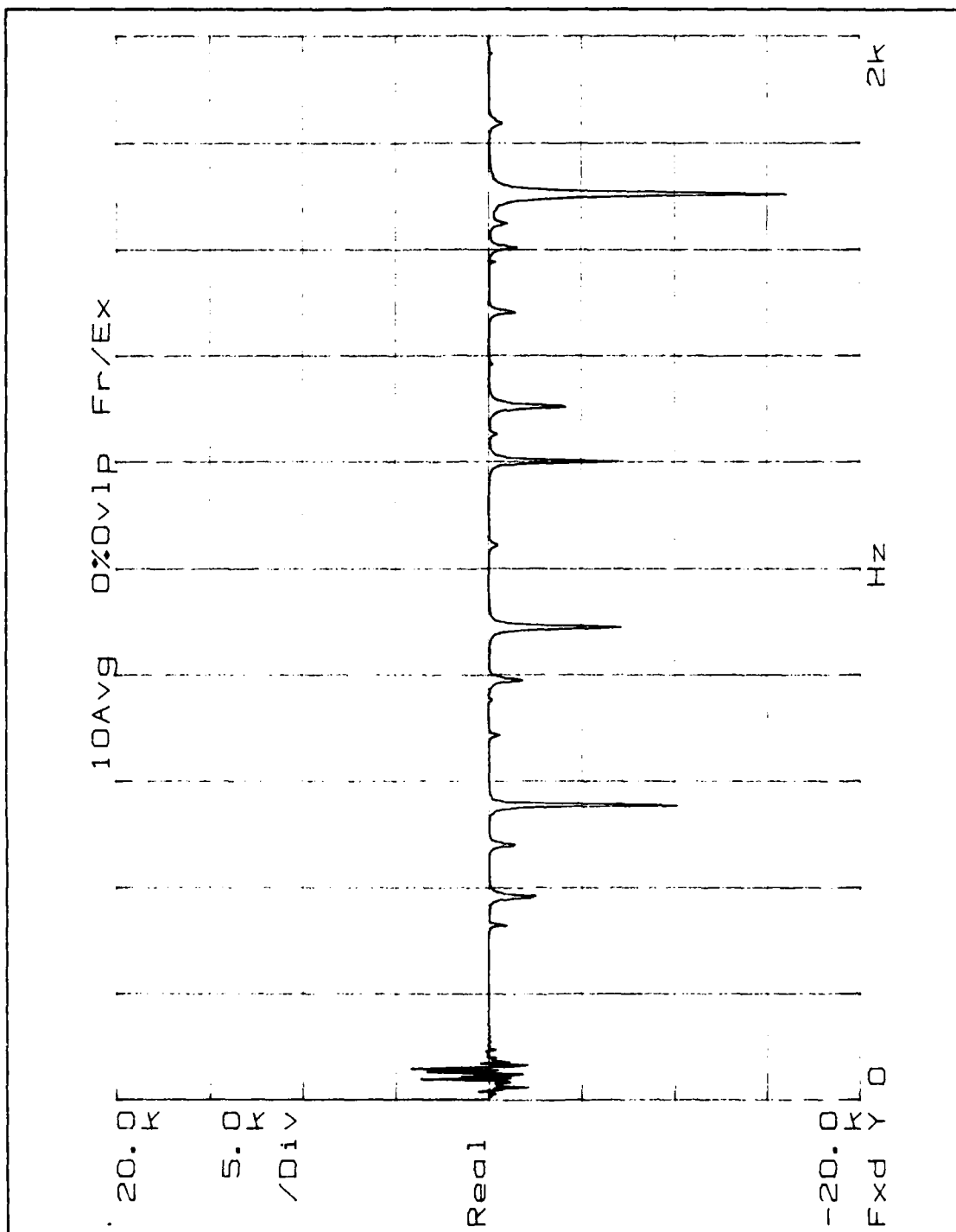


Figure 61. Real part of the test plate's impedance at location A.

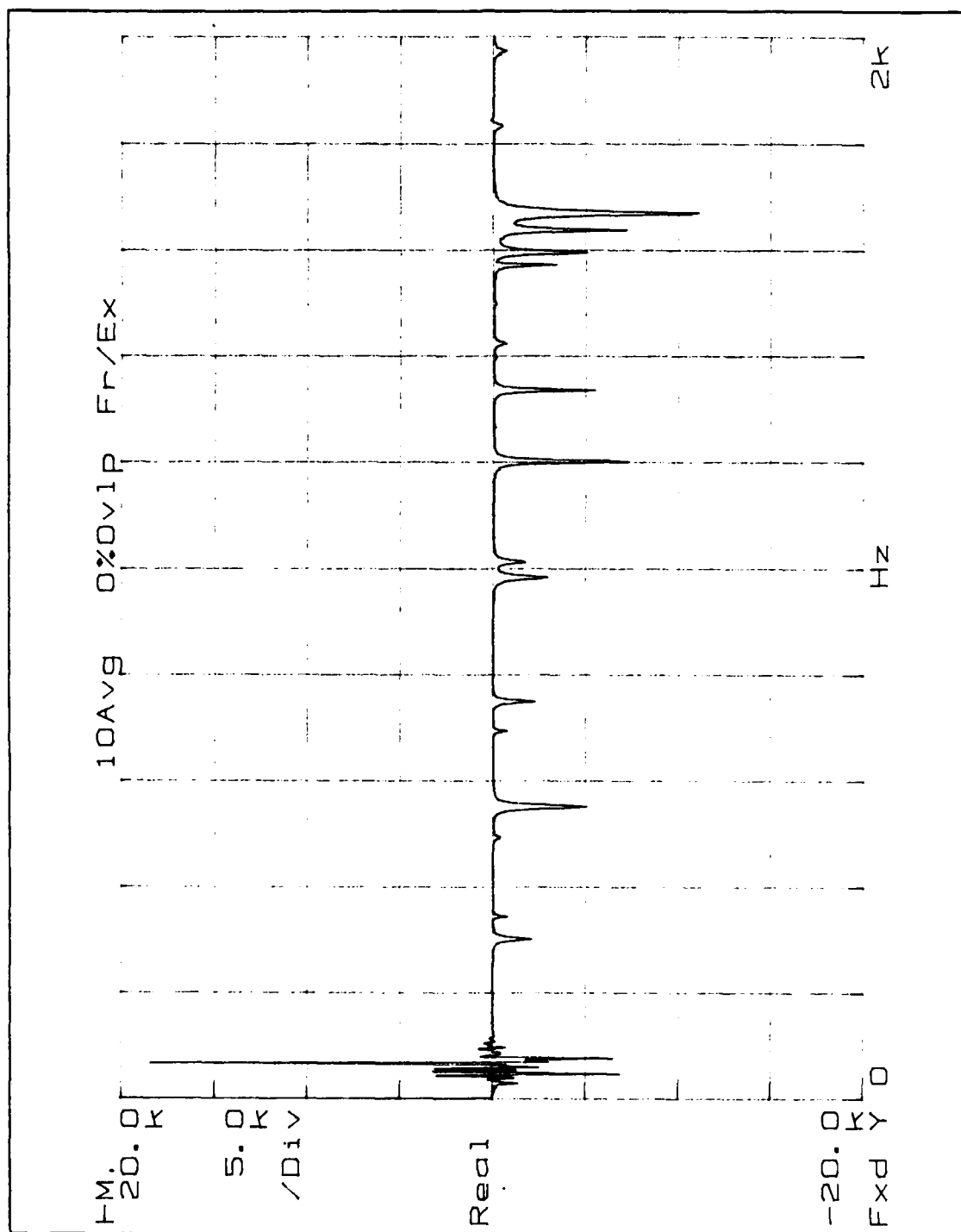


Figure 62. Real part of the test plate's impedance at location B.

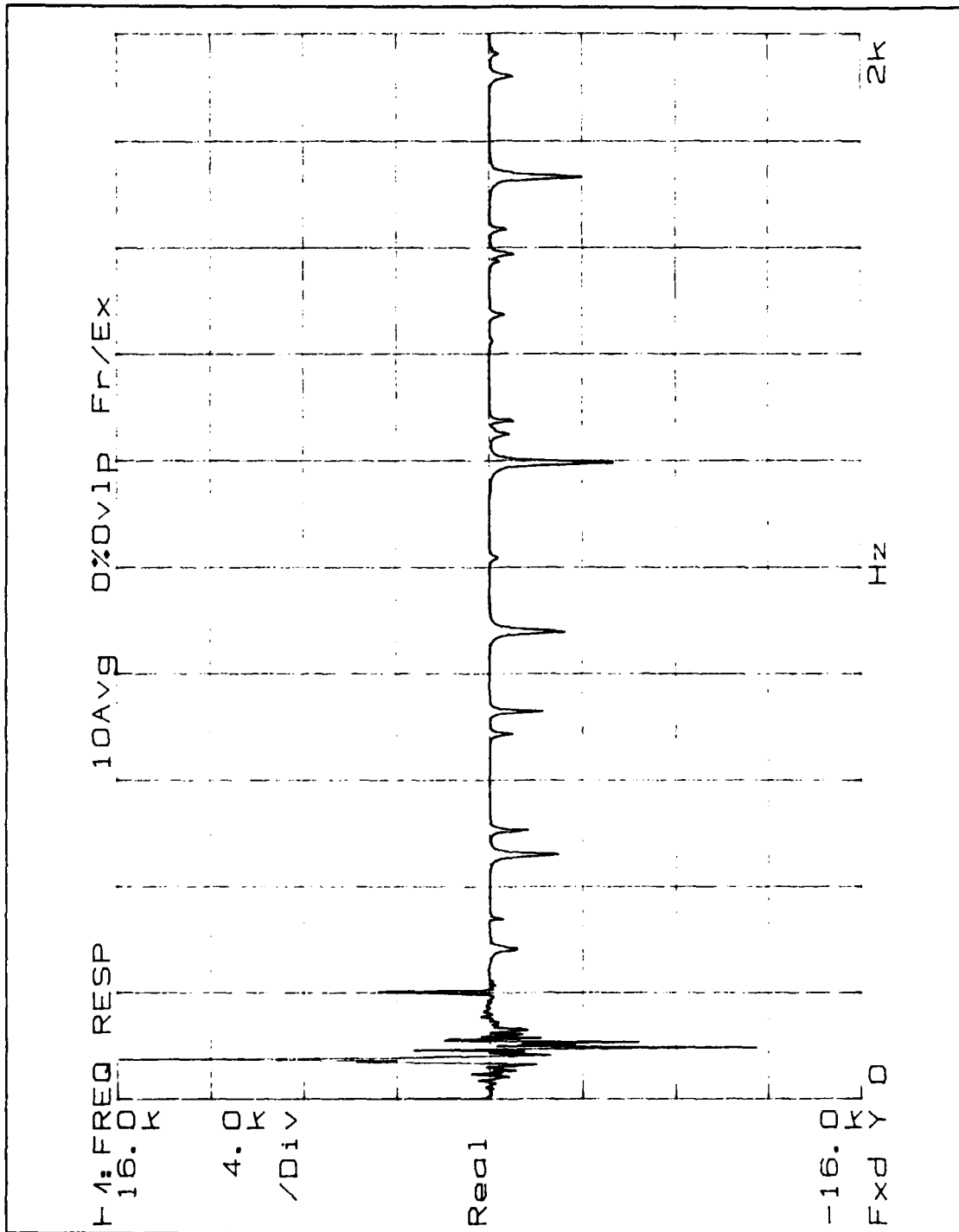


Figure 63. Real part of the test plate's impedance at location C.

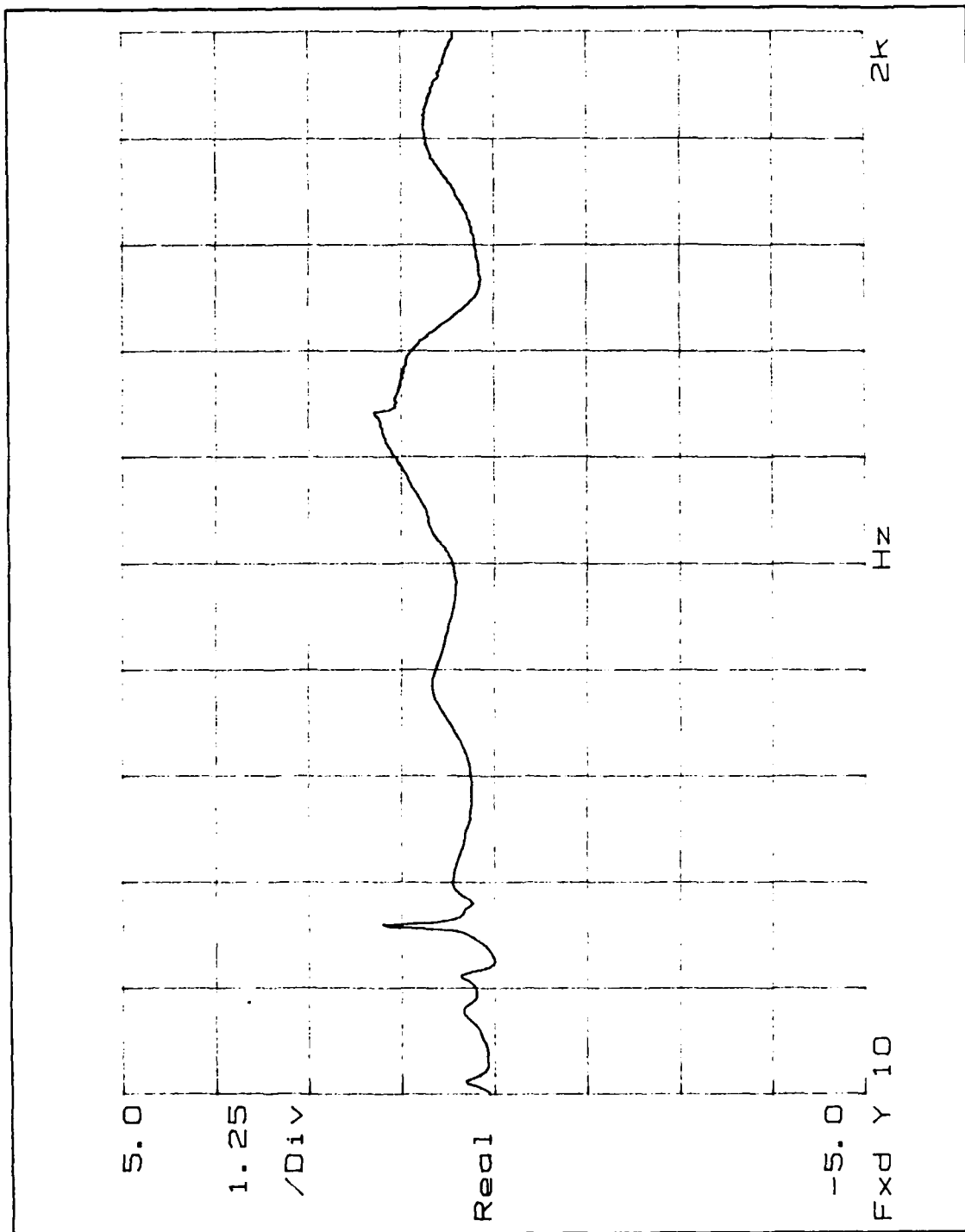


Figure 64. Real part of the 20" constrained layer waveguide absorber's impedance.

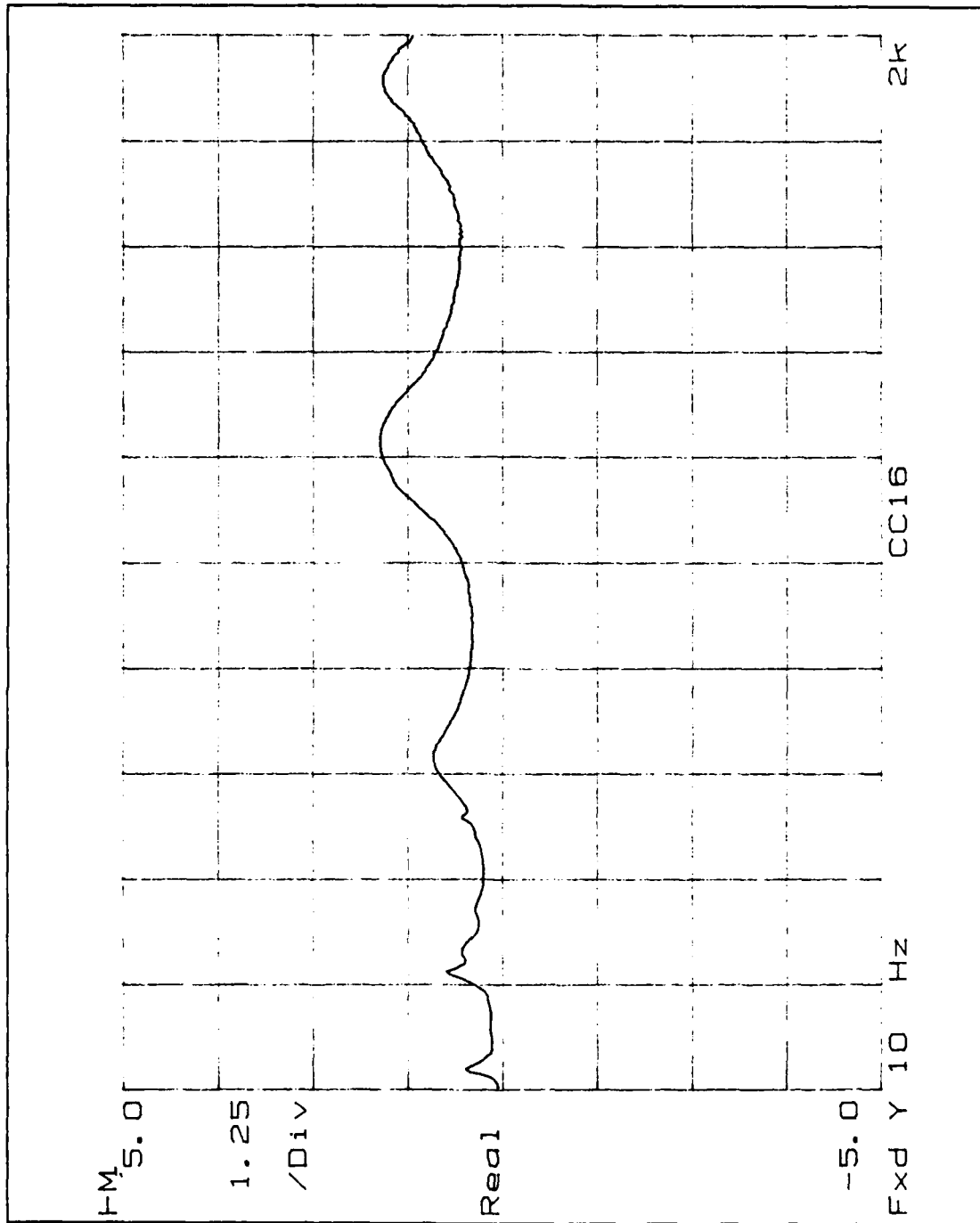


Figure 65. Real part of the 16" constrained layer waveguide absorber's impedance.

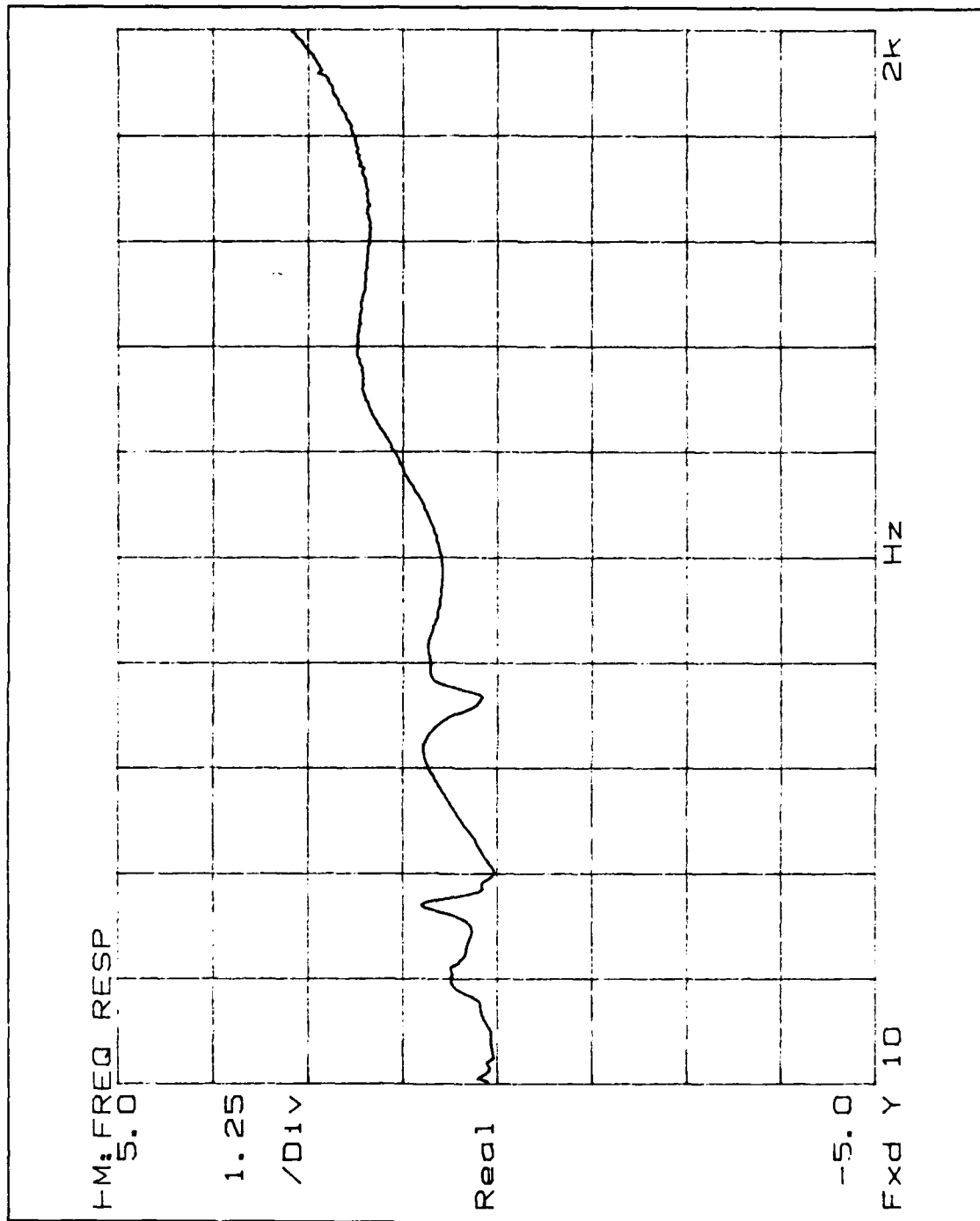


Figure 66. Real part of the 20" viscoelastic waveguide absorber's impedance.

LIST OF REFERENCES

1. Nashif, A. D., Jones, D. I. G., and Henderson, J. P., *Vibration Damping*, John Wiley & Sons, Inc., 1985.
2. Bschoor, O., and Albrecht, H., "Vibration Absorbers for the Reduction of Machinery Noise", *VDI-Zeitschrift*, 121, 1979.
3. Air Force Wright Aeronautical Laboratories Technical Report 83-3125, *Preliminary Evaluation of Waveguide Vibration Absorbers*, by E. E. Ungar and L. G. Kurzweil, January 1984.
4. BBN Laboratories, Inc., Report 6463, *A Study to Guide the Development and Use of Waveguide Absorbers for Structural Damping*, by E. E. Ungar and B. F. Williams, March 1987.
5. Lee, G. G., *Analytical and Experimental Studies of Beam Waveguide Absorbers for Structural Damping*, Master's Thesis, Naval Postgraduate School, Monterey, CA, March 1988.
6. Gockel, M. A., editor, *MSC/NASTRAN User's Manual*, MacNeal-Schwendler Corporation, June 1983.
7. Gockel, M. A., editor, *NASTRAN Handbook for Dynamic Analysis*, MacNeal-Schwendler Corporation, June 1983.
8. Fahy, F., *Sound and Structural Vibration*, Academic Press, 1985.

INITIAL DISTRIBUTION LIST

		No. Copies
1.	Defense Technical Information Center Cameron Station Alexandria, VA 22304-6145	2
2.	Library, Code 0142 Naval Postgraduate School Monterey, CA 93943-5002	2
3.	Dean of Science and Engineering, Code 06 Naval Postgraduate School Monterey, CA 93943-5000	2
4.	Research Administration Office, Code 012 Naval Postgraduate School Monterey, CA 93943-5000	1
5.	Department Chairman Code 69 Naval Postgraduate School Monterey, CA 93943-5000	1
6.	Professor Young S. Shin, Code 69Sg Department of Mechanical Engineering Naval Postgraduate School Monterey, CA 93943-5000	4
7.	Professor Kilsoo S. Kim, Code 69Ki Department of Mechanical Engineering Naval Postgraduate School Monterey, CA 93943-5000	1
8.	Dr. Arthur Kilcullen, Code 1962 David Taylor Naval Research Center Bethesda, MD 20084	2
9.	Mr. Maurice Sevik, Code 19 David Taylor Naval Research Center Bethesda, MD 20084	1
10.	Dr. Lawrence Maga, Code 196 David Taylor Naval Research Center Bethesda, MD 20084	1
11.	Mr. Gordon Eversteine, Code 1844 David Taylor Naval Research Center Bethesda, MD 20084	1

- | | | |
|-----|--|---|
| 12. | Dr. B. Whang, Code 1750.2
David Taylor Naval Research Center
Bethesda, MD 20084 | 1 |
| 13. | Dr. Peter Doubleday
Underwater Sound Research Detachment
Naval Research Laboratory
P.O. Box 8337
Orlando, FL 32856 | 1 |
| 14. | Mr. Bob Ting
Underwater Sound Research Detachment
Naval Research Laboratory
P.O. Box 8337
Orlando, FL 32856 | 1 |
| 15. | Dr. Alfred Tucker
Office of Naval Research
800 North Quincy St.
Arlington, VA 22217 | 1 |
| 16. | Mr. P. Majumdar, Code 55N
Naval Sea Systems Command Headquarters
Washington, DC 20362 | 1 |
| 17. | Mr. Jerry Synder, Code 55Y13
Naval Sea Systems Command Headquarters
Washington, DC 20362 | 1 |
| 18. | Mr. Walter Madigosky
White Oak Laboratory
Naval Surface Weapons Center Detachment
10901 New Hampshire Ave.
Silver Spring, MD 20903 | 1 |
| 19. | Dr. N. T. Tsai
Defense Nuclear Agency
SPSS
Washington, DC 20305-1000 | 1 |
| 20. | Dr. Parviz Mahmoodi
Building 201-BS-08
3M Center
St. Paul, MN 55144 | 1 |
| 21. | Mr. A. Dwayne Nelson
Building 230-1F-02
3M Center
St. Paul, MN 55144 | 1 |